MEASURING THERMAL PROPERTIES AND WATER CONTENT OF SOIL AND OIL SANDS MATURE FINE TAILING USING THE HEAT PULSE PROBE METHOD

A Dissertation Submitted to the College of Graduate Studies and Research

in Partial Fulfillment of the Requirements

for the Degree of Doctor of Philosophy

in the Department of Soil Science

University of Saskatchewan

Saskatoon

By

Min Li

PERMISSION TO USE

In presenting this dissertation in partial fulfillment of the requirements for a Postgraduate degree from the University of Saskatchewan, I agree that the Libraries of this University may make it freely available for inspection. I further agree that permission for copying of this dissertation in any manner, in whole or in part, for scholarly purposes may be granted by the professor or professors who supervised my dissertation work or, in their absence, by the Head of the Department or the Dean of the College in which my dissertation work was done. It is understood that any copying or publication or use of this dissertation or parts thereof for financial gain shall not be allowed without my written permission. It is also understood that due recognition shall be given to me and to the University of Saskatchewan in any scholarly use that may be made of any material in my dissertation. Requests for permission to copy or to make other uses of materials in this dissertation, in whole or part, should be addressed to:

Head, Department of Soil Science

University of Saskatchewan

Saskatoon, Saskatchewan

Canada, S7N 5A8

DISCLAIMER

Reference in this dissertation to any specific commercial product, process, or service by trade name, trademark, manufacturer, or otherwise, does not constitute or imply its endorsement, recommendation, or favoring by the University of Saskatchewan. The views and opinions of the author expressed herein do not state or reflect those of the University of Saskatchewan, and shall not be used for advertising or product endorsement purposes.

ABSTRACT

Measurements of thermal properties and water contents of soil are important for predicting the water and energy balance in terrestrial ecosystems and for many agricultural, environmental, geophysical, and engineering applications. The heat pulse probe method including the single-probe heat pulse (SPHP) and the dual-probe heat pulse (DPHP) is the only approach that can appropriately measure soil thermal properties in situ. Currently, the SPHP can only be used to measure soil thermal conductivity (λ), but the DPHP can measure λ, thermal diffusivity (α), volumetric heat capacity (C), and θ simultaneously. However, little is known about the performance of the DPHP in a saturated suspension medium; for example, the oil sands mature fine tailing (MFT). To the best of my knowledge, no report is available on the determination of θ using the SPHP. In addition, accurate thermal contact conductivity (H) values between the probe and soil are currently unknown, but is a prerequisite for accurately determining soil thermal properties and θ by the SPHP.

This dissertation sought to improve the heat pulse probe method by applying the DPHP in measuring the bulk density (ρ_b) of MFT, and developing the SPHP for θ estimation. Three studies were conducted: 1) to evaluate the feasibility of determining the solid percentage of MFT using the DPHP; 2) to compare θ estimations from the relationships between θ and λ, normalized cumulative temperature increase (TN_{cum}), and normalized maximum temperature increase (TN_{max}) using the SPHP; and 3) to obtain the H values experimentally and evaluate the performance of θ estimation by the $H(\theta)$ relationships using the SPHP.

This dissertation demonstrates that the DPHP can be used to accurately measure the solid percentage of MFT, and the accuracy can be improved by independent measurement of soil specific heat of solids (c_s). It also shows that a combination of the $\lambda(\theta)$, $TN_{cum}(\theta)$, and $TN_{max}(\theta)$

methods facilitates θ determination using the SPHP. Probe independence is the advantage of the λ(θ) method; however, the $TN_{cum}(\theta)$ and $TN_{max}(\theta)$ methods are especially useful when a faster and more frequent measurement is required. The SPHP measured $H(\theta)$ relationships can be used to estimate θ accurately for different textured soils except for coarse sand. More studies should be conducted to build the pedotransfer functions between soil physical properties and the λ(θ), $TN_{cum}(\theta)$, $TN_{max}(\theta)$, and $H(\theta)$ relationships.

ACKNOWLEDGEMENTS

My appreciation goes out to all the help that I have received in completing this dissertation. I would like to express my deepest gratitude to my supervisor Dr. Bing Si for his patient guidance, intelligent inspiration, and financial support throughout my Ph.D. studies. My thanks also go to Drs. Andrew Ireson, Jane Elliott, John Pomeroy, and Steven Siciliano for their service on my advisory committee and their valuable suggestions. Thanks to Dr. Joshua Heitman for his contributions as an external examiner. A special thanks goes to Drs. S. Lee Barbour, Wei Hu, Henry Chau, Gang Liu, and Miles Dyck for their helpful insights and timely conversations. Thanks to Prof. Terry Tollefson, Prof. Jeff schoenau, Dr. Geoff Halferdahl and Miss Kathryn Dompierre for generously providing soil samples. Thanks for the friendship, encouragement and proof reading from my colleagues and friends, Lindsay Tallon, Trent Pernitsky, Kathy Dobrovolskaya, Eric Neil, Mark Sigouin, and Thian Wittayawarakul.

I gratefully acknowledge the financial support from the Natural Sciences and Engineering Research Council of Canada (NSERC) and the scholarships from the Chinese Scholar Council, Canadian Society of Soil Science, the Department of Soil Science, the College of Agriculture and Bioresources, and the College of Graduate Studies and Research at the University of Saskatchewan.

To my mother, Suzhen Ren, parents-in-law, Yiguo Hu and Pinglian Lyu, and my sister, Qiong Li, thanks for your constant support. To my lovely son Terrence, thank you for putting a smile on my face every day. To my wife, Yu Dai, the most important one in my life, thanks for your deeply understanding and love.

DEDICATION

This dissertation is dedicated to my dear dad, Mingyi Li.

He did not tell me what is right. He did it right, I watched and learned.

TABLE OF CONTENTS

LIST OF TABLES

LIST OF FIGURES

LIST OF ABBREVIATIONS

AHFO	Active heated fibre optic
DPHP	Dual-probe heat pulse
DSC	Differential scanning calorimetry
DTS	Distributed temperature sensing
EC	Electric conductivity (S m^{-1})
FFT	Fluid fine tailing
GPR	Ground penetrating radar
MDSC	Modulated differential scanning calorimetry
MFT	Mature fine tailing
MPHP	Multi-probe heat pulse
RMSE	Root mean square error
SPHP	Single-probe heat pulse
TDR	Time domain reflectometry

LIST OF SYMBOLS

A, a	The slope of a linear relationship (-)
B, b	The intercept of a linear relationship (-)
C	Volumetric heat capacity (J m^{-3} K^{-1})
c	Specific heat capacity (J kg^{-1} K^{-1})
C_p	Volumetric heat capacity of probe (J m^{-3} K^{-1})
c_a	Specific heat capacity of air (J kg^{-1} K^{-1})
c_m	Specific heat capacity of mineral (J kg^{-1} K^{-1})
c_o	Specific heat capacity of organic matter (J kg^{-1} K^{-1})
c_s	Specific heat capacity of solids (J kg^{-1} K^{-1})
c_w	Specific heat capacity of water (J kg^{-1} K^{-1})
H	Thermal contact conductivity (W m^{-2} K^{-1})
I	Electrical current (A)
J_0	The zero-order Bessel functions of the first kind (-)
J_1	The first-order Bessel functions of the first kind (-)
m	mass (kg)
m_{solid}	mass of solids (kg)
n	Number (-)
p	Laplace transformation variable (-)
q	heating strength (W m^{-1})
r	Radius (m)
T	Temperature (˚C)
t	Time (s)
Ⓣ	Laplace transforms of ΔT (-)
t_0	Heat pulse duration (s)
T_{cum}	Cumulative temperature increase (K s)
T_{max}	Maximum temperature increase (K)
TN_{cum}	Normalized cumulative temperature increase(K s m W^{-1})
TN_{max}	Normalized maximum temperature increase(K m W^{-1})
Y_0	The zero-order modified Bessel functions of the second kind (-)

Y_1	The first-order modified Bessel functions of the second kind (-)
Z_1, Z_2, and Z_3	Parameters of Eq. 5.14 (-)
α	Thermal diffusivity ($m^2\ s^{-1}$)
γ	Euler's constant (γ = 0.5772)
Δsp	Absolute change of solid percentage (%)
ΔT	Temperature change (K)
θ	Soil water content ($m^3\ m^{-3}$)
θ_e	Estimated soil water content ($m^3\ m^{-3}$)
θ_m	Measured soil water content ($m^3\ m^{-3}$)
θ_{sa}	Saturated water content ($m^3\ m^{-3}$)
λ	Thermal conductivity ($W\ m^{-1}\ K^{-1}$)
ρ_b	Bulk density ($kg\ m^{-3}$)
ρ_p	Particle density of soil ($kg\ m^{-3}$)
ρ_w	Density of water ($kg\ m^{-3}$)
σ	Standard deviation (-)

1 INTRODUCTION

1.1 General Introduction

The thermal properties of soil, including thermal conductivity (λ, W m^{-1} K^{-1}), thermal diffusivity (α, m^2 s^{-1}), and volumetric heat capacity (C, J m^{-3} K^{-1}), are important in agricultural, environmental, hydrological and engineering science. Soil thermal properties control the transport and storage of energy in the soil, the energy balance of the earth's surface, and the temperature regimes of the top soil layer and lower atmospheric layers (de Vries and Peck, 1958a), and also affect the water flux, evaporation, plant growth, chemical reactions, and microbiological activities in the soil.

Another important property of soil, the soil water content (θ, m^3 m^{-3}), is fundamentally important for a wide variety of agricultural, engineering, and hydrological applications and plays important roles in the hydrological cycle and plant growth. An accurate and reliable technique to determine θ is needed for precision irrigation management and hydrological modelling (Dias et al., 2013).

Traditionally, soil thermal properties and θ are studied and measured individually; however, these two properties are interrelated in the field. For example, when soil θ is high, the C value will also be high. Therefore, temperature increases will be smaller and slower for wetter than for drier soils under the same conditions of incoming solar radiation (Fig. 1.1). Conversely, soil thermal properties affect temperature changes in the soil profile, and thus the movement and storage of water in the soil. Therefore, it is important to develop a single instrument that can measure both soil thermal properties and θ at the same time, location, and scale, in order to provide accurate and

reliable data for studies which include coupled heat and water transport and balance (Bristow, 1998; Ren et al., 1999). It is also important to understand the covariance amongst the driving variables and its impact on estimation of λ and θ. In addition, both the temporal and spatial covariance should be studied because the long term and spatially distributed simultaneous soil thermal properties and θ measurements are of value.

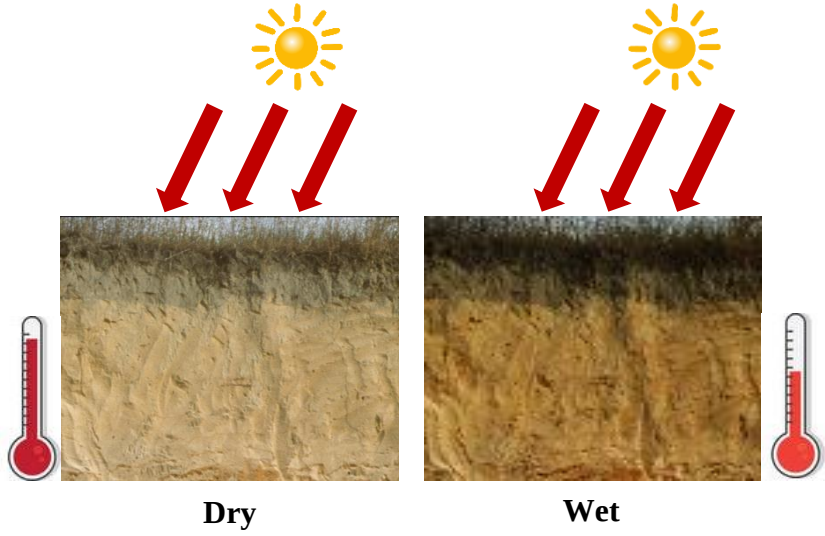

Fig. 1.1. Temperature increases of the same soil at different water contents, when receiving the same amount of solar radiation.

Despite the great importance of soil thermal properties and θ to soil heat and water budgets, the measurements of these properties are challenging. There are several methods that can measure soil thermal properties and θ, individually; however, to obtain both soil thermal properties and θ simultaneously, the heat pulse probe method is the only available option. A large scale application of the heat pulse probe method is called the active heated fibre optic-distributed temperature sensing (AHFO-DTS) (Sayde et al., 2010), which can measure soil thermal properties and θ simultaneously up to the scale of kilometres rather than merely at a point. The heat pulse probe method includes the single-probe heat pulse (SPHP) and the dual-probe heat pulse (DPHP).

Currently, the SPHP can only measure λ (de Vries and Peck, 1958b), but the DPHP can measure all three soil thermal properties and θ simultaneously (Bristow et al., 1994b; Bristow, 1998).

Although the DPHP has been applied to measurements on soil and rock, there are no reports on the performance of the DPHP in a saturated suspension media, such as soils at the bottoms of the bogs, rivers, and lakes, or oil sand tailings. Canada has the largest oil sands reserves in the world (Rowland et al., 2009; Penner and Foght, 2010). The extraction of bitumen from the mined oil sands generates a large volume of mature fine tailings (MFT), which is a saturated medium comprised of approximately 70 % water and 30 % solids. Without any further intervention, MFT could take up to one hundred years to consolidate sufficiently to act as a weight bearing soil for reclamation purposes (Chalaturnyk et al., 2002; Farkish and Fall, 2013). The industry is utilizing a wide variety of methods in an attempt to accelerate the consolidation process (Redfield et al., 2003; Farkish and Fall, 2013), and the characterization of the spatial and temporal distribution in bulk density (ρ_b, kg m^{-3}) (or solid percentage) of large volumes of MFT is critical to the management of these deposits (Dobchuk et al., 2013). Therefore, a nonradioactive, continuous, and automated measurement of MFT's ρ_b (or saturated water content, or solid percentage) is needed to monitor the MFT solidification process, and the DPHP has the potential to be the best choice compared to other methods.

However, the DPHP has several limitations when it is used in field soils. First, it tends to overestimate *C* and θ (Heitman et al., 2003; Ochsner et al., 2003; Liu et al., 2012). Second, the probe needles are easily bent because of their small diameter when the probe is used in the field soils, and thus the distance between two probes changes. It has been proven that small needle deflections can cause significant measurement errors for the DPHP (Liu et al., 2008a). Last, the lengths of the dual probes are usually shorter than 3 cm, because the heterogeneity of the field

soils, choice of the representative location to install the probe is important. If the soil around the probe has rocks or cracks, reliable measurement cannot be obtained.

The SPHP has several advantages over the DPHP: First, the single probe's needle is more robust and suited to field settings due to its larger diameter and thicker wall (Liu and Si, 2011a). Second, the single probe only has one needle and there is no issue about needle deflection (Fig. 1.2). The measurement error is barely affected even the probe is bent. Third, the single probe has a larger zone of influence as a result of its longer needle length. Therefore, it is important to develop the SPHP in order to overcome the limitations of the DPHP for the field soil measurement.

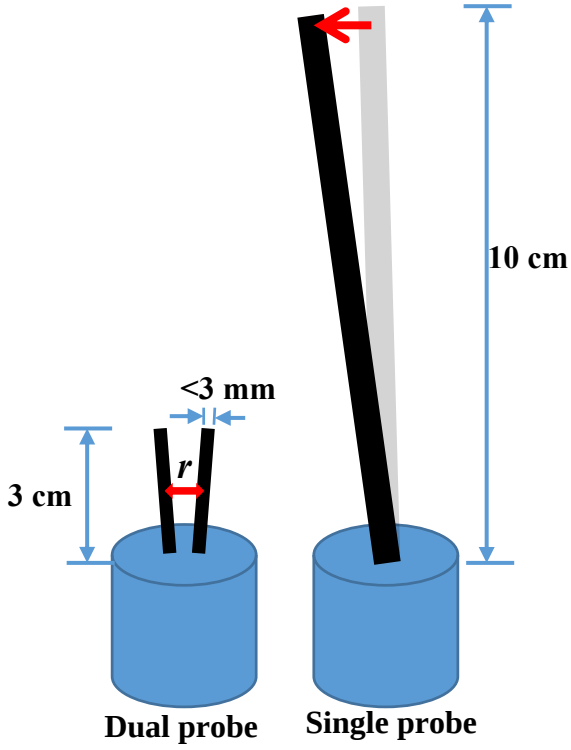

Fig. 1.2. Schematic of the typical sizes of the heat pulse dual probe and single probe (not to scale). The needle deflection can introduce large errors in the dual probe measurement, but not in the single probe measurement.

In recent years, the AHFO-DTS system has been used for in situ monitoring of soil thermal properties and θ (Sayde et al., 2010; Ciocca et al., 2012; Striegl and Loheide, 2012). With the

AHFO-DTS method, θ can be inferred from the λ~θ relationship (Ciocca et al., 2012), the maximum temperature increase (T_{max}, K)~θ relationship (Striegl and Loheide, 2012), or the cumulative temperature increase (T_{cum}, K s)~θ relationship (Sayde et al., 2010). However, reported studies using the AHFO-DTS technique focused only on in situ θ monitoring and did not test the performance on multiple soil textures, nor compare the three methods (i.e., λ(θ), T_{cum}(θ), and T_{max}(θ) methods).

The above three methods for θ determination should all be applicable to the SPHP, since the AHFO-DTS system is based on the SPHP. In order to thoroughly compare the λ(θ), T_{cum}(θ), and T_{max}(θ) methods, it may be more desirable to use the SPHP than to use the AHFO-DTS. The reason is that the stainless steel needle (high λ) of the single probe is in direct contact with soil particles, whereas a fibre optic cable has several protective layers surrounding the fibre optic cable, which may increase contact resistance between the heater, temperature sensor and soil. Therefore, conventional heat pulse probes have better contact with soil than the fibre optic cables in terms of heat conduction (Liu and Si, 2011a; Ciocca et al., 2012), and can obtain more frequent temperature readings during the early time, which is very important for determining the thermal contact conductivity (H, W m^{-2} K^{-1}) and α from the Blackwell (1954) small-time (hereinafter referred to as short-time) solution.

As previously mentioned, the SPHP has been applied in soil to measure λ; however, not for α, C, or θ. This is due to the unknown H at the boundary between the probe body and soil particles. Thermal contact conductivity of soil is the reciprocal of thermal contact resistance, which is a heat transport prohibiting effect due to the limited actual contact areas between the soil particles and the probe. The λ(θ), T_{cum}(θ), and T_{max}(θ) methods can be tested on AHFO-DTS to estimate θ; however, these relationships are soil texture and ρ_b dependent.

In order to obtain all three soil thermal properties from the SPHP without any soil-specific calibration, Blackwell (1954) devised simple approximations for both short-time and large-time (hereinafter referred to as long-term) periods. The long-time solution is used to determine λ, and the short-time solution is used to determine H, and thus α. However, the short-time solution requires nonlinear fitting of the data during the first several seconds, so its application was limited in the 1950s by the lack of high frequency temperature measurement equipment. Benefiting from the development of high frequency dataloggers, Waite et al (2006) measured α of methane hydrate from H obtained using the short-time solution, but the results showed large uncertainty in estimating H. Liu and Si (2011a) measured H of four dry sands using the short-time solution; however, the choice of the time range could be an issue when it is used for the wet soils. Without accurate H values between the probe and soil (de Vries and Peck, 1958a; Hadas, 1974), it is difficult to accurately estimate the α of wet soil using the SPHP. To date, little is known about the H values between the heat pulse single probe and soil (Liu and Si, 2011a). A better understanding of H may improve the SPHP for determining soil thermal properties and θ simultaneously, which also helps improve the heat pulse probe based AHFO-DTS.

The overall goal of this research is to develop both the DPHP and SPHP using laboratory soil column experiments, and this goal is addressed by three objectives: 1) to evaluate the feasibility of applying the DPHP to the measurement of the solid percentage of oil sands MFT; 2) to compare the $\lambda(\theta)$, $T_{cum}(\theta)$, and $T_{max}(\theta)$ methods for θ estimation using the SPHP; and 3) to obtain H experimentally and investigate the potential for θ determination by the $H(\theta)$ relationship using the SPHP.

1.2 Organization of the Dissertation

This dissertation is written in the style of a collection of manuscripts for submission to peer reviewed journals. Following this INTRODUCTION and a LITERATURE REVIEW (Chapter 2), the research presented in this dissertation is a compilation of three research chapters (Chapters 3-5). Each research chapter begins with a preface that describes how the chapter relates to the dissertation as a whole and includes a brief summary of the research (i.e., abstract), a brief introduction that includes a review of the relevant literature, a detailed materials and methods section, a summary and discussion of the results and a conclusion. The three main research chapters address the following objectives:

Chapter 3: To validate the feasibility of the DPHP for measuring solid percentage of oil sands MFT. Soil solid percentages of three MFT samples at a total of 12 bulk densities were measured, and the relationship between the DPHP measured and oven-dried solid percentages of MFT was built. The accuracy of this method was further validated by testing on additional six MFT samples,

Chapter 4: To compare the $\lambda(\theta)$, $T_{cum}(\theta)$, and $T_{max}(\theta)$ methods to determine θ using the SPHP. The precision of θ obtained from the $\lambda(\theta)$, $T_{cum}(\theta)$, and $T_{max}(\theta)$ methods were compared by error analysis. The effects of heating duration on the θ determination errors of the three methods were discussed. Two additional probes with the same materials and sizes as the initial probe were used to examine the effects of the probe itself on λ, T_{cum}, and T_{max} as well as to evaluate the accuracy of θ determined using the SPHP,

Chapter 5: To test the potential of θ determination from the $H(\theta)$ relationships using the SPHP. The H values of four soils at various θ were obtained, the effects of soil physical properties on the H values and $H(\theta)$ relationships were discussed and θ were estimated from the $H(\theta)$ relationships.

Chapters 3-5 are followed by a SYNTHESIS AND CONCLUSIONS (Chapter 6) that connects the individual manuscripts, summarizes the major findings and implications of the research, and highlights the combined contributions of the individual studies. This chapter includes a Summary of Findings section together with Future Research Directions. Literature cited throughout the dissertation are attached in the REFERENCES section (Chapter 7). A guide to fabricate the heat pulse probes, the wiring diagrams and photos of the measurement setup, and the main programs for the datalogger and calculations are attached in the APPENDICES section at the end of this dissertation.

2 LITERATURE REVIEW

2.1 Soil Thermal Properties

Soil temperature is one of the most important controlling factors for the behaviour of soil and affects the physical, biological, and chemical processes occurring in the soil as well as vegetation growing on it (Brady and Weil, 2008). Most plants have a narrow range of soil temperatures for optimal growth (Alexander, 2014), and are more sensitive to soil temperature than air temperature. Seed germinations require specific soil temperatures, and root functions such as nutrient and water uptake will be restricted if the soil temperature falls below its optimum range (Brady and Weil, 2008; Huang et al., 2012). Soil microbial processes and organic matter decomposition are also largely restricted by low soil temperature (Baver, 1956). Fluctuations in soil temperatures above and below 0 ˚C cause thawing and freezing cycles within the soil, where the expansion of water during freezing can damage plant roots and create cracks in the soil (Alexander, 2014).

There are three major sources of heat in surface soils. The majority of surface soil energy is provided by absorbed solar radiation, which is also responsible for diurnal and seasonal changes in soil temperatures (Baver, 1956). Some of the energy in soils is produced by chemical and biological processes occurring at the Earth' surface. Additionally, the Earth's core provides heat to its surface through heat convection in the mantle; however, the amount of heat provided from the centre of the Earth is less than 0.03 % of that from the sun (Alexander, 2014). Soil temperature is determined by two types of factors: factors that influence the amount of heat available to the soil surface and those that influence the dissipation of heat away from the surface. The amount of heat available is controlled by sources of heat such as the sun, soil mulch, and other soil surface

properties. The dissipation of heat is mainly affected by soil water content (θ, $m^3\ m^{-3}$), as θ affects soil thermal properties and evapotranspiration (Hanks, 1992). Various tillage practices also affect soil temperature and thermal properties by changing the microtopography of the soil surface (Johnson and Lowery, 1985).

Heat transport processes in soil are a combination of conduction, convection, radiation, and latent heat (Dane and Topp, 2002). Conduction of heat occurs by transmission of energy between adjacent soil particles. Convection takes place mainly through the movement of a heat-carrying mass (i.e. soil water) through soil pores. At the soil-atmosphere interfaces, laminar flow and turbulence heat flux are the commonest types of convection (Hillel, 1998). Radiation is the transfer of thermal energy from a point to its surroundings in the form of electromagnetic waves, and is usually insignificant and therefore ignored within soils. Latent heat processes occur when the heat is absorbed by the soil to cause the phase change without raising its temperature (Hillel, 1998; Dane and Topp, 2002). If the heat is consumed to convert ice into a liquid water without raising the temperature, it is called latent heat of fusion. If the heat that is consumed to change the liquid water into vapour state is known as the latent heat of vaporization (Ghildyal and Tripathi, 1987).

The soil temperature regime is quantitatively described by soil thermal properties. There are three key soil thermal properties: thermal conductivity (λ, $W\ m^{-1}\ K^{-1}$), volumetric heat capacity (C, $J\ m^{-3}\ K^{-1}$), and thermal diffusivity (α, $m^2\ s^{-1}$) (Huang et al., 2012). The λ of soil describes the property of soil to conduct heat in the presence of a temperature gradient (Canarache et al., 2006) and depends on many factors, such as soil mineral composition, organic matters, and θ (Hillel, 1998). The C of soil characterizes the total of heat energy that can be stored in soil; in other words, it characterizes the quantity of heat that can be added or removed per unit volume of soil per unit change in temperature (Baver, 1956; Gardiner and Miller, 2004). The α is defined as the ratio of

λ to *C* (Canarache et al., 2006), and it measures the heat conduction of soil relative to its heat storage. In other words, α describes the rate of transmission of temperature changes within the soil (Bristow et al., 1994b). When any two of the three soil thermal properties are known, the remaining unknown property can be calculated.

Soil thermal properties are frequently required when studying coupled heat and water transport across the vadose zone, and affect water flow, evaporation, plant growth, and chemical and microbiological soil processes (Lu et al., 2013). Knowledge of soil thermal properties in agricultural lands aids in irrigation and seeding management. Soil thermal properties are especially important for irrigation management in hot, arid regions; as θ and evaporation are affected by soil temperature regime.

The engineering disciplines are interested in soil thermal properties, especially λ of soils, as it affects the heat transfer from buried cables, road construction materials, cross-country oil pipe lines, etc. (de Vries and Peck, 1958a). The values of λ are required in the determination of the electric current-carrying capacity of buried cables and of the heat losses from underground steam and hot water piping (Woodside and Messmer, 1961a; Ochsner et al., 2001a). Thus, soil λ values are a key property influencing the design and simulation of earth-contact engineering facilities.

Soil thermal properties are affected by many factors (Nakshabandi and Kohnke, 1965; Tindall and Kunkel, 1999), which can be divided into two groups. The first group is composed of properties inherent to the soil itself, including soil texture and mineralogical composition. The second group can be manipulated or controlled through soil management, and includes θ, soil bulk density (ρ_b, kg m^{-3}), and temperature (Abu-Hamdeh, 2001). Given the same θ, sandy soils usually have higher λ values than that of finer textured soils. Water has a λ value 30 times greater than

that of air, but smaller than that of soil minerals (Nakshabandi and Kohnke, 1965); therefore, θ affects soil λ substantially. Generally, soil λ increases with θ (Hillel, 1998). As ρ_b of a given soil increases, the contact between the individual particles becomes more extensive, and as a result λ increases. However, this increase in λ is small in comparison to the increase due to θ (Nakshabandi and Kohnke, 1965). When the soil temperature is above 0 ˚C, λ shows relatively low dependence on temperature. However, in frozen soils, the temperature dependent ice content causes variable λ, as λ of ice is more than four times greater than that of water (Penner, 1970). Several studies on the thermal properties of frozen soils have been conducted (Penner, 1970; Penner et al., 1975; Slusarchuk and Watson, 1975), which focused on thaw prevention of permafrost soils used in highway design in cold regions, resulting in decreased maintenance cost.

2.1.1 Soil thermal conductivity

Soil thermal conductivity is described by Fourier's law of heat conduction and is usually defined as the quantity of heat that flows through a unit area in a unit time under a unit temperature gradient (Kirkham and Powers, 1972)

$$\lambda = -Q/(A\frac{dT}{dx}) \quad \text{(Eq. 2.1)}$$

where *Q* is the quantity of heat passed through soil per unit time (W), *A* is the cross-sectional area (m^2), and *dT/dx* is the temperature gradient (K m^{-1}). This definition is only suitable in a homogenous, isotropic, rigid solid material. However, the soil is porous media, and heat flows in soil are from one component to another in series as well as parallel to the different components (solids, water, and air); therefore, there is no simple function to describe the relationship between λ and volume fractions of each soil components, and a theoretical model to accurately describe

this complex series-parallel behavior of λ of soil is not available (Dane and Topp, 2002). The typical λ and *C* values of different soil materials are listed in Table 2.1.

Table 2.1. Thermal conductivities and volumetric heat capacities of soil solids and related materials (Koorevaar et al., 1983; Bristow, 2002a)**.**

Material	Thermal conductivity ($W\ m^{-1}\ K^{-1}$)	Volumetric heat capacity ($\times 10^6\ J\ m^{-3}\ K^{-1}$ at 20 °C)
Soil mineral (average)	NA	1.9
Quartz	8.8	NA
Clay mineral	2.9	NA
Organic matter	0.25	2.5
Water	$0.552 + 2.34 \times 10^{-3}T$† $- 1.10 \times 10^{-5}T^2$	4.18
Air	$0.0237 + 0.000064T$	0.0012
Ice (°C)	2.18	1.9

† *T* stands for temperature (°C).

The λ of soil is strongly influenced by the composition, shape, and configuration of soil components; such as soil texture, ρ_b, and θ. As shown in Fig. 2.1, most of the air-dried soils have similar values of λ around 0.3 $W\ m^{-1}\ K^{-1}$, because soil solids have limited contact with each other. As θ increases, there is a rapid increase in λ, which is caused by the increase in the contact areas as a result of the water films formed between solids particles, increasing the connectivity between solid particles. As θ continues to increase, more air spaces are replaced with water, and more heat passes through liquid water rather than solid, thus the increases in λ become slowly. The rapid increases from low to high λ usually occur earlier at lower θ in a sandy soil than a clay soil. This is because sand particles, made of quartz, have a high λ and any increase in connectivity through water films would drastically improve thermal conduction. At low water contents, water forms films surrounding clay particles and thus heat conduction in clay soils increases more substantially later on when small pores are filled with water.

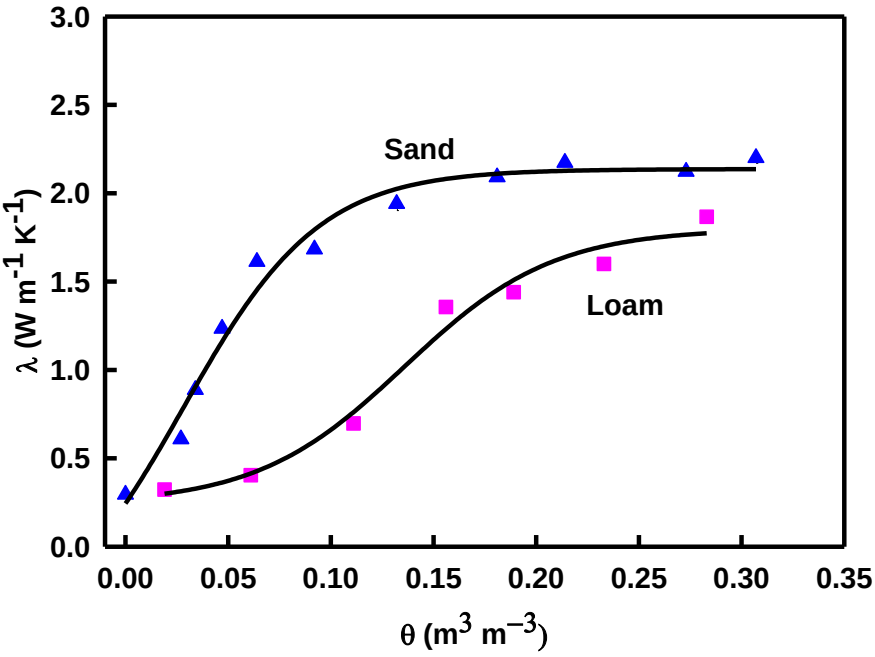

Fig. 2.1. Typical soil thermal conductivity (λ) as a function of soil water content (θ) for sand and loam.

Because of the difficulty in deriving theoretical models, efforts have been made to develop semi-theoretical and empirical models (Barry-Macaulay et al., 2015; Dong et al., 2015). Numerous soil λ models have been developed. In the following I will present two of them. The macroscopic "apparent" λ of soil is a spatially averaged heat flow over microscopically complex paths and cannot be calculated exactly (Dane and Topp, 2002). In 1963, de Vries developed a semi-theoretical model by assuming that λ of any mixture can be expressed as the weighted sum of λ of the components of the mixture (Ghildyal and Tripathi, 1987):

$$\lambda = \frac{k_m x_m \lambda_m + k_w x_w \lambda_w + k_a x_a \lambda_a}{k_m x_m + k_w x_w + k_a x_a} \quad \text{(Eq. 2.2)}$$

where λ_i, x_i, and k_i are thermal conductivity, volume fraction, and weighting factor of i, respectively. The subscript i (i.e. m, w, and a) stands for mineral, water, air, respectively; and k_m, k_w, and k_a can be determined empirically.

Based on a large number of λ measurements on repacked soils in the laboratory, Campbell (1985) developed an empirical model of λ as a function of θ:

$$\lambda = P_1 + P_2\theta - (P_1 - P_4)\exp[-(P_3\theta)^{P_5}] \quad \text{(Eq. 2.3)}$$

where P_1, P_2, P_3, P_4, and P_5 are soil dependent coefficients being related to relatively readily available soil properties. The relationships are

$$P_1 = \frac{0.57+1.73\phi_q+0.93\phi_{rm}}{1-0.74\phi_q-0.49\phi_{rm}} - 2.8\phi_s(1-\phi_s) \quad \text{(Eq. 2.4)}$$

$$P_2 = 2.8\phi_s \quad \text{(Eq. 2.5)}$$

$$P_3 = 1 + (2.6/{m_c}^{0.5}) \quad \text{(Eq. 2.6)}$$

$$P_4 = 0.03 + 0.7{\phi_s}^2 \quad \text{(Eq. 2.7)}$$

$$P_5 = 4 \quad \text{(Eq. 2.8)}$$

where ϕ_q, ϕ_{rm}, and ϕ_s are the volume fraction of quartz, minerals other than quartz, and total solids, respectively; and m_c is the clay mass fraction. P_3 is a strong function of clay content, which is used to capture the rapid transition of λ from low to high as θ increases (Fig. 2.1).

2.1.2 Soil volumetric heat capacity

The volumetric heat capacity of soil is simply defined as

$$C = dQ/dT \quad \text{(Eq. 2.9)}$$

where dT (K) is the temperature change of the system as a result of heat addition (dQ) (J m^{-3}) through an infinitesimal process (Ghildyal and Tripathi, 1987; Dane and Topp, 2002). The calculation of C is easier than that of λ for soils, as the total storage of heat can be simply added up of the heat stored in each component of soil. Therefore, C of soil is expressed as the weighted sum of the C of soil constituents (Koorevaar et al., 1983):

$$C = \sum_{i=1}^{n} x_i C_i = \sum_{i=1}^{n} x_i \rho_i c_i \qquad \text{(Eq. 2.10)}$$

Where x_i, ρ_i, c_i, and C_i are the volume fraction, density, specific heat capacity, and volumetric heat capacities of n soil constituents. It is more convenient to express the Eq. 2.10 in terms of mass fractions ϕ_i defined on a dry-mass basis than x_i in practice, and

$$x_i = (\phi_i \rho_b)/\rho_i \qquad \text{(Eq. 2.11)}$$

Substitution of Eq. 2.11 into Eq. 2.10 leads to

$$C = \rho_b \sum_{i=1}^{n} \phi_i c_i = \rho_b(\phi_m c_m + \phi_o c_o + \theta_g c_w + \phi_a c_a) \qquad \text{(Eq. 2.12)}$$

where the subscripts m, o, w, and a indicate mineral, organic matter, water, and air, respectively; and θ_g is the gravimetric soil water content. As seen in Table 2.1, soil air makes a negligible contribution to C of soil. Because it is difficult to separate the mineral and organic fractions of soil, Eq. 2.12 can be written as

$$C = \rho_b(\phi_s c_s + \theta_g c_w) = \rho_b(c_s + \theta\rho_w/\rho_b c_w) = \rho_b c_s + \theta\rho_w c_w \qquad \text{(Eq. 2.13)}$$

where c_s is the averaged specific heat of the solids. Therefore, with other soil properties kept constant, the C increases linearly with increasing θ.

2.1.3 Soil thermal diffusivity

If both λ and *C* of soil are known, then soil thermal diffusivity α can be calculated by (Ghildyal and Tripathi, 1987)

$$\alpha = \lambda / C \qquad \text{(Eq. 2.14)}$$

Or α can be determined from temperature observations using transient heat conduction equation. For a steady heat conduction, Eq. 2.1 can be described by

$$q = -\lambda(dT/dz) \qquad \text{(Eq. 2.15)}$$

where q is the steady heat flux density (W m^{-2}). Substituting Eq. 2.15 into the equation of continuity (Eq. 2.16)

$$\partial CT/\partial t = -(\partial q/\partial z) \qquad \text{(Eq. 2.16)}$$

we can obtain

$$\partial CT/\partial t = (\partial/\partial z)[\lambda(\partial T/\partial z)] \qquad \text{(Eq. 2.17)}$$

Assuming the soil is a homogeneous and isotropic system, Eq. 2.17 can be simplified as

$$C\partial T/\partial t = \lambda(\partial^2 T/\partial z^2) \qquad \text{(Eq. 2.18)}$$

Dividing both sides of Eq. 2.18 by *C* yields

$$\partial T/\partial t = \alpha(\partial^2 T/\partial z^2) \qquad \text{(Eq. 2.19)}$$

Equation 2.19 has been frequently used as the governing expression to describe heat transfer in soil. For most soils, α increases with increasing θ from dry soil, reaches a maximum and then decreases again (Fig. 2.2).

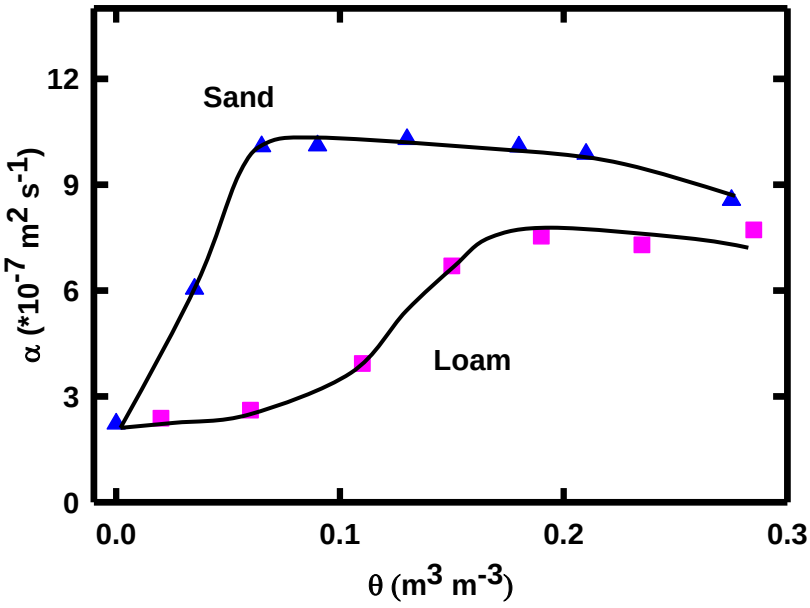

Fig. 2.2. Typical soil thermal diffusivity (α) as a function of soil water content (θ) for sand and loam.

2.1.4 Soil thermal properties measurement

Knowledge of soil thermal properties including λ, *C*, and α is of great importance; however, accurate determination of soil thermal properties is quite challenging and there are few options available.

The λ can be predicted by several semi-theoretical and empirical models (Beck, 1976; Sepaskhah and Boersma, 1979; Gangadhara Rao and Singh, 1999; Singh and Devid, 2000; Gori and Corasaniti, 2003). To experimentally measure λ, there are only two methods available: the steady-state method (i.e. guarded hot plate method) (Bristow et al., 1994b) and the transient-state

method (i.e. the heat pulse probe method and the active heated fibre optic-distributed temperature sensing (AHFO-DTS) method) (Sayde et al., 2010; Benítez-Buelga et al., 2014).

The guarded hot plate method has been well established for the measurement of λ of relatively large samples of concrete, insulation and other industrial materials (Bristow, 2002b). This method, however, employs steady-state principles and hence is subject to many conditions and uncertainties associated with soil water movement caused by temperature gradient during measurement. When the guarded hot plate method is used on wet soils, the water movement that occurs during the relative long heating time makes it difficult to reach a steady state (Dubois and Lebeau, 2013). In addition, the poor contact between the heater plates and soil samples can introduce substantial error (Dane and Topp, 2002).

The transient-state methods, on the other hand, employ a heat pulse probe which generates a pulse of heat at a given heating rate. The heat pulse probe includes the single-probe heat pulse (SPHP) method and the dual-probe heat pulse (DPHP) method (Bristow et al., 1994b; Liu and Si, 2011a). The SPHP can only be used to measure λ; however, the DPHP can measure λ, *C*, α, and θ simultaneously. In addition, based on the heat pulse probe theory, the AHFO-DTS system extends soil thermal property measuring scale from cm to up to kilometer scale (Striegl and Loheide, 2012). The heat pulse probe and AHFO-DTS methods will be discussed in detail in section **2.3**.

The *C* of soil can be obtained either by indirect or direct methods. The indirect methods include De Vries approximation, adiabatic calorimetry, drop calorimetry, and differential scanning calorimetry (DSC) (Dane and Topp, 2002). The De Vries approximation is widely used in practice and requires a known θ. Inversely, if *C* is measured by other methods, the De Vries

method can be used to calculate θ even in frozen soils containing ice (Liu and Si, 2011b; Kojima et al., 2014; Tian et al., 2015). The adiabatic calorimetry and drop calorimetry require a substantial amount of time, expertise, and specialized instrumentation to obtain reliable values of *C*; therefore, they are not introduced here and are rarely used in soil science. The DSC method has not been thoroughly evaluated for soil samples (Reading et al., 1994; Liu and Si, 2011a), and is a destructive method suitable only for small sample sizes. The only direct and in situ measurement of soil *C* is the DPHP (Campbell et al., 1991; Bristow et al., 1994a; Kluitenberg et al., 1995).

The α can be determined by observing soil temperature changes with time at two or more locations (Dane and Topp, 2002) or can be measured using the DPHP, by determining the time required for the maximum temperature rise of the temperature sensor to be reached (Bristow et al., 1994a; Kluitenberg et al., 1995; Bristow, 1998), or can be calculated from λ and *C*.

2.2 Soil Water Content

Water in the soil is an important resource for both human beings and natural ecosystems. It is a vital link in the hydrological cycle that influences most of the physical, chemical, and biological processes that occur in soils. Physically, soil water acts as a lubricant and a binding agent between soil particles (Dane and Topp, 2002). The high *C* value of water modifies the diurnal and seasonal temperature cycles at the soil surface. Changes in θ and its energy status affect soil strength, compressibility, penetrability and ρ_b (Huang et al., 2012). Soil water content information can be useful for evaluation of the water balance. Chemically, water serves as the transport agent of dissolved inorganic chemicals and suspended biological components, making them available to microbes and vegetation (Dane and Topp, 2002; Gardiner and Miller, 2004). The biological production from soil, either as forest products or agricultural crops, is influenced primarily by

water availability in soil (Foth, 1990). A limited number of plants can survive on water taken directly from the atmosphere, whereas most plants access water in the soil using their roots (Anderson and Hopmans, 2013; Alexander, 2014). Typical agricultural crops use an average of 500 to 700 kg of water to produce 1 kg of dry plant matter (Plaster and Reiley, 1992). Soil formation and weathering rate are also controlled by θ (Huang et al., 2012).

Soil water content is traditionally expressed as the ratio of the mass of water to the mass of dry solids in a soil sample, which is called the gravimetric water content. Alternatively, the volume of water present in a unit volume of soil is called the volumetric water content. Sometimes water content is expressed as the degree of saturation, which is the ratio of water-filled pore space to the total soil pore space (Huang et al., 2012). In meteorology and hydrology, θ and precipitation are expressed in terms of water depth (Plaster and Reiley, 1992).

In addition to θ, soil water status can also be expressed through the soil water energy state. The two primary forms of energy that are of interest are kinetic and potential. When soil water movement is very slow, the kinetic energy is negligible. The total soil water potential is composed of the matric potential, osmotic potential, pressure potential and gravitational potential (Gardiner and Miller, 2004). The relationship between θ and soil water potential is called the soil water retention curve, which is one of the most frequently used characterisations in soil physics and is used to predict the soil water storage, water supply to plants and soil aggregate stability. Nearly all soils show hysteresis in their soil water retention curves due to the ink bottle meniscus effect arising from the high surface tension of water, trapped air in soil, and the shrink-swell effect (Miyazaki et al., 1993).

When all soil pores are filled with water, the soil is said to be saturated and θ is referred to as the saturated water content. Once the excess gravitational water, or water that will freely flow under the force of gravity, has fully drained away from the soil over the course of several days, the water content is referred to as field capacity (Baver, 1956; Gardiner and Miller, 2004). The matric potential of soil usually ranges between -10 and -30 kPa at the field capacity (Brady and Weil, 2008). If the θ continue to decrease through evapotranspiration until it is so low that plants are not able to extract water fast enough for their growth, it is said to be at its permanent wilting point (Gardiner and Miller, 2004). For most plants the permanent wilting point develops when the soil water potential is about -1500 kPa (Brady and Weil, 2008). The determination of permanent wilting point and field capacity is frequently required to guide irrigation management and optimize plant production.

2.2.1 Soil water content measurement

The state of water in the soil is highly dynamic and the movement of water is affected by evapotranspiration, precipitation, irrigation, soil temperature and soil thermal properties (Ghildyal and Tripathi, 1987). The determination of θ is one of the most common soil physical analyses, and is necessary for many agricultural, hydrological, and engineering studies.

Soil water content can be measured directly or indirectly. The direct methods involve the removal or separation of water from the soil matrix by heating, the extraction and replacement of water by a solvent, or by chemical reaction (Dane and Topp, 2002). By heating, water is vaporised and removed from the soil and θ is determined by measuring the resulting change in mass. By extraction and replacement by solvent, θ is determined through chemical or physical analysis of the extracting solvent. By chemical reaction, θ is determined through quantitative measurement

of the reaction products (Dane and Topp, 2002). In practice, the removal of water by heating is referred to as the gravimetric method, which is the only direct θ measurement method commonly used in soil science. The indirect methods involve measurement of soil physical or chemical properties that rely on θ. For example, the dielectric constant, electrical conductivity (EC, S m^{-1}), *C*, hydrogen content, and magnetic susceptibility of the soil.

For gravimetric methods, soil samples are dried in various ways including incandescent heating at a controlled temperature to achieve a constant weight, microwave heating for a selected time period in order to achieve a constant weight, and vacuum distillation of water to reach a desired vapor pressure level (Dane and Topp, 2002; Huang et al., 2012). The advantages of the gravimetric method are that the principles are straightforward, it can be used in the laboratory, it is inexpensive, and is considered the standard method with random errors of < 1 % water content (Warrick, 2002). The gravimetric method is the only mass-based method for determining water content, whereas other methods measure the volume-based or volumetric water content.

However, the traditional heating gravimetric method is time-consuming, destructive to the soil, and may be subject to two additional sources of error. First, water is retained by the soil components at a wide range of energy levels, and even after several days of heating and drying the mass of soil may still be decreasing (Dane and Topp, 2002). Therefore, there is no standard on absolute time at which the soil reaches a "dry" state when exposed to the recommended temperature of 105 ˚C. Second, part of the mass loss may be due to evaporation of components other than soil water, such as organic matter (Dane and Topp, 2002). Additionally, due to the destructive nature to the soil, the gravimetric methods cannot be used as a series of in situ dynamic measurements (Huang et al., 2012).

The dielectric constant-based methods for determining θ include time domain reflectometry (TDR), capacitance probe, ground penetrating radar (GPR), radar scatterometry, and passive microwave (Baver, 1956; Dirksen, 1999; Carter and Gregorich, 2008). The TDR method utilizes a fast rise time electromagnetic pulse guided along a transmission line through a soil sample (Noborio, 2001). The time delay between the reflections of the pulse from the beginning and end of the soil transmission line is used to determine the velocity of propagation through the soil along the transmission line. The dielectric constant of the soil controls this velocity, and θ is inferred from the dependence of the dielectric constant on θ (Topp and Davis, 1985). The TDR method can be used for both laboratory and in situ field measurements. Another advantage of TDR is that it can be coupled with other equipments, such as the heat pulse probe (Noborio et al., 1996), tensiometer (Dane and Topp, 2002) and penetrometer (Manoel et al., 2001). The measurement of θ is typically only slightly susceptible to changes in soil ρ_b (for non-swelling soils) and temperature (Noborio, 2001). Limitations of TDR include relatively high equipment expense, large errors for saline soils, and soil-specific calibration required for soils with high levels of organic matter or clay (Warrick, 2002).

The capacitance devices, GPR, radar scatterometry and passive microwave are all the primarily used methods in field measurements. The advantage of the dielectric constant-based methods is that the EC of the soil can be obtained as well (Dane and Topp, 2002).Similar to TDR, capacitance devices also measure soil dielectric constant. With these devices; however, capacitance electrodes are placed in the soil which act as the dielectric of a capacitor in a capacitive-inductive resonant circuit (Dane and Topp, 2002). Capacitance devices are relatively cheap, safe, and easy to operate. However, the sensors require a soil-specific calibration, and the accuracy is affected by soil salinity and soil temperature (Kelleners et al., 2004). The GPR

generates radio frequency signals in a wide range of angles from an antenna into the ground, and another antenna receives the return signals (Galagedara et al., 2005). The intermediate measuring scale of GPR fills the measuring scale gap between large scale remote sensing and point scale measurements (Huisman et al., 2001, 2003). Similar to GPR, the radar scatterometry's transmitting and receiving antennae are located above the soil, allowing it to measure θ of the near-surface soils (Dane and Topp, 2002). Differing from the other methods, the passive microwave remote sensing technique applies no signal, and the soil itself is the electromagnetic source (Njoku and Entekhabi, 1996). A sensitive microwave receiver placed above the ground is used to measure the temperature and dielectric properties of the surface soil. This passive microwave remote sensing can use the ground, aircraft and orbiting satellites as platforms. The passive microwave method has relatively poor spatial resolution, so it is usually used to measure an average θ over a large area.

Another indirect method is electromagnetic induction, where the instrument employs low frequency signals and measures the signal loss to determine the EC of the soil. Soil water content can then be determined by the relationship between θ and EC (Reedy and Scanlon, 2003). Electromagnetic induction instruments are non-contacting, non-destructive, and rapid. As the measurements can be taken instantaneously, it is suitable for the rapid survey of a large area (Sheets and Hendrickx, 1995). The electromagnetic induction method is susceptible to salinity as it is based on EC.

Neutron scattering probes release a radioactive source of high energy fast neutrons, which interact with hydrogen atoms in the soil that slowing down the neutrons (Dirksen, 1999; Dane and Topp, 2002). As most of the hydrogen in soil is associated with water, the number of soil hydrogen can be used to infer the volumetric water content. The advantages of the neutron probe method

are that it is non-destructive, water can be measured in any phase and it may be performed repetitively (Huang et al., 2012). It also works well in stony soils and cracking clays in which other methods work poorly. However, the neutron probe can only be used in the field to measure θ at multiple depths if pre-installed tubes are present. Calibrations are required to account for background hydrogen sources and other local effects (Carter and Gregorich, 2008). In addition, it is radiative, costly, and unsuitable for surface soils (Huang et al., 2012). Operation of the neutron scattering probe requires the attendant to complete specialized training and possess a license (Warrick, 2002).

The cosmic-ray probe is another instrument to measure θ by counting fast neutrons in the soil, but produced by secondary cosmic ray particles (Zhu et al., 2015). It can measure the areal-average θ of an effective depth at an intermediate scale on the order of from cm to several hundred meters (Lv et al., 2014). The cosmic-ray probe is a low-power passive method that can continuously monitor θ in the field, and its self does not release radioactive source. It is non-invasive, non-contact, and insensitive to soil salinity, ρ_b, texture and surface roughness (Zreda et al., 2008). However, the measurement depth decreases as increasing θ (Zreda et al., 2012) and calibration is required as it is susceptible to aboveground biomass (Baatz et al., 2015).

The nuclear magnetic resonance technique can measure θ and water retention parameters in soils and rocks by counting the number of protons associated with water molecules in the soil (Costabel and Yaramanci, 2013). The nuclear magnetic resonance images can present us with the distribution of water and pores in soil (Bird et al., 2005), and can be used in laboratory or the field settings. However, it is destructive as it requires a soil sample be removed for measurement and it is radioactive.

The gamma ray attenuation device uses a radioactive source to emit a beam of gamma rays into a soil sample (Corey et al., 1971). The attenuation of the beam is recorded by a gamma ray detector after the beam has passed through a known length of soil (Pires et al., 2005). With known density of soil solids and water, the measured density can be used to determine θ. By using two radioactive sources in a single collimator, the gamma ray method can measure both ρ_b and θ simultaneously (Corey et al., 1971). It can also be used to measure soil particle size distribution (Oliveira et al., 1997). The gamma ray method has greater depth resolution than the neutron scattering method; however, it is radioactive, restricted to soil thicknesses, and affected by ρ_b changes (Dane and Topp, 2002).

The DPHP is another popular method to measure θ based on the linear relationship between *C* and θ (Bristow et al., 1993, 2001; Peron et al., 2012). Based on both the SPHP and DPHP methods, an AHFO-DTS system was developed to monitor in situ θ on an intermediate scale (Sayde et al., 2010; Ciocca et al., 2012; Striegl and Loheide, 2012). The details on the DPHP and AHFO-DTS methods will be discussed in section **2.3**.

In comparison, the gravimetric method is accurate, standard, and direct; however, it is destructive and time consuming. The indirect methods are less destructive or non-destructive; however, the accuracies and precisions of those methods depend upon the strength of the relationship between the measured property and θ.

2.3 Simultaneous Measuring Soil Thermal Properties and Water Content

Soil thermal properties and θ are interactive in the field (Hillel, 1998); therefore, in order to provide reliable data for coupled soil heat and water transport studies (Bristow, 1998), it is

important to develop a single instrument that can measure both soil thermal properties and θ at the same time, location, and scale. However, from the above discussions on different methods to measure soil thermal properties and θ, we can see that the DPHP and the AHFO-DTS are the only two methods that can measure λ, *C*, α, and θ simultaneously (Bristow, 1998; Ren et al., 1999; Olmanson and Ochsner, 2006; Young et al., 2008; Liu et al., 2012; Benítez-Buelga et al., 2014). Therefore, the heat pulse probe method and the AHFO-DTS method will be discussed in detail as follows.

2.3.1 Heat Pulse Probe Method

The heat pulse probe method was originally developed from a thermal based apparatus to measure λ of various of liquids (Van Der Held and Van Drunen, 1949). This non-stationary method was subsequently improved and designed as a heat probe element to measure λ of soil in situ (de Vries, 1952), which was based on the mathematical analysis of conduction of heat in solids presented by Carslaw and Jaeger (1946).

The SPHP has been firstly used to measure λ of different materials. However, due to the difficulties to obtain accurate thermal contact conductivity (*H*, W m^{-2} K^{-1}) values, obtaining accurate *C* and α values by the SPHP is still challenging (Hadas, 1974; Riha et al., 1980; van Loon et al., 1989). Therefore, in 1990s, the DPHP was developed to measure all three soil thermal properties and several other properties. If the probe has three or more needles, consisting of one or more heater needles and two or more sensor needles, it is called a multi probe (Larson, 1988; Saito et al., 2007; Xiao et al., 2012). A comparison of the properties that the SPHP, DPHP, and multi-probe heat pulse (MPHP) methods can measure is listed in Table 2.2. A picture of the heat pulse probe set-up is shown in Fig. A.7 in Appendix2.

Table 2.2. Typical applications of the heat pulse probe methods in different media.

Probe	Property	Unfrozen soil	Frozen soil	Peat	Rock	Snow
Single probe	Thermal conductivity	(de Vries, 1952)	(Penner, 1970)	/	(Woodside and Messmer, 1961b)	(Jaafar and Picot, 1970)
Dual probe	Thermal conductivity	(Bristow et al., 1994a)	(Ochsner and Baker, 2008)	(Kettridge and Baird, 2007)	/	/
	Volumetric heat capacity	(Campbell et al., 1991)	(Putkonen, 2003)	(Kettridge and Baird, 2007)	/	/
	Water content	(Bristow et al., 1993)	(Zhang et al., 2011)	(Campbell et al., 2002)	/	/
	Density	/	/	/	/	(Liu and Si, 2008)
	Ice content	/	(Liu and Si, 2011b)	/	/	/
Multi probe	Thermal conductivity	(Hopmans et al., 2002)	/	/	/	/
	Volumetric heat capacity	(Bristow et al., 2001)	/	/	/	/
	Water content	(Bristow et al., 2001)	/	/	/	/
	Water flux	(Ren et al., 2000)	/	/	/	/
	Evaporation	(Xiao et al., 2012)	/	/	/	/
	Electric conductivity	(Bristow et al., 2001)	/	/	/	/

† Contents in bracket are example references of the related studies.

2.3.1.1 Single-probe heat pulse method

Currently, the SPHP can only be used to determine λ of soil. In the SPHP method, both a heating wire and a thermistor (or thermocouple) are installed in the same needle, and the probe is inserted into soil. Then the probe is heated for a period of time by passing an electrical current through the heating wire, and the temperature in the centre of the probe is monitored during the heating or cooling. The simplest model to measure λ using the SPHP is to treat the single probe as a linear heat source of infinite length. Therefore, the diameter, λ and *c* of the probe are ignored, and the contact between probe and soil is assumed to be perfect (de Vries, 1952). With this

simplification, an analytical solution to the radial heat flow equation can be used to obtain λ from the slope of the temperature increase as a function of logarithmic time curve when the curve reaches a straight line at a later time.

For more realistic results and to obtain α and *C*, the model was modified by a cylindrical configuration, and the probe diameter (only outer diameter, or both inner and outer diameter), *H*, the specific heat of the probe, and λ of probe (perfect conductor or poor conductor) were all considered (Blackwell, 1954). However, the solutions of the Blackwell equations involve the Laplace transformation, and complicated integrals need to be calculated numerically. To simplify the calculations, Blackwell (1954) devised the simple approximations for both short-time and long-time periods. The long-time solution is used to determine λ (Manohar et al., 2000).

Since the long-time solution of Blackwell equation is simple and accurate, the SPHP has been widely tested for λ measurement of different materials, such as unfrozen soils (de Vries, 1952; de Vries and Peck, 1958a; b; Penner et al., 1975; Dang and Leong, 2015), frozen soils (Penner, 1970; Slusarchuk and Watson, 1975), rocks (Woodside and Messmer, 1961b; Beck et al., 1971; Cull, 1974; Beck, 1976), snow (Jaafar and Picot, 1970; Sturm and Johnson, 1992), glass beads (Hopmans and Dane, 1986), and methane hydrate (Waite et al., 2006, 2007).

The λ of different soil textures at various θ and temperatures with different densities calculated by different models have been widely investigated (Sepaskhah and Boersma, 1979; Riha et al., 1980; Hopmans and Dane, 1986; Ewen and Thomas, 1987; Hiraiwa and Kasubuchi, 2000; Tarnawski et al., 2009, 2011, 2013; Tarnawski and Leong, 2012; Nikolaev et al., 2013). The results show that soil λ increases with higher θ (Sepaskhah and Boersma, 1979). Coarser soil texture has higher λ with the same θ (Riha et al., 1980). When soil temperature increases, the λ

tends to increase (Hiraiwa and Kasubuchi, 2000; Nikolaev et al., 2013). The effects of salt concentration and organic matter on soil λ were also tested (Abu-Hamdeh and Reeder, 2000). If θ is known, two other thermal properties (α and *C*) can also be calculated (Nakshabandi and Kohnke, 1965; Wierenga et al., 1969; Moench and Evans, 1970; Ghuman and Lal, 1985). However, without θ, SPHP cannot obtain α and *C* independently.

The accuracies and errors associated with the SPHP have been investigated. To ensure the assumption of an infinite long probe, the calculation to determine the minimum length/diameter ratio for radial flow theory to meet different error requirement has been provided (Blackwell, 1954, 1956). The experimental results of soil λ measurement proved that the calculation to account for the finite λ of the probe provided more realistic results (de Vries and Peck, 1958a). To ensure all temperature changes are caused by the heat pulse probe, the background temperature should be corrected before and during measurement to reduce measuring errors (Jury and Bellantuoni, 1976).

When soil temperature is above 0 ˚C, soil thermal properties are more dependent on soil texture, ρ_b, and θ, and less dependent on temperature (Abu-Hamdeh and Reeder, 2000; Hiraiwa and Kasubuchi, 2000; Abu-Hamdeh et al., 2001). However, when soil temperature is below 0 ˚C, ice begin to form in soil. Therefore, a constant λ cannot be assumed. As ice has a λ four times greater than that of water, λ of frozen soils increases when soil temperature decreases and ice content increases (Penner, 1970). The amount of water in frozen soils varies at the same temperature depending on specific surface area, mineral type, exchangeable ions, soluble salt content of the pore water, and pore size distribution (Penner, 1970; Slusarchuk and Watson, 1975). When soil temperature is around -2 to 0 ˚C, the ice content is very sensitive to the temperature. The heating from the heat pulse probe will cause latent heat flow and phase change of the ice. Therefore, accurate measurement of λ in soil at -2 to 0 ˚C by the heat pulse probe is impractical.

When the temperature of the sample is carefully controlled to a sufficiently low temperature, the SPHP method can be applied to measure λ of snow (Jaafar and Picot, 1970).

The SPHP method has been applied to rocks which are far denser than soil. Compared to field soils, measuring rocks through boreholes is more challenging due to the difficulty in drilling the holes with the same small diameter as the probe (Cull, 1974). Therefore, the probe-rock contact resistance is relative large. However, the accuracy of the λ measurement is less affected by *H*, and λ of coarse granular media such as pebble beds can also be accurately obtained (Jones, 1988a).

The SPHP has been used to measure λ (Blackwell, 1954; de Vries and Peck, 1958b); however, measuring θ using a single probe and the relationship between temperature change or λ and θ has not been widely investigated. Shaw and Baver (1939) applied a Wheatstone bridge to an eletrothermal method in order to measure the electrical current (*I*, A) changes of their setup with changing θ in various soils. The *I*~θ relationship was developed for the tested soil; however, the prediction of θ from this relationship was not performed. The λ of different soils at various θ has been widely tested (Sepaskhah and Boersma, 1979; Horton and Wierenga, 1984; Hopmans and Dane, 1986; Abu-Hamdeh and Reeder, 2000; Momose and Kasubuchi, 2002), and attempts to develop the expressions of the λ~θ relationship have been reported (Ewing and Horton, 2007). Among them, Kasubuchi (1992) attempted to measure θ using the λ~θ relationship obtained from the heat pulse method; however, the accuracy was not reported and the results were limited to two soils within a limited range of θ.

To obtain more information besides the λ as determined from the long-time solution of Blackwell equation, the short-time solution of Blackwell equation may be used to determine *H* hence α, *C*, and θ. Following the Blackwell solutions, Jaeger (1956) and de Vries and Peck (1958a;

b) derived two additional solutions to the cylindrical heat pulse probe method, respectively. However, due to the complicated expressions and difficulty in obtaining accurate *H*, it is difficult to measure other properties such as α, *C*, or θ. Obtaining λ, *H*, and *C* simultaneously without previously knowing θ has been attempted, but produced unsatisfactory accuracies of about 5, 10, and 25 %, respectively (van Loon et al., 1989). The short-time solution was used to obtain *H* of methane hydrate (Waite et al., 2006, 2007), but showed large uncertainty due to the arbitrary time range selection of the data points to fit the short-time solution.

Thermal resistance (the reciprocal of λ) is the resistance effect caused by the finite heat transport in a material; similarly, thermal contact resistance is an additional heat transfer resistance due to the incomplete contact area across the interface between two media. Thermal contact resistance presents when a junction is formed by pressing two similar or dissimilar metallic materials together, only a small fraction of the nominal surface area is actually in contact because of the non-flatness and roughness of the contacting surfaces (Cooper et al., 1969; Sauer et al., 2007). While a uniform temperature gradient may exist in a homogeneous material, the boundary of two materials creates a temperature difference (Fletcher, 1988) as shown in Fig.2.3. The reciprocal of thermal contact resistance, *H*, is more commonly used in practice. The definition of *H* is given by (Wang et al., 2012)

$$H = -q/\Delta T \qquad \text{(Eq. 2.20)}$$

where q is the heat flux density and ΔT is the temperature drop at the interface. Note that the definition and unit between *H* and λ are different.

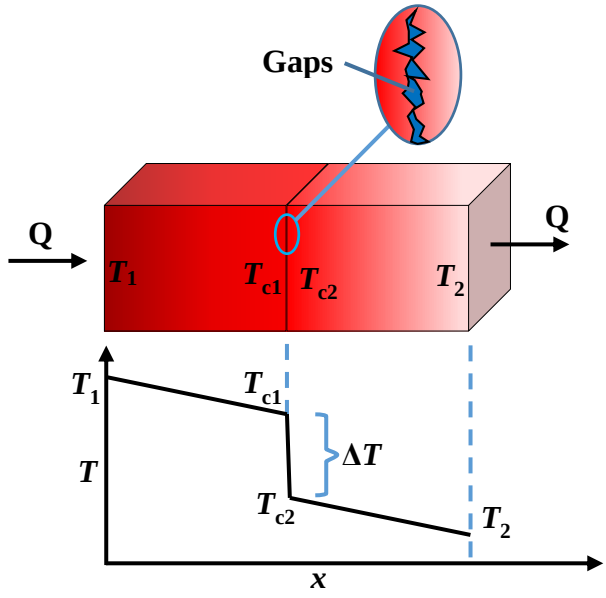

Fig. 2.3. The temperature distribution at the interface between two materials due to imperfect contact.

The definition of *H* is simple; however, it has not been possible to develop a single analytical expression for the prediction of *H* at a junction between two materials, except for cases of highly idealized single and multiple contacts (Jeng et al., 2006). Despite the availability of these models, *H* is largely determined experimentally in order to provide a measure of the thermal performance of a specific configuration or system.

Currently, the values of *H* between the single probe and different soils at various θ have not been investigated. Assuming perfect contact between the probe and the soil is not realistic, so the influence of the contact resistance between probe and soil was evaluated (Hadas, 1974). The results showed that large errors occur in poor contact situations particularly at higher θ. Compared to the dual probe, the single probe needle is more robust in the field, measures larger scales, and is not affected by needle deflection. Therefore, it is important to understand how θ, soil properties and the probe affect *H* to facilitate the application of the SPHP and also the SPHP based AHFO-DTS method in simultaneous determination of soil thermal property and θ.

2.3.1.2 Dual-probe heat pulse method

To break through the limitations of the SPHP, the DPHP was developed to measure all three soil thermal properties (Campbell et al., 1991; Bristow et al., 1994b; Liu and Si, 2011a). The dual probe has two needles, one containing the heating wire and the other the temperature sensor. An instantaneous heat pulse is applied into a line source (the heater), and the maximum temperature rise of another needle (the sensor) at a certain distance from the heater is inversely related to the volumetric specific heat of soil (Bristow et al., 1994a). The time for the sensor to reach maximum temperature is inversely related to α of soil, and the value of the maximum temperature is inversely related to C of soil. As long as C and α are known, λ can be calculated by $\lambda=C/\alpha$. Therefore, all of the three soil properties can be obtained by the DPHP (Bristow et al., 1994a, 1995).In addition, θ can also be determined by the linear relationship between C and θ (Bristow et al., 1993; Tarara and Ham, 1997; Bristow, 1998; Song and Ham, 1998; Song et al., 1999; Basinger et al., 2003; Heitman et al., 2003; Ochsner et al., 2003; Ren et al., 2003b).

The dual heat pulse probe was originally used to measure C of soil by an instantaneous line source of infinite length model (Campbell et al., 1991). Bristow et al. (1993) applied the DPHP in the field to estimate θ from C, showed well agreement between the DPHP measured θ with that from the standard oven-dry method.

The possible errors associated with the DPHP were discussed by comparing models for the instantaneous infinite line source with pulsed infinite line source, pulsed finite line source and pulsed infinite cylindrical source, and accounting for different probe and heat pulse apparatus designs as well as errors in probe spacing and heat input (Kluitenberg et al., 1993). Additional error analysis (Kluitenberg et al., 1995) showed that soil α and C estimates are sensitive to the

error in probe spacing, but λ is unaffected by it. The errors and solutions when the dual probe is used in a heterogeneous situation (for example, surface soil at the soil-air interface) was also investigated (Kluitenberg and Philip, 1999; Philip and Kluitenberg, 1999).

The temperature versus time data obtained using dual heat pulse probe can be analyzed using two different approaches: 1) the single-point method and 2) nonlinear fitting (Knight and Kluitenberg, 2004). The single-point method is based on accurate identification of the peak in the temperature curve, which is difficult when the data is sparse and contains noise. Currently, the nonlinear fitting is more commonly used. Bristow et al. (1995) compared these two methods and concluded that both methods should be checked by comparing the fitted model with the measured temperature-time data.

To obtain more accurate estimates, several studies were conducted on the corrections and calibrations (Ren et al., 2003b; Ham and Benson, 2004; Olmanson and Ochsner, 2006; Liu et al., 2008a; Young et al., 2008; Kluitenberg et al., 2010), sensitivity analysis (Knight et al., 2007) and errors analysis (Liu et al., 2007, 2012; Liu and Si, 2010; Knight et al., 2012) of the DPHP. Even though all three thermal properties can be obtained from the DPHP without knowing H, ignoring H and finite probe body contributes to the overestimation of C from the infinite line source model (Basinger et al., 2003; Liu et al., 2012).

The DPHP is an inexpensive, automatic, non-destructive, and non-radioactive method for θ measurement. However, it also requires calibration in the field (Ren et al., 2003b; Ham and Benson, 2004), and the biggest limitation of the DPHP is that the accuracy is greatly affected by needle deflections (Liu et al., 2008a; Kluitenberg et al., 2010) when it is inserted into soils, especially hard and clay soils. To overcome this drawback, a self-calibrated dual probe with two

thermistors in the sensor needle was designed to quantitatively correct the inward and outward deflections, reducing measurement errors (Liu et al., 2013a). The prevalent use of the DPHP with infinite line source model assumes the probe is embedded in an infinite soil, which is invalid at the soil surface. Therefore, the adiabatic boundary condition solutions were built for the situation that the probe is inserted into soil near the soil-air interface (Liu et al., 2013b; Zhang et al., 2014).

The DPHP works better than the guarded hot plate method in frozen soils. For the guarded hot plate method, a relatively large temperature difference and a longer measurement time are necessary. Therefore, water movement and evaporation at the hot side and condensation at the cold side can introduce large errors (Carter and Gregorich, 2008). However, the DPHP uses much smaller measuring time and the temperature increase can be controlled smaller, thus the errors caused by ice melting are relatively small.

When the soil temperature is below -10 ˚C, the DPHP performs well. However, at the range of -10 to 0 ˚C, the phase change of ice into water and back to ice causes large measurement uncertainty (Putkonen, 2003). The DPHP measurement with a 60 s heat pulse duration and heating rate < 15 W m^{-1} were successfully applied on ice and various kinds of snow for snow density measurement when the temperature was below 0 ˚C and there was no water in the snow (Liu and Si, 2008). The ice content measurement of a frozen soil by the DPHP is possible when the soil temperature is below -18 ˚C and the majority of water is ice; however, it still overestimates ice content with the appearance of water in the soil (Liu and Si, 2011b). An alternative way to determine the ice content is to use the empirical relation of the soil-specific ice to unfrozen water ratio at different temperatures and measure total water content by the DPHP (Zhang et al., 2011), or by the sensible heat balance method (Kojima et al., 2014). However, the sensible heat balance method showed large errors in field tests.

2.3.1.3 Multi-probe heat pulse method

For soil thermal property measurement, the principle of the MPHP is the same as the DPHP, but with more replicates of temperature readings from each thermistor. The advantage of the MPHP compared to the DPHP is that, since it has two or more sensor needles, it can be used to measure soil water flux (Ren et al., 2000; Hopmans et al., 2002), soil heat flux (Cobos and Baker, 2003), soil water evaporation (Trautz et al., 2014), and EC (Bristow et al., 2001; Mori et al., 2003) based on the different temperature responses between sensors.

The three-needle design heat pulse probe was widely studied to estimate water flux density from the temperature response differences of two sensors placed upstream and downstream of the heat source (Ren et al., 2000; Kluitenberg and Warrick, 2001; Wang et al., 2002; Hopmans et al., 2002; Ochsner et al., 2005). For a four-needle heat pulse probe, an equivalent four-electrode Wenner array can be used to obtain soil apparent EC (Bristow et al., 2001; Mori et al., 2003). Combining the MPHP and TDR (Ren et al., 2003a) is especially useful for studying the coupled flow of heat, water, and solute in the vadose zone. With known θ from the TDR measurement, the thermo-TDR can also be used to measure soil ρ_b (Liu et al., 2014). Wang et al. (2002) and Kluitenberg et al. (2007) simplified and improved the mathematically complex data analysis procedures. Xiao et al. (2012) made an 11-needle heat pulse probe to provide an improved way to monitor in situ the depth and time pattern of subsurface soil-water evaporation at fine-scales.

The MPHP has the same limitations as the DPHP, and more deflections will occur as it is more difficult to install it in the field as a result of more needles. Besides, when soil water flux is too small, it is also difficult to obtain accurate measurement (Wang et al., 2002; Ochsner et al., 2005).

Beside the typical commonly used single probe, dual probe and multi probes, there are several other special probe designs. A DPHP-TDR probe was designed to combine the DPHP for soil thermal property measurement and TDR for θ measurement (Baker and Goodrich, 1987; Noborio et al., 1996), and it can be used to measure all three soil thermal properties, as well as θ, ρ_b, EC, and salt concentration simultaneously (Ren et al., 1999, 2003a; Bristow et al., 2001; Mori et al., 2003; Lu et al., 2013; Liu et al., 2014).

A multi-functional probe with one heater and four sensors, combined with four aluminium ring electrodes working as the Wenner array were designed to measure soil thermal properties, θ, and EC at small scales simultaneously (Valente et al., 2006). A five-needle multi-probe with one heater, two long sensors and two short sensors was built to numerically evaluate the probe sensitivity to smaller water fluxes (Saito et al., 2007). Within each sensor needle of the five-needle multi-probe there are three or four thermistors placed at different locations.

A ring shape heat pulse probe was developed to measure λ of rocks, allowing a smaller sampling size and shorter heating time (Somerton and Mossahebi, 1967). Following Somerton and Mossahebi, a similar button heat pulse probe without needles was made and tested for θ measurement (Kamai et al., 2009).

As the accuracy of the dual probe is affected by needle deflections, a partial cylindrical thermo-TDR sensor was designed to make the sensors stronger to reduce the needle deflections (Olmanson and Ochsner, 2008). Kasubuchi (1977) designed a twin cylindrical probe to measure λ of soil, consisting of the same two single probes. One of the single probe measures the reference material with known λ and another probe measures the soil. Changes in the temperature of two

probes are drawn, and the tangent of the line is the ratio of the λ between the two materials. The advantage of the twin cylindrical probe is that calibration is eliminated.

2.3.2 Active heated fibre optic-distributed temperature sensing system

The fibre optic-DTS system was first developed for fire monitoring, pipeline monitoring, and other industrial applications in the 1980s (Tyler et al., 2009). It is a relatively new technique in hydrology to measure and monitor temperatures of ground surface (Freifeld et al., 2008), snowpack base (Tyler et al., 2008), lake bottom, mine shaft, and stream (Selker et al., 2006b) and was introduced in soil science recently to measure soil temperature, soil thermal properties and θ (Weiss, 2003).

The DTS system sends a pulsed laser into the fibre optic cable, and parts of the laser pulse are reflected back along the cable with either an original, longer or shorter wavelength. The reflections with shorter or longer wavelengths are called Anti-Stokes backscatter or Stokes backscatter, respectively (Selker et al., 2006b; a; Sayde et al., 2010). Since the amplitude of the Anti-Stokes backscatter is sensitive to temperature, the Stokes/Anti-Stokes ratio can be used to calculate soil temperature (Weiss, 2003; Selker et al., 2006b; a). By reading the return time of the laser, it is possible to determine the distance from where the light was reflected. Therefore, the temperature along the entire length of the fibre optic cable can be obtained.

As the fibre optic-DTS system provides soil temperature measurements at much higher spatial and temporal frequencies than any previous measurement method (Tyler et al., 2009), it is possible to use the temperature change information and the fact that soil water influences soil thermal properties (Steele-Dunne et al., 2010) to estimate θ along the entire length of fibre optic cable. As it does not require an external heat source, this method is considered a passive fibre optic-DTS

method (Steele-Dunne et al., 2010). However, its application is limited when there are insufficient diurnal temperature changes, and calibrations are required as a result of the uncertainty and non-uniqueness of the $\lambda(\theta)$ relationship.

By contrast, the AHFO-DTS method was developed to detect soil water intrusions into a landfill cap in order to prevent underground water contamination (Weiss, 2003). This method utilizes knowledge of the soil thermal response as a function of θ. In the AHFO-DTS method, a metal sheath armoring the fibre optic cable serves as an electrical heater to actively heat the surrounding soils, while the resulting temperature changes are measured by the fibre optic cable within the sheath and recorded by the DTS system (Ciocca et al., 2012). The SPHP based AHFO-DTS method of analyses can be used to determine λ (Freifeld et al., 2008). Soil water content can then be inferred using the relationships between θ and λ (Ciocca et al., 2012), the maximum temperature increase (T_{max}, K) (Striegl and Loheide, 2012), or the cumulative temperature increase (T_{cum}, K s) (Sayde et al., 2010, 2014).

By installing two or more fibre optic cables paralleling each other, C was measured by the AHFO-DTS based on the DPHP principles, and then θ was obtained by the linear relationship between C and θ (Benítez-Buelga et al., 2014). However, the DPHP based AHFO-DTS requires two or more cables buried in the soil parallel each other which is difficult to control in practice (Striegl and Loheide, 2012; Benítez-Buelga et al., 2014; Sayde et al., 2014)

The AHFO-DTS system has been widely tested in the laboratory and field (Sayde et al., 2010, 2014; Ciocca et al., 2012; Striegl and Loheide, 2012), and the advantages of the AHFO-DTS system are obvious: 1) it extends the measurement scale from the traditional point scale to an intermediate scale of up to 30 km along the fibre optic cable (Selker et al., 2006b), 2) it has a

temperature resolution of 0.01 ˚C, spatial resolution of 20 cm, and temporal resolution of 1s (Selker et al., 2006a), 3) it can be applied in many situations, such as soils, lake bottoms, mine shafts, air-snow interfaces, air-water interfaces, and streams (Selker et al., 2006b), 4) it can be used to measure several soil properties and hydrological processes, such as soil temperature and its gradients in time and space, soil thermal properties, θ, soil energy balance, groundwater inflow, soil water movement and wetting bulbs (Selker et al., 2006b; Striegl and Loheide, 2012; Gil-Rodríguez et al., 2013; Read et al., 2014; Sayde et al., 2014), and 5) it can be automated and are user-friendly.

Currently, the AHFO-DTS method also has several limitations:

1) The SPHP based AHFO-DTS method can obtain λ and θ, but not C or α. Moreover, θ is derived from the relationship between λ (or T_{max}, T_{cum}) and θ, which are soil specific relationships that require soil specific calibrations (Steele-Dunne et al., 2010; Sayde et al., 2010; Ciocca et al., 2012).

2) The DPHP based AHFO-DTS method can measure both C and θ, but soil ρ_b and the specific heat capacity of solids are required for calibration (Benítez-Buelga et al., 2014).

3) For the SPHP based AHFO-DTS method, the measurement errors are relatively large at the middle and high range of θ (Ciocca et al., 2012; Striegl and Loheide, 2012). For the DPHP based AHFO-DTS method, the accuracies need to be improved, especially at the lower range of θ (Benítez-Buelga et al., 2014).

4) The accuracy of the AHFO-DTS system is affected by many factors, including the fibre optic cable design, signal size, instrument configuration, the cable-to-DTS connection quality, and

the operator's skill (Tyler et al., 2009; Rose et al., 2013; Krause et al., 2014; Suárez, 2014). Calibrations accounting for signal attenuation and temperature offset are also required in order to obtain accurate temperature readings.

2.4 Oil Sands Mature Fine Tailing

With an estimated reserve of 1.7 trillion barrels (Allen, 2008; Han et al., 2009), northern Alberta, Canada has the largest oil sands reserves in the world (Garven, 1989; Madill et al., 2001). Currently, more than 1.3 million barrels are extracted daily, and the production is expected to reach 3 million barrels per day by 2018 with new projects added annually (Chen et al., 2013).

Following the surface mining, bitumen is separated from the oil sands ore by a warm water based extraction process, resulting in tailings that is a slurry mixture of about 70% waste water, 30% solids, and some non-recovered bitumen (Herman et al., 1994; Chen et al., 2013). The tailings mixture is called fluid fine tailing (FFT) and is conventionally deposited hydraulically in on-site tailing ponds (Penner and Foght, 2010). Once FFT have undergone some degree of consolidation and the sand settles down to the bottom of the pond, they are referred to as mature fine tailings (MFT). The MFT take around 100 years to dewater from the fluid state without any further intervention (Chalaturnyk et al., 2002; Farkish and Fall, 2013). The Canadian oil sands industry generates approximately 2500 m^3 of MFT per 1000 m^3 of synthetic crude oil daily, and around 7.5×10^8 m^3 of MFT has accumulated in tailing ponds in the Alberta oil sands region (Luna Wolter and Naeth, 2014). Therefore, managing large volumes of MFT for reclamation has remained a challenge for the oil sands industry since oil sands mining began four decades ago (Dobchuk et al., 2013).

2.4.1 Monitoring oil sands mature fine tailing consolidation

The management of mature fine tailing (MFT) deposits is a critical element of both mine operations and future mine closure plans. The oil sand industry uses a wide variety of physical and chemical methods in an attempt to accelerate the solidification process for re-vegetation (Chalaturnyk et al., 2002; Proskin et al., 2010; Dobchuk et al., 2013; Farkish and Fall, 2014), but a technique to characterize the spatial and temporal distribution of MFT dewatering in tailings ponds is critically needed (Dobchuk et al., 2013).

A direct indicator of solidification success is an increase in ρ_b of the MFT. The most commonly used methods to measure soil ρ_b are: the core method, the clod method, the excavation method and the gamma ray attenuation method (Dane and Topp, 2002). The core, clod, and excavation methods are destructive, not repeatable, and cannot be automated. The gamma ray attenuation method is nondestructive to MFT, has sufficient depth resolution, and enables measurements in transient systems with considerable precision. However, the gamma ray attenuation instrument is radioactive, heavy, and cannot be automated. There is also a restriction on the use of radioactive sources by the Canadian government. Soil water content θ can be used to monitor the consolidation process of MFT; however, none of available methods can be used for long-term automated measurement on multiple locations and depths in the tailing ponds, because of the salinity. Therefore, a nonradioactive, continuous, and automated method is needed to monitor the MFT solidification process.

Ochsner et al (2001b) and Liu et al (2008b) used the combined heat pulse probe-TDR technique to determine ρ_b of soil, displaying the potential of the DPHP as an automatic and nonradioactive method to monitor in situ soil ρ_b. In their methods, the probe served as both the

dual heat pulse probe and TDR probe. The *C* of MFT was obtained from the heat pulse probe measurement and θ was obtained from the TDR measurement, and ρ_b was then obtained from:

$$\theta_{sa} = (C - \rho_b c_s)/(c_w \rho_w) \quad \text{(Eq. 2.20)}$$

Where θ_{sa} is the saturated water content ($m^3\ m^{-3}$); c_s and c_w are the specific heat capacity of MFT solids and water, respectively ($J\ kg^{-1}\ K^{-1}$); and ρ_w is the density of water ($kg\ m^{-3}$).

However, there are no studies describing the use of an independent DPHP to measure ρ_b of MFT. The DPHP also has not been tested in a suspension system like the MFT (Fig. 2.4), which is very different from the normal field soils.

Fig. 2.4. Photo of an oil sands mature fine tailing sample

3 MEASURING SOLID PERCENTAGE OF OIL SANDS MATURE FINE TAILINGS USING THE DUAL-PROBE HEAT PULSE METHOD[1]

3.1 Preface

The dual-probe heat pulse (DPHP) method has been widely used for the thermal properties and water content measurement of soils and rocks. However, the performance in the saturated media such as oil sands mature fine tailing (MFT) is unknown. The MFT is quite different from natural field soils, in which solid particles dispersed in water. To the best of our knowledge, there are no studies describing the use of an individual heat pulse probe method to measure the bulk density (or solid percentage) of a medium (soil or MFT), without additional water content measurement in the medium. In this chapter, the feasibility of the DPHP method for MFT's solid percentage measurement was examined.

[1] This chapter has been published previously in Li, M., S. L. Barbour, and B. C. Si. 2015. Measuring solid percentage of oil sands mature fine tailings using the dual probe heat pulse method. Journal of Environmental Quality. 44(1): 293-298. doi: 10.2134/jeq2014.06.0262. The published paper was also invited to publish a summary in Li, M., S. L. Barbour, and B. C. Si. 2015. Consolidation of oil sands mature fine tailings using the heat pulse probe. CSA News Magazine. 60: 15-15. doi:10.2134/csa2015-60-2-6. The co-author contributions to this manuscript were greatly appreciated and consisted of: S.L. Barbour (provided methodological guidance and manuscript editing) and B. C. Si (provided financial assistance, methodological guidance, laboratory work support, and manuscript editing). Minor modifications have been made for consistency.

3.2 Abstract

The reclamation of mature fine tailings (MFT) is a critical challenge for the oil sands industry in Western Canada, and a nonradioactive, automated and inexpensive method to monitor the MFT solidification is needed. The objective of this paper is to evaluate the feasibility of a dual-probe heat pulse (DPHP) method to measure MFT solid percentage. Three MFT samples, each at various solid percentages, were measured by the DPHP method. A linear relationship $y = 0.9495x + 0.0558$ was established between the DPHP measured solid percentage (y) and that of oven-drying method (x). Additional six MFT samples were collected and measured to validate the DPHP method. The specific heats of the six MFT solids were measured independently using a modulated differential scanning calorimetry (MDSC) method, and the sensitivity of DPHP measured MFT solid percentage to the specific heat of MFT solids was evaluated. The result shows that the DPHP method can be used to accurately measure MFT solid percentages, and the accuracy can be further improved if the specific heat of the MFT solids is measured independently.

3.3 Introduction

Canada has the largest oil sands reserves in the world (Rowland et al., 2009; Penner and Foght, 2010). The extraction of bitumen from mined oil sands generates a large volume of fluid fine tailings (FFT) - a high water content mixture of water, sand, fines (silt and clay < 50 μm in diameter), and residual hydrocarbons. The standard industry practice to deal with the byproducts is to hydraulically place these tailings into large surface impoundments or in mined out pits. Following an initial stage of sedimentation and self-weight consolidation, the larger particles settle to the bottom leaving a thick slurry layer known as mature fine tailing (MFT), which is comprised of about 70 % water and 30 % solids. Without any further intervention, MFT could take hundreds

of years to consolidate sufficiently to act as a weight bearing soil (Chalaturnyk et al., 2002; Farkish and Fall, 2013). As a consequence, managing these large volumes of mine tailings has been a challenge for the oil sands industry since oil sands mining began four decades ago (Renault, 2003; Dobchuk et al., 2013).

The industry is utilizing a wide variety of methods in an attempt to accelerate the consolidation process (Redfield et al., 2003; Farkish and Fall, 2013). A direct measure of the consolidation success is the dry bulk density (ρ_b, kg m^{-3}), which is the dry solid mass (m_{solid}, kg) in a unit volume of MFT. An alternative measurement often used by industry is the solid percentage (m_{solid} in a unit mass of MFT). The standard method for measuring ρ_b is the Gamma ray attenuation method (Costa et al., 2013). This non-destructive method has a good depth resolution and enables measurements in transient systems with considerable precision (Dane and Topp, 2002). However, Gamma ray equipment is heavy, radioactive, and non-automatic. It is also time-consuming to measure the ρ_b of MFT at different sites and depths. Soil water content (θ, m^3 m^{-3}) is another indication to monitor the consolidation process of MFT; however, none of available methods can be used for long-term automated measurement on multiple locations and depths in the tailing ponds. Therefore, an alternative automated, inexpensive and clean method to evaluate the MFT consolidation is of value.

The heat pulse probe method has been widely used in soil science to determine soil thermal properties (Bristow et al., 1994b; Abu-Hamdeh, 2001). It is nonradioactive, light, and compact and easily automated. The single-probe heat pulse (SPHP) method can be used to determine soil thermal conductivity (λ, W m^{-1} K^{-1}) (de Vries, 1952; Tarnawski et al., 2009) whereas a DPHP method has been used to measure λ (Kluitenberg et al., 2010), thermal diffusivity(α, m^2 s^{-1}) (Liu et al., 2013a), and volumetric heat capacity (C, J m^{-3} K^{-1}) (Campbell et al., 1991). The C of soil is

a function of ρ_b and θ. If ρ_b is known, the DPHP method can be used to measure θ (Bristow et al., 1993) from *C*. Inversely, Ochsner et al. (2001b) and Liu et al. (2008b) tried to measure ρ_b using a DPHP-time domain reflectometry (DPHP-TDR) combined technique, by measuring *C* from the DPHP method and volumetric θ from the TDR. However, due to the high salinity of MFT, it is not possible to measure θ of MFT using TDR. Therefore, a simple nonradioactive method is needed for measuring solid percentage of MFT. To the best of our knowledge, there are no studies describing the use of an individual heat pulse probe method to measure ρ_b (or solid percentage) of a medium (soil or MFT), without additional θ measurement in the medium.

The objective of this study was to evaluate the potential use of the DPHP method to measure the solid percentage of MFT. There are three important differences between natural field soils and oil sands MFT, which have to be addressed in undertaking this evaluation. Firstly, the ρ_b of soil in the natural sites usually keeps constant over long time periods. As a result, there is small temporal variability. However, both ρ_b and θ of MFT keep changing considerably during consolidation and a better measurement method is needed as mentioned above. In addition, MFT is always a suspension with different water content in a sense that solid particles suspend in liquid, while soil is a porous medium with water filled in the pore space between solid particles. Little is known about the performance of heat pulse probe method in these media. Finally, the volume of water is temperature dependent; because of the diurnal and seasonal changes of temperature of MFT, the solid percentage is more accurate and convenient in practice compared to ρ_b, as the volume measurement is avoided.

3.4 Materials and Methods

3.4.1 Dual-probe heat pulse theory

A dual probe can be used to estimate soil thermal properties by releasing a short pulse of heat and measuring the concomitant temperature response of the soil to the heat pulse (Liu and Si, 2008). A typical DPHP has two needles: a heater needle to provide the heat pulse and a sensor needle to measure the temperature response of the soil. The temperature change (ΔT, K) at a radial distance of r (m) from an infinite line heat source due to a heat pulse duration t_0 (s) in an infinite soil can be expressed (Kluitenberg et al., 1993) as

$$\Delta T(r,t)=\begin{cases} \dfrac{-q}{4\pi\alpha C}Ei[\dfrac{-r^2}{4\alpha t}] & 0<t\le t_0 \\ \dfrac{q}{4\pi\alpha C}\{Ei[\dfrac{-r^2}{4\alpha(t-t_0)}]-Ei[\dfrac{-r^2}{4\alpha t}]\} & t>t_0 \end{cases} \quad \text{(Eq. 3.1)}$$

where t is time (s), q is the rate of heat liberated (W m^{-1}), α and C are the thermal diffusivity (m^2 s^{-1}) and volumetric heat capacity (J m^{-3} K^{-1}) of soil, respectively; and $Ei(-x)$ is the exponential integral.

The single-point method and the non-linear fitting method are two methods that are used to calculate the thermal properties using the pulsed infinite line source DPHP method. The comparison of these two methods was conducted by Bristow et al. (1995). Equation 3.1 produces identifiable and unique C and α value from the maximum-temperature single-point method (Kluitenberg et al., 1993; Bristow et al., 1994b). As the noise or error of the single-point can produce large errors in the calculated C and α (Bristow et al., 1995), the nonlinear least squares fitting of Eq. 3.1 to experimental data points in this study was used to obtain a set of C and α value

for each sample. The thermal conductivity (W m^{-1} ˚C^{-1}) of soil can be obtained by $\lambda = C \times \alpha$. Mathcad15.0 (PTC Inc., Needham, MA) software was used for the curve fittings and calculations, and the "minimize" function with the conjugate gradient algorithm was used for the nonlinear curve fitting.

The saturated volumetric water content (θ_{sa}, m^3 m^{-3}) of MFT is a function of its *C* (Bristow et al., 1993) as follows

$$\theta_{sa} = (C - \rho_b c_s)/(c_w \rho_w) \quad \text{(Eq. 3.2)}$$

where ρ_b is the bulk density of MFT (kg m^{-3}), c_s is the specific heat of oven-dried MFT solids (J kg^{-1} K^{-1}), c_w is the specific heat of water (c_w = 4180 J kg^{-1} K^{-1} at 20 ˚C), and ρ_w is the density of water (ρ_w =1000 kg m^{-3}). Because the amount of residual hydrocarbons in MFT is less than 1 to 3 % by weight (Chalaturnyk et al., 2002; Ramos-Padrón et al., 2011), the effects of hydrocarbons on specific heat of water, density of water and particle density of solids are negligible. The ρ_b of MFT can be related to θ_{sa} by

$$\rho_b = (1 - \theta_{sa})\rho_p \quad \text{(Eq. 3.3)}$$

where ρ_p is the particle density of MFT solids (ρ_p = 2650 kg m^{-3}, corresponding to the typical particle density of soil mineral. The effect of the small amount of hydrocarbons is ignored). Substituting Eq. 3.3 into Eq. 3.2, we obtain

$$\theta_{sa} = (C - \rho_p c_s)/(c_w \rho_w - \rho_p c_s) \quad \text{(Eq. 3.4)}$$

where c_w, ρ_p, and ρ_w are constants. Unique θ_{sa} value can be obtained from Eq. 3.4 by measuring *C* by DPHP method and knowing c_s. The solid percentage can be calculated as follows

$$solid\ percentage = \rho_p(1-\theta_{sa})/[\rho_p(1-\theta_{sa}) + \theta_{sa}\rho_w] \quad \text{(Eq. 3.5)}$$

3.4.2 Modulated differential scanning calorimetry

As mentioned above, the specific heat of MFT solids c_s is required to calculate θ_{sa} and solid percentage of MFT. To evaluate the value of an independent measurement of c_s, an improved differential scanning calorimetry (DSC) method was used to obtain better estimation of c_s. The DSC determines the temperature and heat flow associated with material transitions as a function of time and temperature, whereas the MDSC combines traditional DSC and temperature modulated calorimetry (Kozlowski, 2012). It is a thermo analytical technique to measure evaporation, crystallization, melting, and specific heat of a dry material. The MDSC is a new technology to measure the specific heat (Reading et al., 1994). However, only a few researchers (Smidt and Tintner, 2007; Liu and Si, 2011a; Kozlowski, 2012) have applied it to soil samples. The MDSC machine (Model Q2000, TA instruments, New Castle, DE) was used to measure the specific heat of oven-dried MFT solids samples (Fig. 3.1).

Fig. 3.1. Photo of a modulated differential scanning calorimetry system manufactured by TA instruments.

The MDSC technique uses two simultaneous heating rates: a linear heating rate that provides information similar to standard DSC, and a sinusoidal modulated heating rate that permits the specific heat measurement. It measures the difference between a sample and a reference in the amount of heat required to increase the temperature by one unit as a function of time (Liu and Si, 2011a). The DSC heat flow signal $dH(T,t)/dt$ (J s^{-1}) is a function of specific heat c (J kg^{-1} K^{-1}) as

$$\frac{dH(T,t)}{dt} = cm\frac{dT}{dt} + f(T,t) \quad \text{(Eq. 3.6)}$$

where T is temperature (˚C), t is time (s), m is the sample mass (kg), dT/dt is the heating rate, $f(T,t)$ is the non-reversing (kinetic) heat flow, and cmdT/dt is the reversing heat flow. The temperature change of the sample as a function of t under a heat flow signal was recorded by the MDSC machine, and the specific heat can be obtained through the TA Universal Analysis software (TA instruments, New Castle, DE).

Most reports used simultaneous reversing and non-reversing heat flows for specific heat measurement (Reading et al., 1994; Smidt and Tintner, 2007; Liu and Si, 2011a; Kozlowski, 2012). The non-reversing heat flow increases the sample temperature with a constant rate and the reversing heat flow adds a sinusoidal signal to measure the specific heat at that temperature. In order to obtain accurate results, Thomas (2005) suggested using longer modulation period to allow sufficient time for complete heat transfer from DSC machine to sample. However, smaller average heating rate results in a less accurate total heat capacity signal to obtain absolute specific heat values.

The specific heat of MFT solids can either be assumed as 750 J kg^{-1} K^{-1} for all samples or measured by an independent MDSC method. Therefore, the sensitivity of solid percentage on c_s was analyzed to determine whether an independent c_s measurement is needed to satisfy the required accuracy. Based on the concept of small perturbation (Yeh, 1986), the absolute change of solid percentage (Δsp, %) caused by small increment or decrement of c_s (Δc_s, J kg^{-1} K^{-1}) can be calculated by substituting Eq. 3.4 and 3.5 into:

$$\Delta sp = sp(c_s + \Delta c_s) - sp(c_s) \quad \text{(Eq. 3.7)}$$

where $sp(c_s)$ represents solid percentage as a function of c_s.

3.4.3 Mature fine tailing samples and measurement

Three MFT samples were taken at different locations from the surface of the Syncrude's Aurora Mine MFT ponds in Alberta, Canada. Samples were collected and put into buckets and shipped to the University of Saskatchewan for laboratory measurements. The solid percentages of three samples were 70.4, 50.8, and 40.7 % as determined by the oven-dry method. The textures of all three samples were silt loam (U.S. Department of Agriculture Classification) as tested by the Coulter laser diffraction method (Coulter, 2011). In order to create a wider range in solid percentage, each MFT sample was diluted to three to five different solid percentages by adding distilled water to the sample and mixing it uniformly. In this way, samples with twelve different solid percentages (ranges from 20.9 to 70.4 %) were obtained from the three samples. After each heat pulse probe measurement, a subsample was taken to obtain the solid percentage by the oven-dry method.

To validate our measurement results from three MFT samples, six more samples were collected at different locations and at depths from 8 m to 45 m within the Aurora Mine MFT ponds. The range of solid percentage of the six MFT validation samples covers all possible solid percentages in the ponds. The different depths also correspond to different times of deposition. The samples were obtained using a piston suction sampler lowered from a boat using a wire line. Following retrieval the sample was extruded into a container under atmospheric conditions. The samples were then sealed and shipped to the University of Saskatchewan laboratory for analyses. The locations and physical properties of these six validation samples are listed in Table 3.1. All six validation samples had the texture of a silt loam.

Table 3.1. Depth, location, particle size distribution, texture and pH of six validation samples.

Sample	Depth (m)	UTM-East (m)	UTM-North (m)	Clay (%)	Silt (%)	Texture (-)	pH (-)
1	8.0	462006	6317800	21	78	Silt loam	7.6
2	9.5	461224	6317243	18	81	Silt loam	6.7
3	19.5	461224	6317243	26	74	Silt loam	7.9
4	35.0	461194	6318606	20	71	Silt loam	7.5
5	38.0	462376	6319428	14	59	Silt loam	7.3
6	45.0	461903	6318397	17	75	Silt loam	7.4

The dual probe used in this study was similar to Liu and Si (2010). It has five needles: one heater needle and four temperature sensor needles at different locations on the circumference for replications. All needles are 28 mm in length. The heater needle is at the centre of a square and there is a temperature needle at each corner of the square. Each temperature needle is around 6 mm from the heater needle. The apparent needle spacing was calibrated using water stabilized with 5 kg m^{-3} of agar (Liu and Si, 2008). A thermistor (10 kΩ at 25 ^{o}C, Model 10K3MCD1, BetaTHERM Corp., Shrewsbury, MA) was placed in the center of each needle. A two-loop nichrome wire (Nichrome A, electrical resistance is 205 Ω m^{-1}, Pelican Wire Co., Naples, FL) was inserted into the heater needle.

The needle was secured into a predrilled hole in a 32-mm-diameter and 32-mm-long plastic plug. The plug was then installed at the bottom of a cylindrical PVC container which works as a soil column. The soil columns were 4.5 cm high and 11 cm in diameter. The ends of heating wire and thermistor of the probe were soldered to 18 AWG electrical wires and connected to a datalogger. More detailed information on probe construction and setup can be found in Mori et al. (2003) and Liu and Si (2010). A datalogger (Model CR10X, Campbell Scientific, Logan, UT) and multiplexers (Model AM16/32, Campbell Scientific, Logan, UT) were used to control the heat pulse, to monitor the electric current through the heater, and to measure the temperatures as a function of time. Heat pulse measurements consisted of a 180 s sequence (1 s measurement interval) including 8 s heating (q ~ 45 W m^{-1}). The q values were inferred from the measured voltage drop across a precision 1 Ω resistor. Each MFT sample was measured once by four sensors of the dual probe.

Four temperature response curves by four sensor needles were obtained for each MFT sample during the same heat pulse released by the heater needle. The thermal properties were derived by fitting Eq. 3.1 to the temperature rise curves. The values of C, ρ_p, ρ_w, and c_s were used to calculate θ_{sa} and solid percentage based on Eq. 3.4 and 3.5. To obtain c_s values for each MFT solids by the MDSC method, three replicates of each MFT solids ($m_{soil} \approx 10$ mg) were prepared by compressing a sample of MFT solids into a hermetic aluminum pan ($m \approx 55$ mg). The small samples were put in the MDSC machine and equilibrated at 20 ˚C followed by a modulated temperature at ±0.5 ˚C every 120 s. This temperature condition was kept for five minutes while the temperature data was recorded for 10 minutes. A plot of the reversing specific heat signal versus time from the TA Universal Analysis software provided the specific heat of the samples at 20 ˚C. The MDSC was calibrated by using a standard sample with a known specific heat (sapphire, in this study).

Subsamples were taken and the wet and oven-dried weights of MFT subsamples were also obtained. These subsamples were oven-dried for 72 hours at the temperature of 65 ˚C. The lower temperature as opposed to 105 ˚C was selected to prevent loss of hydrocarbons.

3.5 Results and Discussion

A typical temperature-time curve for the MFT samples is presented in Fig. 3.2A. Heat was released into the soil for 8 s and the temperature at the first measurement needle began to increase noticeably after about 10 s, reaching a maximum temperature at around 20 s. Equation 3.1 provides an excellent fit to the experimental data (Fig. 3.2A), and C and α of the MFT sample were obtained by fitting the theoretical curve to the experimental data with the nonlinear least squares method.

In order to obtain MFT water content, the specific heat of dry MFT must be known (Eq. 3.2). There has been a range of values of specific heat for mineral soils reported in the literature (Liu and Si, 2011a) and the specific heat of mineral soils measured by the DPHP method ranged from 800 to 1000 J kg^{-1} K^{-1}, which were overestimated compared to the standard DSC method. Therefore, the solid percentages of three MFT samples were inferred by assuming c_s of all MFT samples to be 750 J kg^{-1} K^{-1}, which corresponding to the typical specific heat of mineral soil measured by DSC (Liu and Si, 2011a).

The influence of hydrocarbons on the specific heat of MFT solids will be discussed in a later section. There were two reasons for this assumption. Firstly, the MFT is composed of much more homogenous fines (silt and clay particles) than natural soils. Consequently, the specific heat of MFT minerals has less variation than natural soils. Secondly, the amount of solid hydrocarbons

in MFT is more than that in natural soils, but still negligible compared to the fines, so the contribution of hydrocarbons to the total *C* of MFT can be ignored.

The results of DPHP measured solid percentages of three MFT samples at different θ were shown in Fig. 3.2B. It is evident that the DPHP measured solid percentages has a linear relationship with that of oven-dry method ($y = 0.9495x + 0.0558, r^2 = 0.95$). The small standard deviations (as shown by error bars) indicated that the good repeatability of the measurements between the four temperature sensors of the probe. Therefore, the DPHP method is precise and accurate in measuring MFT solid percentage. It is of note that convection in MFT is negligible due to the viscous nature of the MFT mixture. This is also supported by the linear relationship between the DPHP measured solid percentage and the oven-dry method (Fig. 3.1). However, the development of free convection in very dilute MFT suspensions is likely.

The λ of six validation MFT samples ranged between 0.79 and 1.09 W m^{-1} with *C* between 2.76×10^{6} and 3.81×10^{6} J m^{-3} K^{-1} (Table 3.2). This corresponded to α values between 2.09×10^{-7} and 3.96×10^{-7} m^2 s^{-1}. The values of thermal properties were in reasonable ranges compared to other reports (Noborio et al., 1996; Bristow, 1998; Mori et al., 2003). The water content of the MFT samples decreased with increasing depth (Table 3.2). This decrease in water content is associated with a decrease in *C* and an increase in λ and α (Table 3.2) due to the higher *C* and lower λ of water relative to the MFT solids.

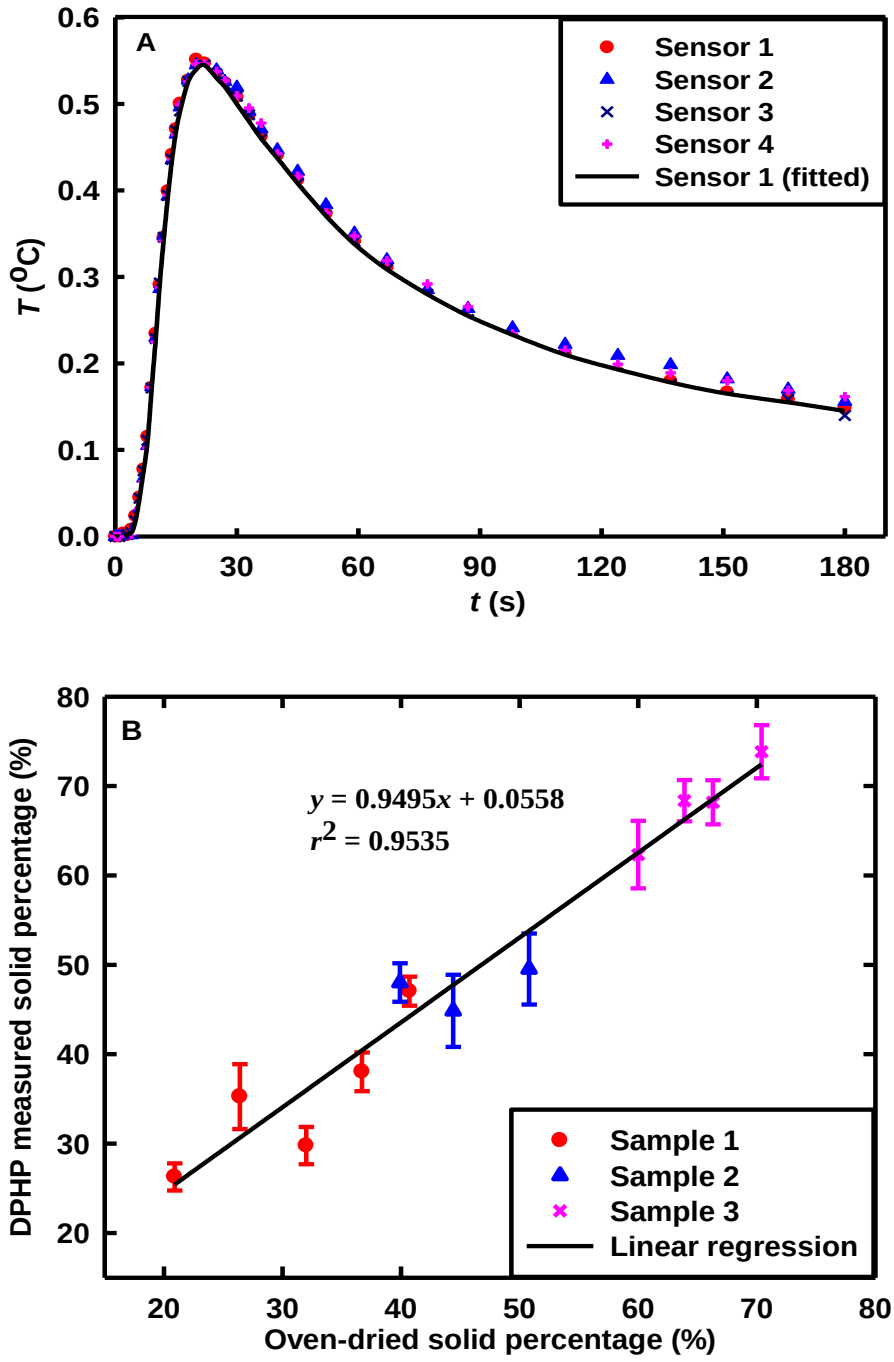

Fig. 3.2. (A) Measured temperatures by four sensors and fitted curve for the 1st sensor of testing sample 3 at 70 % solid percentage following an 8 s duration heat pulse; and (B) Scatter plot of measured solid percentage from the dual-probe heat pulse method and that of oven-dry method for three mature fine tailing samples.

Assuming that the specific heats of MFT solids (c_s) of six validation MFT samples were 750 J kg^{-1} K^{-1}, the solid percentages were calculated from DPHP measurements. Based on the linear equation in Fig. 3.2B, the DPHP method provided good estimate of the MFT solid percentage (Fig. 3.3), even though each MFT sample in this study contains different amount of hydrocarbons. The different choices of default c_s value cause underestimation or overestimation of solid percentage. However, the underestimation or overestimation can be eliminated by calibration. In order to determine if the estimation of solid percentage by the DPHP is sensitive to the actual c_s values of each MFT sample, the c_s of MFT was measured independently using the MDSC method.

The temperature of MFT ponds varied between 0 to 25 ˚C. Within this temperature range, the dependence of specific heat on temperature has a negligible effect on estimated thermal properties of MFT samples (Liu and Si, 2011). For convenience, all the samples in this study were equilibrated initially at 20 ˚C (instead of heating up) followed by application of the modulated heat flux. Fig. 3.4 is an example from TA Universal Analysis software. It shows that the measurement of specific heat value took about 8 minutes (i.e., after 4 modulation cycles) to converge to a stable range. This indicates that reliable soil specific heat values can be obtained only after a minimum number of modulation cycles at certain temperature.

Table 3.2. Thermal properties and water content of six validation samples by dual-probe heat pulse measurement assuming the specific heats of all mature fine tailing solids are 750 J kg^{-1} K^{-1}.

Sample	Thermal conductivity (W m^{-1} K^{-1})	Volumetric heat capacity ($\times 10^6$ J m^{-3} K^{-1})	Thermal diffusivity ($\times 10^{-7}$ m^2 s^{-1})	Volumetric water content (%)
1	0.79 (0.014†)	3.81 (0.42)	2.09 (0.05)	83 (1.9)
2	0.87 (0.036)	3.79 (0.92)	2.29 (0.15)	83 (4.2)
3	0.89 (0.032)	3.71 (0.67)	2.41 (0.08)	79 (3.1)
4	0.93 (0.027)	3.52 (0.82)	2.66 (0.07)	70 (3.8)
5	1.09 (0.082)	2.76 (0.20)	3.96 (0.49)	36 (9.1)
6	1.05 (0.021)	3.13 (0.13)	3.36 (0.13)	53 (5.9)

† Numbers in bracket stands for standard deviations of four replicates.

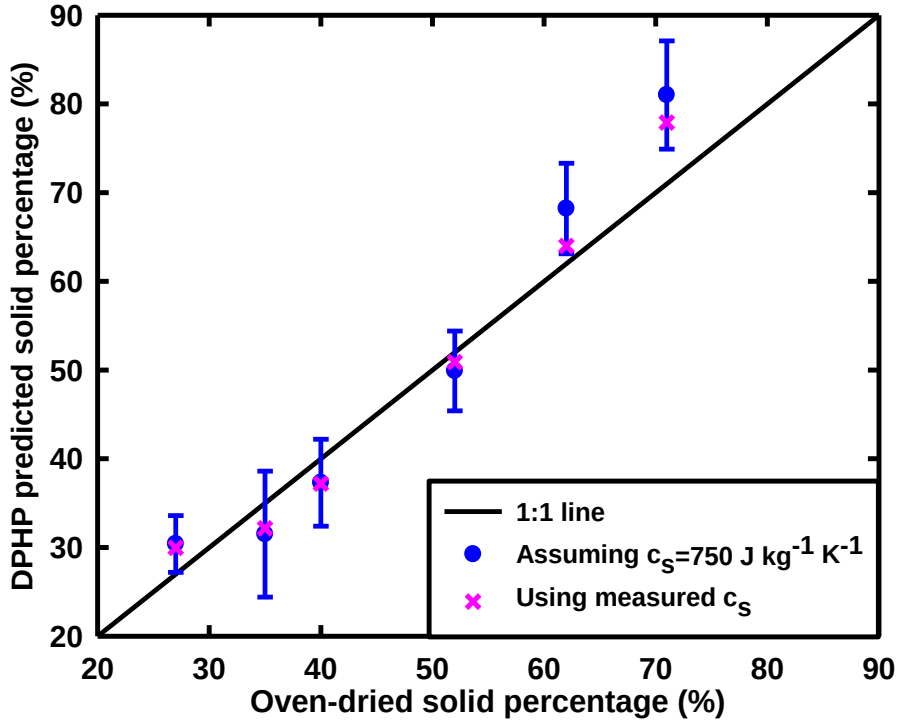

Fig. 3.3. Plot of predicted solid percentages from the dual-probe heat pulse method and that of measured by oven-dry method for six validation samples.

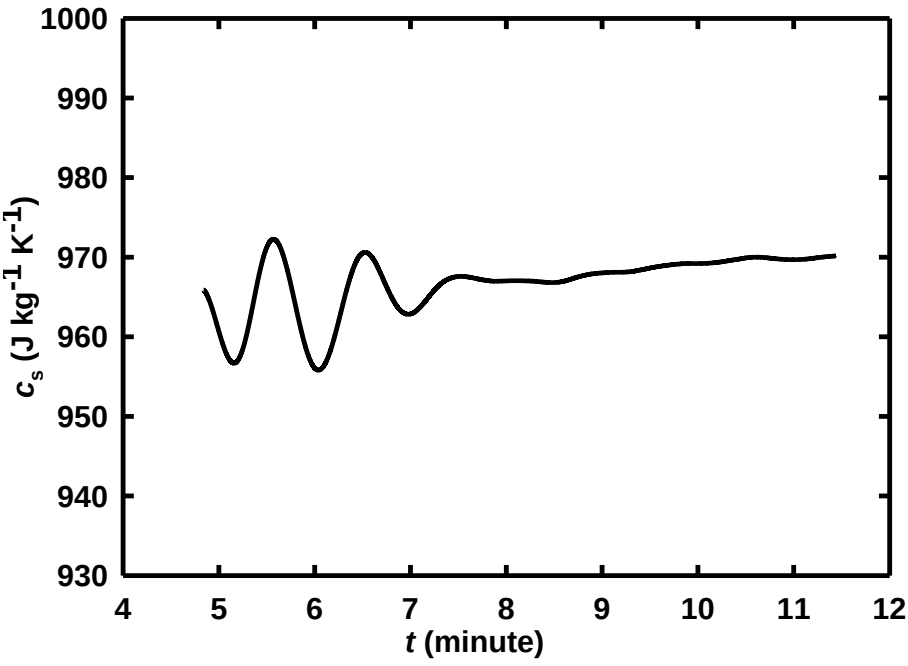

Fig. 3.4. An example of the specific heat (c_s) as a function of time (t) curve of one mature fine tailing sample from the modulated differential scanning calorimetry measurement.

The specific heats of the solids of the six MFT validation samples were 737, 769, 749, 772, 688, and 662 J kg^{-1} K^{-1}. These values are close to the default value, but still different from each other (within 750 ± 88 J kg^{-1} K^{-1}). Using each sample's actual c_s values from the MDSC measurement for the MFT resulted in an improvement of the solid percentage estimate, particularly at high solid percentages (Fig. 3.3). However, independent measurements of c_s in the laboratory is not convenient for field measurement, so the sensitivity of MFT solid percentage on c_s was analyzed using Eq. 3.7. Note that C in Eq. 3.4 is not a constant. Therefore, Δsp values over a wide range of C and Δc_s for given c_s = 750 J kg^{-1} K^{-1} are shown (Fig. 3.5).

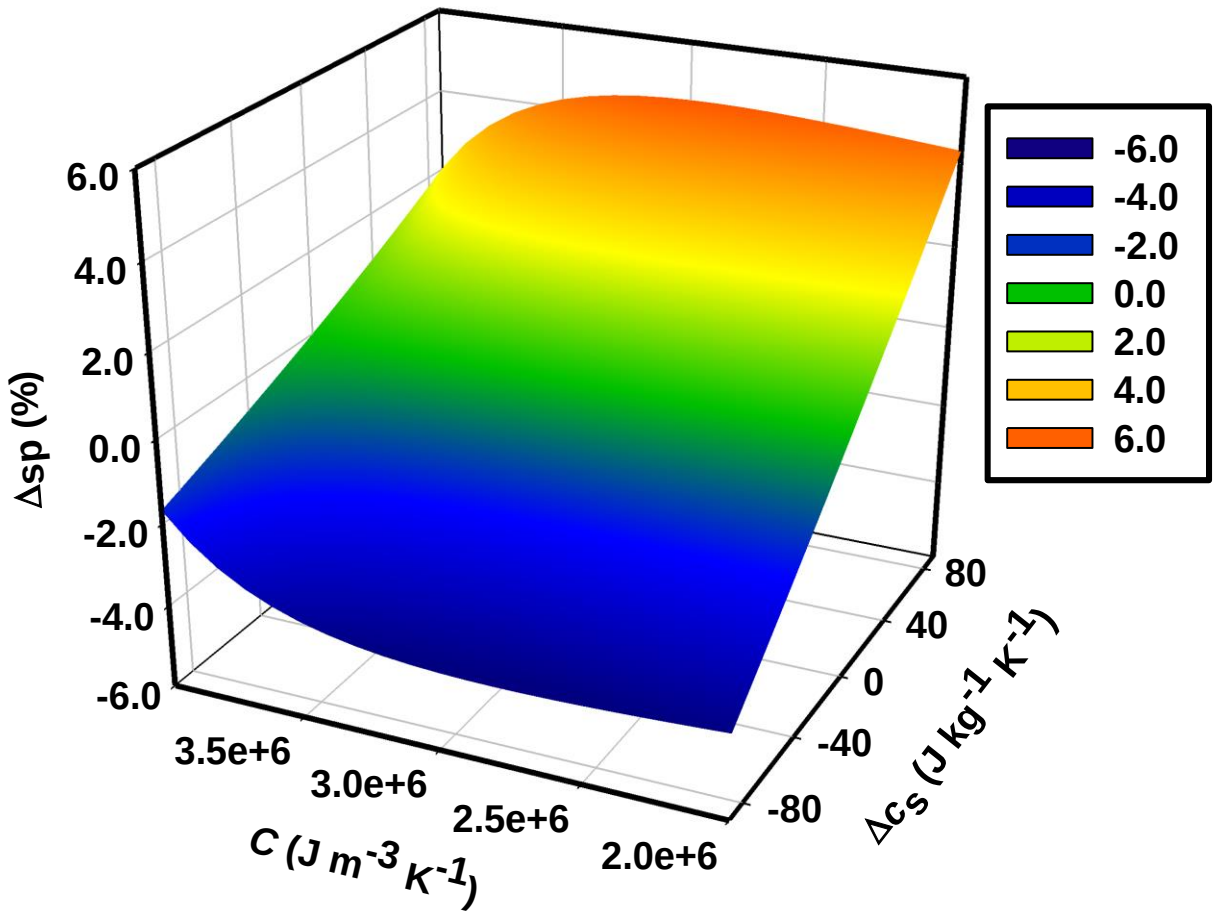

Fig. 3.5. Sensitivity of the solid percentage (Δ*sp*) towards the specific heat (c_s) of MFT solids at different volumetric heat capacities (*C*) of MFT when the specific heat of solids is assumed 750 J m^{-3} K^{-1}.

The use of maximal and minimal c_s values (772 (= 750 + 22) J kg^{-1} K^{-1} and 662 (= 750 - 88) J kg^{-1} K^{-1}) caused, at most, 1.1 % and -4.1 % changes to the absolute MFT solid percentage values, respectively. If a more accurate default c_s was chosen (i.e. 715 J kg^{-1} K^{-1}), then the range of c_s in the MFT pond would be 715 ± 60 J kg^{-1} K^{-1}, and Δ*sp* is less than 3.0 %. Therefore, independent measurement of c_s is not necessary for typical oil sands MFT, especially when the HPDP method was used to monitor the MFT solid percentage changes rather than the absolute values. However, if the variance of c_s is more than that in this study or this method is used in other saturated media, the MDSC method may require accurate c_s values of each sample.

3.6 Conclusions

Our experiment demonstrated that the DPHP method is accurate in determining solid percentage of MFT. There is a linear relationship between the DPHP-measured MFT solid percentage and that of the oven-dry method. The accuracy of DPHP-obtained MFT solid percentage can be further improved by measuring the specific heat of different MFT samples using the MDSC method. This accurate, inexpensive, and automated method can be easily adapted to monitor the thermal properties and the solid percentage of MFT in the oil sand tailing ponds. Multiple dual probes can be installed at different depths and locations in MFT ponds for determining the thermal properties, water content, and solid percentage during the MFT solidification process.

4 SINGLE-PROBE HEAT PULSE METHOD FOR SOIL WATER CONTENT DETERMINATION: COMPARISON OF METHODS[2]

4.1 Preface

Chapter 3 shows that the dual-probe heat pulse (DPHP) can be used for oil sands mature fine tailings' solid percentage measurement. However, the DPHP is subject to large errors due to the needle deflections when the dual probe is used in natural soils, especially those with a high clay content. This problem can be avoided by the single-probe heat pulse (SPHP). Therefore, developing the SPHP for both soil thermal properties and soil water content (θ, $m^3\ m^{-3}$) measurement to eliminate the drawbacks of the DPHP would be beneficial. In this chapter, the possibility of θ determination by the SPHP was tested and six different methods of data interpretation (λ, TN_{cum}, and TN_{max}, as well as the reciprocal of each) applied in the AHFO-DTS technique were compared.

[2] This chapter has been submitted for publication in Li, M., B. C. Si, W. Hu, and M. Dyck. Single-probe heat pulse method for soil water content determination: comparison of methods. Vadoze Zone Journal. The co-author contributions to this manuscript were greatly appreciated and consisted of: B. C. Si (provided financial assistance, methodological guidance, laboratory work support, and manuscript editing), W. Hu and M. Dyck (provided methodological guidance and manuscript editing). Minor modifications have been made for consistency.

4.2 Abstract

The estimation of soil thermal conductivity (λ, W m^{-1} K^{-1}) using the single-probe heat pulse (SPHP) method is well-known, but estimation of soil water content (θ, m^3 m^{-3}) using the SPHP is poorly understood. This study was to examine six methods – λ, normalized cumulative temperature increase (TN_{cum}, K s m W^{-1}), normalized maximum temperature increase (TN_{max}, K m W^{-1}), and the reciprocals of each – for θ estimation using the SPHP. The temperature response curves of four soils at different θ were measured following 600-s heat pulses with heating strengths of about 6 W m^{-1}, from which λ, TN_{cum}, and TN_{max} values were determined. The maximal measurement errors of the three methods were 0.11 m^3 m^{-3} for the coarse sand and 0.01 m^3 m^{-3} for the fine sand, sandy loam, and silty clay, except for 0.05 m^3 m^{-3} for the fine sand by the λ(θ) method. The predicted θ from all of the λ, TN_{cum}, and TN_{max} methods agreed well with that from the oven-dry method for all soils with exception given to the TN_{cum}(θ) and TN_{max}(θ) methods for the coarse sand when θ > 0.20 m^3 m^{-3}. The measurement errors and θ predictions of the 1/λ(θ) method were similar to that of the TN_{cum}(θ) and TN_{max}(θ) methods, and that of the 1/TN_{cum}(θ) and 1/TN_{max}(θ) methods were similar to that of the λ(θ) method. As each of the six methods worked well only for some soils, improved estimations were obtained when the λ(θ) method was combined with the 1/TN_{cum}(θ) (or 1/TN_{max}(θ)) method for coarse textured soils, and the 1/λ(θ) method was combined with the TN_{cum}(θ) (or TN_{max}(θ)) method for fine textured soils.

4.3 Introduction

Soil water plays an important role in the hydrological cycle and plant growth, so accurate and reliable techniques to measure θ are needed for precision irrigation management and hydrological modelling (Huisman et al., 2003; Dias et al., 2013). There are several instruments available to

measure θ, such as the frequently used time-domain reflectometry (TDR) and neutron scattering probe. The TDR provides convenient surface soil θ measurements, but it cannot be used in soils with high EC (Nadler et al., 1999; Steele-Dunne et al., 2010). The neutron scattering probe can be used to measure θ non-destructively at different soil depths, but it is costly and radioactive (Huang et al., 2012). In addition, the neutron probe requires a site-specific calibration and cannot measure θ in the surface 15 cm layer (Dane and Topp, 2002). Another inexpensive, nonradioactive and widely used θ measurement technique is the heat pulse probe, which is based on the dissipation of an applied heat pulse in the soil (Bristow et al., 1994a; Ochsner et al., 2003; Tarnawski et al., 2009). The heat pulse probe method including the single-probe heat pulse (SPHP) and the dual-probe heat pulse (DPHP), has the advantages of continuous measurement on soil thermal properties (and θ for the DPHP), even in surface layers (Xiao et al., 2012; Liu et al., 2013b; Zhang et al., 2014), and is not sensitive to soil salinity (Shaw and Baver, 1939; Bristow et al., 1994a; Tarnawski et al., 2011). Currently, the DPHP can be used to measure λ, thermal diffusivity (α), volumetric heat capacity (*C*), and θ, whereas the SPHP has only been used to measure λ.

The SPHP method has been used to measure λ of dry and wet soils through the release of a continuous or a long heat pulse from the probe and then measure the temperature rise and/or fall in the same probe (Blackwell, 1954; de Vries and Peck, 1958b; Bristow et al., 1994b). However, there is limited progresses in obtaining soil thermal diffusivity (α, $m^2 s^{-1}$) or heat capacity (*C*, $J m^{-3} K^{-1}$) needed to calculate θ, due to the unknown thermal contact conductivity (*H*, $W m^{-2} K^{-1}$) at the boundary between the probe body and soil particles (Liu and Si, 2011a). Obtaining *H* from Blackwell (1954) small-time solution is difficult; several other solutions were provided, but they all require that *C* be known in advance (Moench and Evans, 1970; Jones, 1988b).

Contrary to the single probe method, the dual-probe heat pulse (DPHP) method releases a short heat pulse in the heater probe and measures the temperature response curve by a temperature sensor probe at a small distance away from the heater. As a result, the DPHP can measure all three soil thermal properties (Bristow et al., 1994b; Bristow, 1998) and hence θ can be obtained from *C* independent of soil type (Bristow et al., 1993), but it tends to overestimate *C* and hence θ, particularly when θ is small (Heitman et al., 2003; Ochsner et al., 2003; Liu et al., 2012). The accuracy of the DPHP is also affected by needle deflection, which may cause large errors when the needles are installed in the field (Basinger et al., 2003; Heitman et al., 2003; Liu et al., 2008a; Kluitenberg et al., 2010). Recently, a self-calibrated dual probe was designed (Liu et al., 2013a; Wen et al., 2015) to automatically calculate in situ needle space deflection without calibration. However, only two sandy soils at dry and saturated conditions were tested and a calibration for the initial needle space is still needed.

The SPHP has multiple advantages over the DPHP: The single probe needle is more robust in the field because of its larger diameter and thicker wall (Liu and Si, 2011a), and is not affected by needle deflection; also, the single probe has a larger zone of influence as a result of longer probe. Unlike the DPHP, the SPHP cannot be used to determine θ from *C*. In order to measure θ by a single probe, the relations between temperature changes (or λ) and θ from the SPHP measurements need to be investigated. Shaw and Baver (1939) applied a Wheatstone bridge on an electro-thermal method, which is similar to the SPHP method, to measure the electrical current changes of their setup with θ in different soils. They found that the electrical current~θ relation depended on soil textures, and the relation was not affected by salt content or external temperature conditions. However, the prediction and accuracy of θ measurement was not mentioned. The λ of different soils at various θ has been widely tested (Sepaskhah and Boersma, 1979; Horton and

Wierenga, 1984; Hopmans and Dane, 1986; Abu-Hamdeh and Reeder, 2000; Momose and Kasubuchi, 2002), and attempts to develop the expressions of λ~θ relations have been reported (Ewing and Horton, 2007). Among them, Kasubuchi (1992) tried to measure θ using the λ~θ relations obtained from the heat pulse method; however, the accuracy was not reported and the results were limited to two soils within a limited range of θ.

In recent years, an active heated fibre optic-distributed temperature sensing (AHFO-DTS) system has been used for in situ monitoring of soil thermal properties and θ (Sayde et al., 2010; Ciocca et al., 2012; Striegl and Loheide, 2012). AHFO-DTS is similar to the SPHP in theory, but uses the fibre-optic cable to measure soil temperature, and thus could potentially extend the temperature, thermal properties, and θ measurement scale from a point to an intermediate landscape scale. The DPHP based AHFO-DTS system was also tested to measure *C* and θ, by installing two or more fibre optic cables paralleling each other, which has the same drawbacks as the DPHP (Benítez-Buelga et al., 2014). To further develop the SPHP based AHFO-DTS, there is a need to extend the measurements from λ to C and θ for the SPHP.

The SPHP can be used to measure λ accurately; therefore, if θ can also be estimated, then *C* can be determined from the linear relationship between *C* and θ, and α can be obtained from λ and *C* (Bristow et al., 1993). Therefore, the ability to accurately estimate θ is critical to extend the measurement of the SPHP and AHFO-DTS from λ to α and *C*. With the AHFO-DTS method, attempts have been made to infer θ from the λ~θ relation (Ciocca et al., 2012) or the maximum temperature increase (T_{max}, K)~θ relation (Striegl and Loheide, 2012). However, the θ estimation errors were high (> 0.05 m^3 m^{-3}) at high θ for both methods. Sayde et al. (2010) applied a new interpretation of temperature data called the cumulative temperature increase (T_{cum}, K s), and found θ measurements from the $T_{cum}(\theta)$ method were more precise than those from the $T_{max}(\theta)$

method. However, published studies with the AHFO-DTS system only focused on in situ θ monitoring and did not test their performance on different textured soils, or compare the three methods (i.e., λ(θ), T_{cum}(θ), and T_{max}(θ) method) (Gil-Rodríguez et al., 2013; Sayde et al., 2014).

The above methods should be compared more thoroughly with more soil types and a wider range of θ. To do this, it may be more convenient to use the SPHP than to use the AHFO-DTS because the stainless steel needle (high in λ) of the single probe is in direct contact with soil particles, whereas a fibre optic cable has several protective layers surrounding the fibre optic cable (temperature sensors), which may increase contact resistance between the heater, temperature sensor and soils. Therefore, the conventional heat pulse probe may have better contact with soil than the fibre optic cable in terms of heat conduction (Liu and Si, 2011a; Ciocca et al., 2012), and have more frequent temperature readings at early time, which allows for more accurate determinations in *H* and α (Liu and Si, 2011a).

Different ranges of the heating duration of the SPHP have been chosen in previous studies (Abu-Hamdeh and Reeder, 2000; Liu and Si, 2011a), and there are both advantages and disadvantages for the short and long heating durations. Therefore, the possible effects of the heating duration on θ estimation errors need to be understood for effective application of this method. In the field, soil thermal property estimates using longer heating duration are representative of a larger volume of soil around the heat pulse probe. However, longer heating consumes more power and is time consuming, which can be a potential problem in an automated system with a solar panel based power supply. In addition, the SPHP assumes that soil thermal properties are uniform within the zone of influence (Liu and Si, 2011a). A longer heating duration increases the zone of influence, and the soil heterogeneity within the zone of influence may be large enough to violate the assumption of homogeneous soil thermal properties within the

sampling volume. However, θ generally changes slowly and longer heating duration would not be a problem, but there are situations where θ may change rapidly; for example, an advancing wetting front following a high intensity precipitation, which requires more frequent measurements of θ and thus shorter heating duration.

The objective of this study was to further develop and thoroughly compare the $\lambda(\theta)$, $T_{cum}(\theta)$, and $T_{max}(\theta)$ methods for θ estimation using the SPHP. The temperature response curves of four soils with different textures at various range of θ were measured by a single probe. The λ and newly defined normalized T_{cum} and T_{max} (denoted as TN_{cum} and TN_{max}) values were obtained and the precisions of θ by the $\lambda(\theta)$, $TN_{cum}(\theta)$, and $TN_{max}(\theta)$ methods as well as the reciprocals of each were compared through error analysis. The effects of the heating duration on the θ estimation errors from all of the six methods were discussed. Probe dependence of the six methods and combination of the methods to reduce estimation errors were also discussed.

4.4 Materials and Methods

4.4.1 Probe construction and soil column setup

The SPHP uses a probe consisting of a single cylindrical rod acting as both the heater and the temperature sensor. Three probes with the same dimensions and materials were built. The probe body was made of a hollow stainless steel tube (Penn Stainless Products, Quakertown, PA), with a length of 11 cm, and an outer and inner diameter of 2.108 and 1.240 mm, respectively. The small diameters were chosen to reduce the effect of probe body on heat transfer and make the probe closer to a line heat source (Kluitenberg et al., 1995; Liu et al., 2012). A thermistor (10 kΩ at 25 ˚C, Model 10K3MCD1, BetaTHERM Corp., Shrewsbury, MA) was installed in the center of the needle. The heater was a loop of nichrome wire (Nichrome A, electrical resistance equals to 69.06 $\Omega\ m^{-1}$, Pelican Wire Co., Naples, FL) inserted into and spanning the entire length of the stainless steel tubing. The tubing was subsequently filled with Omegabond® 101 epoxy (Omega Engineering, Stamford, CT), which has a relatively high λ and is an excellent electrical insulator.

When the epoxy was dry, the needle was secured into a predrilled hole in a 32-mm-diameter and 32-mm-thick plastic plug. The plug was then installed at the bottom of a cylindrical PVC container (13 cm in height and 10 cm in diameter), which housed the soil sample. Three soil columns with the same dimensions were built. The ends of the heating wire and thermistor of the probes were soldered to 18 AWG electrical wires and connected to a datalogger (Model CR9000XC, Campbell Scientific, Logan, UT). The datalogger was used to control and monitor the heat input, and to measure the temperature changes with time. An adjustable resistor and a heater-control relay circuit were used to control and measure the amount of heat released from the probe.

A continuous heating time of 600 s with a heating strength of $q \approx 6$ W m^{-1} was applied and the temperature was recorded with a frequency of 20 Hz. The relatively long heating period was chosen to examine the time effect on θ determinations, and the relatively high frequency was selected to ensure more accurate TN_{cum} estimates. The temperature increases were controlled to less than 10 ˚C in order to avoid water movement caused by a temperature gradient (Shiozawa and Campbell, 1990). To ensure all the temperature changes were caused by the heat pulse probe, the temperatures within the soil columns needed to reach equilibrium before each measurement. The heat pulses were executed at four hours interval to allow enough time for equilibrium and the temperatures were recorded five minutes before each heat pulse execution to double check the equilibrium. In the cases of non-equilibrium during our measurement, corrections were applied using the linear interpolation method presented by Jury and Bellantuoni (1976) .

4.4.2 Soil sample preparation

Four soils were tested: one industrial silica sand (coarse sand) and three field soils: fine sand, sandy loam, and silty clay, according to the U.S. Department of Agriculture textural Classification. The coarse sand was chosen to examine the θ determinations at the extreme case of very poor contact between the heat pulse probe and soil particles. The clay, silt, and sand contents of each soil are shown in Table 4.1.

Table 4.1. Sand, silt, and clay contents and dry bulk densities (ρ_b) of tested soils.

Soil	Clay content	Silt content	Sand content	ρ_b
	%			kg m^{-3}
Coarse sand	0.0 (0.0†)	0.0 (0.0)	100.0 (0.0)	1.75×10^3
Fine sand	2.3 (0.3)	0.3 (0.01)	97.4 (0.3)	1.56×10^3
Sandy loam	12.3 (0.3)	22.3 (0.8)	65.5 (0.6)	1.43×10^3
Silty clay	43.6 (1.2)	41.9 (0.2)	14.5 (1.0)	1.25×10^3

† Numbers in parentheses are standard deviations of four replicates.

A pre-determined amount of soil and water were mixed and shaken in a plastic bag to obtain uniform θ, and then the soil in the bag was packed into the PVC columns at a fixed ρ_b (Table 4.1) for each soil. After equilibration for two days, a 600 s duration heat pulse was released and the temperature rise during the heating was recorded at a frequency of 20 Hz. The heat pulse experiment was repeated four times at four hours interval for each soil sample. The actual gravimetric water content of each sample was confirmed by the oven-dry method and multiplied by ρ_b to get θ after the SPHP measurements. The above procedure was repeated at water content increments of about 0.03 m^3 m^{-3} from air dry to near saturation for each soil. Complete saturated soil samples were not measured because it was difficult to pack very wet soil samples to reach full saturation, which was most probably caused by the entrapped air in the non-interconnected pores in soils (Faybishenko, 1995; Sakaguchi et al., 2005).

4.4.3 Methods to estimate soil water content

Mathcad15.0 (PTC Inc., Needham, MA) software was used for the data analysis. Using the SPHP method, the λ values were estimate based on the Blackwell model (Blackwell, 1954) for a single probe made of a good conductor. In this model, an infinite cylindrical heat source of radius r (m) is surrounded by a homogeneous infinite soil with the same initial temperatures in the heat source and soil. The cylindrical probe has a thermal contact conductivity H (W m^{-2} K^{-1}) between the heat source and surrounding soil particles. If the heat is released continuously at a heating strength q (W m^{-1}), the temperature increase ΔT (˚C) at the heat source at time t (s) is given as

$$\Delta T\left(q, r, C_{\mathrm{p}}, H, \alpha, \lambda\right) = \frac{1}{2\pi i}\int_{\gamma-i\infty}^{\gamma+i\infty} \frac{q\Gamma}{\pi p\left[r^2 C_{\mathrm{p}} p\Gamma + 2\lambda Y_1\left(\sqrt{pr^2/\alpha}\right)\right]} \exp(tp)\mathrm{d}p \qquad \text{(Eq. 4.1)}$$

where λ and α are the soil thermal conductivity (W m^{-1} K^{-1}) and soil thermal diffusivity (m^2 s^{-1}), respectively; C_p is the heat capacity of the probe (J m^{-3} K^{-1}), p is the Laplace transformation variable, γ is Euler's constant=0.5772, i is the imaginary unit, and

$$\Gamma = \frac{1}{\sqrt{pr^2/\alpha}} Y_0\left(\sqrt{pr^2/\alpha}\right) + \frac{\lambda}{rH} Y_1\left(\sqrt{pr^2/\alpha}\right) \quad \text{(Eq. 4.2)}$$

where Y_0 and Y_1 are the zero-order and first-order modified Bessel functions of the second kind, respectively. The solution of Eq. 4.1 is given as (Blackwell, 1954)

$$\Delta T\left(q, r, C_p, H, \alpha, \lambda\right) = \frac{8\lambda q}{\pi^3 r^4 {C_p}^2 \alpha^2} \int_0^\infty \frac{\left[1-\exp(-\alpha t x^2)\right]}{x^3 (P^2+Q^2)} dx \quad \text{(Eq. 4.3)}$$

where

$$\begin{aligned} P &= xJ_0(rx) + J_1(rx)\left[x^2/H - 2/\left(C_p r\alpha\right)\right] \\ Q &= xY_0(rx) + Y_1(rx)\left[x^2/H - 2/\left(C_p r\alpha\right)\right] \end{aligned} \quad \text{(Eq. 4.4)}$$

where J_0 and J_1 are the zero-order and first-order Bessel functions of the first kind, respectively.

Equation 4.3 can be greatly simplified using the long-time approximation (Blackwell, 1954)

$$\Delta T(t) = A\ln(t) + B = q/(4\pi\lambda)\ln(t) + B \quad t \gg r^2/\alpha \quad \text{(Eq. 4.5)}$$

where A and B are the slope and intercept of the ΔT~ln(t) curve. Therefore, λ can be calculated by

$$\lambda = q/(4\pi A) \quad t \gg r^2/\alpha \quad \text{(Eq.4.6)}$$

and the λ(θ) relationships can be built to estimate θ.

Another way to estimate θ using the AHFO-DTS system is the $T_{max}(\theta)$ relationship (Shaw and Baver, 1939; Striegl and Loheide, 2012), which can be easier obtained than λ(θ) relationships and was further compared and improved by the $T_{max}(\theta)$ method (Sayde et al., 2010). Both T_{cum} and T_{max} can be calculated from the SPHP measurement data without previous knowledge of *C*, *H*, or θ. The value of T_{max} is simply the maximal temperature increase when the heat pulse stops. As the datalogger recorded temperature readings at a frequency of 20 Hz, T_{cum} can be approximated by the sum of each temperature increase measurement from the datalogger multiplied by a 0.05s duration. Therefore, T_{cum} and T_{max} are calculated, respectively, by

$$T_{\mathrm{cum}} = \int_{t_0}^{t_1} \Delta T dt = \sum \Delta T_i \cdot 0.05 \text{ s} \quad \text{(Eq. 4.7)}$$

$$T_{\mathrm{max}} = T_1 - T_0 \quad \text{(Eq. 4.8)}$$

where t_1 and T_1 are time and temperature at the end of heating, and t_0 and T_0 are time and temperature at the beginning of heating.

As the temperature increase is proportional to q (Eq. 4.3), it is unreasonable to compare T_{cum} and T_{max} values obtained from temperature response curves for different q values. Even for the same experimental setting, it may be difficult to keep a constant q between heat pulses, as there is always more or less a voltage drop after each heat pulse for a DC power supply. To eliminate the dependence on q, we defined two new terms: the normalized T_{cum} and T_{max} (denoted as TN_{cum} and TN_{max}) here, which are calculated by

$$TN_{\mathrm{cum}} = T_{\mathrm{cum}}/q \quad \text{(Eq. 4.9)}$$

$$TN_{\mathrm{max}} = T_{\mathrm{max}}/q \quad \text{(Eq. 4.10)}$$

4.4.4 The λ(θ), $TN_{cum}(\theta)$, and $TN_{max}(\theta)$ models

Different from *C*, λ is not a simple function of the volume fraction and thermal conductivity of each soil component, making it difficult to build a purely theoretical model for λ (Bristow, 2002a). However, several semi-theoretical and empirical models has been developed (Barry-Macaulay et al., 2015; Dong et al., 2015) and the semi-theoretical Campbell (1994) model was used to describe λ(θ) relationships here. The Campbell model assumes that the λ of soil is the weighted sum of the thermal conductivity of water, gas, and mineral in the soil:

$$\lambda = \frac{k_w x_w \lambda_w + k_a x_a \lambda_a + k_m x_m \lambda_m}{k_w x_w + k_a x_a + k_m x_m} \quad \text{(Eq. 4.11)}$$

where *k* and *x* are a weighting factor and volume fraction, respectively; and the indexes w, a, and m represent water, air, and mineral, respectively. The λ_a of soil is the sum of the λ of dry air and a vapor term due to latent heat transfer. However, all the soil samples were measured at room temperature and the temperature increases caused by the heat pulses were less than 10 ^oC. Therefore, λ of the vapor term was ignored here, thus λ_w and λ_a can be calculated by (Campbell et al., 1994):

$$\lambda_w = 0.554 + 2.24 \times 10^{-3} T - 9.87 \times 10^{-6} T^2 \quad \text{(Eq. 4.12)}$$

$$\lambda_a = 0.024 + 7.73 \times 10^{-5} T - 2.60 \times 10^{-8} T^2 \quad \text{(Eq. 4.13)}$$

where *T* is the soil temperature (^oC). Thermal conductivity of the soil mineral λ_m is obtained by fitting Eq. 4.11 to the experimental data. The volume fractions of soil components are calculated by:

$$x_a = 1 - x_w - x_m \quad \text{(Eq. 4.14)}$$

where:

$$x_{\mathrm{w}} = \theta \tag{Eq. 4.15}$$

$$x_{\mathrm{m}} = \frac{\rho_{\mathrm{b}}}{\rho_{\mathrm{p}}} \tag{Eq. 4.16}$$

where ρ_b and ρ_p are soil bulk density and particle density, respectively (kg m^{-3}), and $\rho_p = 2.65 \times 10^3$ kg m^{-3}. The weighting factors can be obtained by (Campbell et al., 1994):

$$k_{\mathrm{a}} = \frac{1}{3}\left[\frac{2}{1+\left(\frac{\lambda_{\mathrm{a}}}{\lambda_{\mathrm{f}}}-1\right)g_{\mathrm{a}}} + \frac{1}{1+\left(\frac{\lambda_{\mathrm{a}}}{\lambda_{\mathrm{f}}}-1\right)(1-2g_{\mathrm{a}})}\right] \tag{Eq. 4.17}$$

$$k_{\mathrm{w}} = \frac{1}{3}\left[\frac{2}{1+\left(\frac{\lambda_{\mathrm{w}}}{\lambda_{\mathrm{f}}}-1\right)g_{\mathrm{a}}} + \frac{1}{1+\left(\frac{\lambda_{\mathrm{w}}}{\lambda_{\mathrm{f}}}-1\right)(1-2g_{\mathrm{a}})}\right] \tag{Eq. 4.18}$$

$$k_{\mathrm{m}} = \frac{1}{3}\left[\frac{2}{1+\left(\frac{\lambda_{\mathrm{m}}}{\lambda_{\mathrm{f}}}-1\right)g_{\mathrm{a}}} + \frac{1}{1+\left(\frac{\lambda_{\mathrm{m}}}{\lambda_{\mathrm{f}}}-1\right)(1-2g_{\mathrm{a}})}\right] \tag{Eq. 4.19}$$

where g_a is a shape factor that is to be determined; λ_f is defined as a "fluid" thermal conductivity (W m^{-1} K^{-1}) and calculated by:

$$\lambda_{\mathrm{f}} = \lambda_{\mathrm{a}} + f_{\mathrm{w}}(\lambda_{\mathrm{w}} - \lambda_{\mathrm{a}}) \tag{Eq. 4.20}$$

where f_w is an empirical weighting function ranging from 0 in dry soil to 1 in saturated soil, and given by:

$$f_{\mathrm{w}} = 1/\left(1 + \frac{x_{\mathrm{w}}}{x_{\mathrm{w0}}}\right)^{-q} \tag{Eq. 4.21}$$

where q and x_{w0} are soil properties that relate to the value of θ at which water starts to affect λ and the rapidity of the transition from air- to water-dominated conductivity. The q is temperature dependent and obtained by (Campbell et al., 1994):

$$q = q_0(T + 273.15/303)^2 \quad \text{(Eq. 4.22)}$$

The liquid recirculation cut-off water content x_{w0} is correlated to soil texture and can be obtained from the geometric mean particle diameter d_g (10^{-3} m) by (Campbell et al., 1994):

$$x_{w0} = 0.267 {d_g}^{-0.2} \quad \text{(Eq. 4.23)}$$

The value of d_g can be obtained following Shiozawa and Campbell (1991) by:

$$d_g = \exp(5.756 - 3.454 m_{silt} - 7.712 m_{clay}) \quad \text{(Eq. 4.24)}$$

where m_{silt} and m_{clay} are the silt and clay fractions of soil solids particles. Therefore, when fitting Eq. 4.11 to measured λ(θ) curves, only the three parameters λ_m, q_0, and g_a are unknown.

As the values of TN_{cum} and TN_{max} were calculated from the measured temperature increase data, and the trends in TN_{cum} and TN_{max} with changing θ were similar, an empirical rational model was used to describe the $TN_{cum}(\theta)$ and $TN_{max}(\theta)$ relationships:

$$TN_{cum}(\text{or } TN_{max}) = (a + b\theta)/(1 + c\theta) \quad \text{(Eq. 4.25)}$$

where a, b, and c are empirical parameters. From the temperature response curve of each heat pulse measurement, the values of λ, TN_{cum}, and TN_{max} were obtained from Eq. 4.6, 4.9 and 4.10. By repeating the above analyses for soil samples at various water contents, λ, TN_{cum}, and TN_{max} as a function of θ were obtained, and the least squares regression was used to fit Eq. 4.11 and 4.25

to the measured data (Sayde et al., 2010). Equation 4.11 was used for the $\lambda(\theta)$ curve and Eq. 4.25 was used for the $TN_{cum}(\theta)$ and $TN_{max}(\theta)$ curves (Table 4.2). Equation 4.11 was chosen as it is a physically based model, and Eq. 4.25 was chosen to fit the data as it is relatively simple (few parameters) and works reasonable well. The estimated error in θ, σ_θ, was calculated as:

$$\sigma_\theta = \sigma_x / \left| \frac{df(\theta)}{d\theta} \right| \quad \text{(Eq. 4. 26)}$$

where σ_x is the standard deviation of x, where x represents λ, TN_{cum}, or TN_{max}, respectively. The standard deviations were obtained from repeated heat pulse measurements of the same sample at the same θ. The $df(\theta)/d\theta$ is the local slope of the $\lambda(\theta)$, $TN_{cum}(\theta)$, or $TN_{max}(\theta)$ curves. A smaller σ_x indicates a higher precision and reproducibility of the measurement.

To examine the probe-dependence of θ measurements associated with the three methods and to evaluate the accuracy of θ predictions by λ~θ, TN_{cum}~θ, and TN_{max}~θ relations obtained from the first probe, two additional probes with dimensions and materials identical to the first probe were built and used to measure all four soils at various θ. The predicted θ values provided by the second and third probes obtained from the λ~θ, TN_{cum}~θ, or TN_{max}~θ curves were compared with the measured θ values obtained by the oven-dry method. Because the measurement errors and θ predictions of the $1/\lambda(\theta)$ method were similar to that of the $TN_{cum}(\theta)$ and $TN_{max}(\theta)$ methods, and that of the $1/TN_{cum}(\theta)$ and $1/TN_{max}(\theta)$ methods were similar to that of the $\lambda(\theta)$ method, the results of $1/\lambda(\theta)$, $1/TN_{cum}(\theta)$, and $1/TN_{max}(\theta)$ methods were not shown here.

Table 4.2. The model, parameter, and coefficient of determination (r^2) of soil thermal conductivity (λ), normalized cumulative temperature increase (TN_{cum}), and normalized maximum temperature increase (TN_{max}) as a function of soil water content (θ) of tested soils, measured by the first probe with a heating duration of 600 s.

Property	Parameter	Soil			
		Coarse sand	Fine sand	Sandy loam	Silty clay
λ	λ_m	5.30	3.40	3.02	2.53
	q_0	10.00	28.00	20.18	12.26
	g_a	0.1236	0.0200	0.0114	0.0200
	r^2	0.95	0.98	0.99	0.99
TN_{cum}	a	662	784	889	811
	b	64,086	6,251	-1,648	-1,481
	c	479	56.22	6.48	-0.04
	r^2	0.99	0.98	0.97	0.99
TN_{max}	a	1.30	1.57	1.79	1.44
	b	111.70	11.94	-3.45	-2.64
	c	453.45	58.18	6.78	-0.03
	r^2	0.99	0.98	0.97	0.99

4.5 Results and Discussion

4.5.1 Comparison of the λ(θ), TN_{cum}(θ), and TN_{max}(θ) methods

The estimated λ values using Eq. 4.6 increased rapidly with increasing θ from 0 to 0.05 m^3 m^{-3} for the coarse sand and fine sand, but rather slowly for the sandy loam and silty clay (Fig. 4.1A). The increase in λ with the increase in θ was quasi-linear from 0.05 m^3 m^{-3} to near saturation for all soils except the silty clay soil. Our results were consistent with Riha et al. (1980) , Hopmans and Dane (1986), and Tarnawski et al. (2009, 2011). The increase in λ with increasing θ is a result of the displacement of air with water and consequently increased contact areas between soil particles and enhanced heat conduction in the solid phase and liquid phase.

Both TN_{cum} and TN_{max} of the four soils decreased with increasing θ (Fig. 4.1B, C). Although the absolute values of TN_{cum} and TN_{max} differed, the shapes of TN_{cum}(θ) curves were similar to that of TN_{max}(θ) for all soils. TN_{cum} and TN_{max} of the coarse sand and the fine sand decreased

dramatically with increasing θ from 0 to 0.05 m^3 m^{-3}, and then decreased gradually when θ > 0.05 m^3 m^{-3}. TN_{cum} and TN_{max} of the sandy loam decreased gradually over the whole range of θ, and that of the silty clay decreased roughly linearly with θ. The decrease in TN_{cum} and TN_{max} is because of elevated heat transfer in soil as θ increased, resulting in a smaller temperature rise in the centre of the probe where the temperature sensor was located.

There were striking differences in λ(θ), $TN_{cum}(\theta)$, and $TN_{max}(\theta)$ curves among different soils (Fig. 4.1). For example, when the soils were dry, λ values of all soils were approximately 0.3 W m^{-1} K^{-1} and then increased with increasing θ (Fig. 4.1A). However, the rate of increase was smaller for the finer textured soil. When the soils were near saturation, the λ values of coarse sand, fine sand, sandy loam, and silty clay were approximately 3.6, 2.4, 1.9, and 1.0 W m^{-1} K^{-1}, respectively. When the soils were dry, TN_{cum} and TN_{max} of all soils except the coarse sand were around 780 K s W^{-1} m and 1.5 K W^{-1} m, respectively. When soils were near saturation, TN_{cum} and TN_{max} of all soils except the silty clay decreased to approximately 150 K s W^{-1} m and 0.3 K W^{-1} m, respectively. The differences among different textured soils were likely caused by the different bulk densities and quartz content. As soil texture became finer and ρ_b decreased, both soil temperature increases and λ decreased (Singh and Devid, 2000) because λ of quartz is about three times greater than λ of clay minerals (Dane and Topp, 2002), and, therefore, lower soil temperature increases and λ estimates were observed it finer textured soils, which have lower quartz content (Sepaskhah and Boersma, 1979)

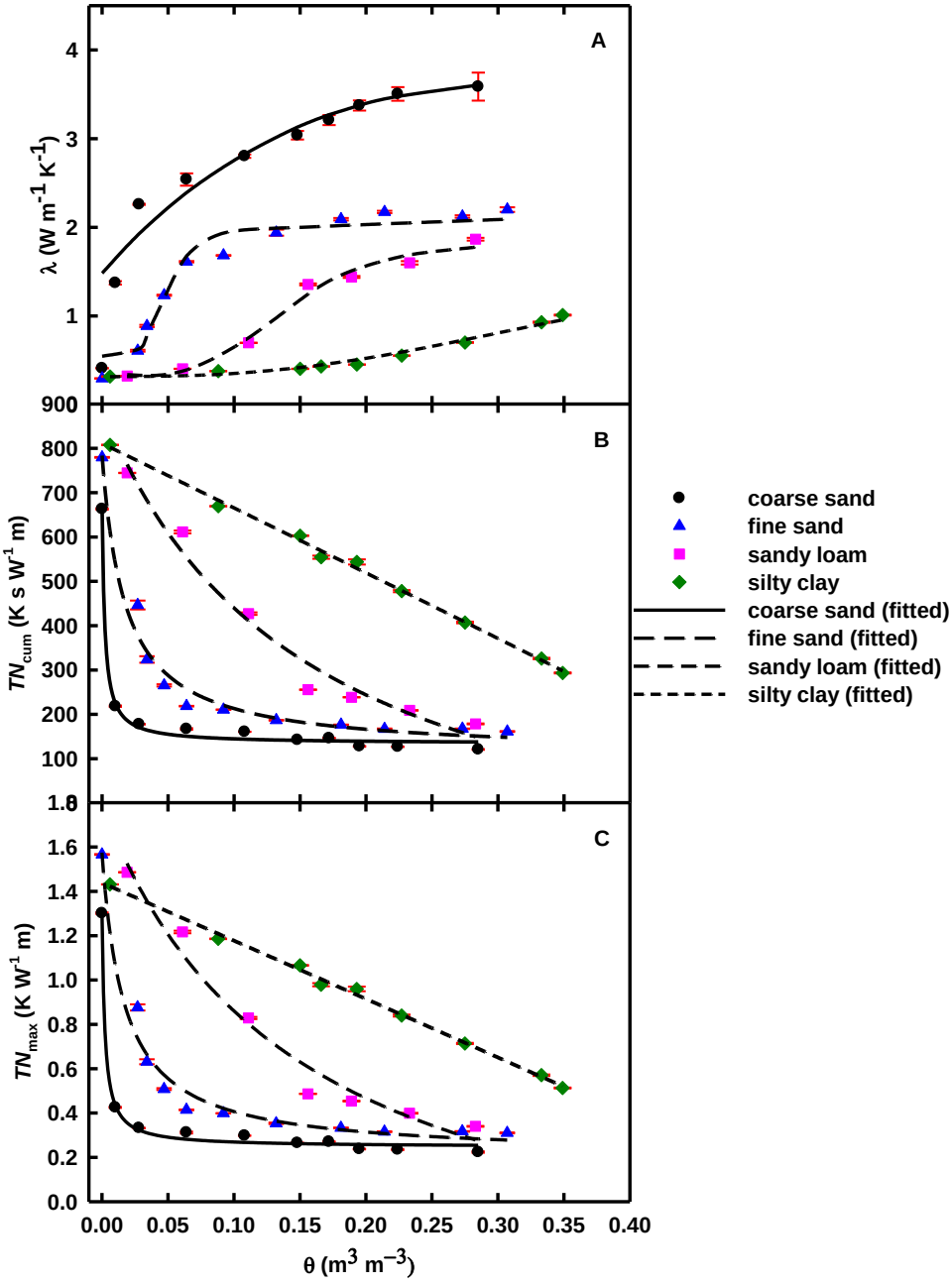

Fig. 4.1. Measured and fitted thermal conductivity (λ) (A), normalized cumulative temperature increase (TN_{cum}) (B), and normalized maximum temperature increase (TN_{max}) (C) of tested soils as a function of soil water content (θ), measured by the first probe with a heating duration of 600 s. Error bars indicate the standard deviation of four replications.

Many attempts have been made to examine and model the relationships between λ and soil texture and ρ_b (Gangadhara Rao and Singh, 1999; Singh and Devid, 2000; Côté and Konrad, 2005; Tarnawski and Leong, 2012); however, as shown by Lu et al. (2014), these models have limited success beyond a few soils. There is also limited information on the relationships between soil physical properties and $TN_{cum}(\theta)$ or $TN_{max}(\theta)$ (Sayde et al., 2010; Ciocca et al., 2012). Because of the small number of soils investigated in this study, it is still difficult to quantitatively relate the differences in $\lambda(\theta)$, $TN_{cum}(\theta)$, and $TN_{max}(\theta)$ relations among different soils to soil physical properties such as soil texture and ρ_b.

In order to predict θ, two models (Eq. 4.11 and 4.25) were fitted to the measured $\lambda(\theta)$ and $TN_{cum}(\theta)$ (and $TN_{max}(\theta)$), respectively. All curves fit the measured values well (Fig. 4.1), with correlation coefficients > 0.95. To evaluate the non-uniqueness of best-fit parameters, Monte Carlo simulation analysis was carried out according to the method of Wagener et al. (2003) and the results showed that the values of all model parameters were unique. As shown in Table 4.1 and 4.2, the parameters of the models had clear trends with the particle size fractions and ρ_b; however, these relationships are only applicable to some of the investigated soils. To fit λ, the semi-theoretical model we used described the sharp rises at the middle ranges of θ more effectively, but most of the empirical models may fit better for the coarse sand at low θ. As different models provided similar local slopes of the $\lambda(\theta)$ relationships, the θ estimation errors discussed below are not significantly affected by the choice of the models. The accuracies of the θ estimates may be affected more, depending on the accuracy of the fittings, which should be considered when selecting the $\lambda(\theta)$ models.

All error bars were very small (Fig. 4.1), indicating good repeatability among the four replicates for all measurements. The exception was the $\lambda(\theta)$ for coarse sand (0.02 to 0.16 W m^{-1}

K^{-1}) when $\theta > 0.05$ m^3 m^{-3}, but it was still small compared to the typical λ values. From the trends and slopes of the curves we can visually and qualitatively conclude that λ was more sensitive to θ for the coarser soils (coarse sand and fine sand) than for the finer soils (sandy loam and silty clay) over the full range of θ (Fig. 4.1A), due to the higher quartz contents and more continuous water films between soil particles which conducted heat better in the coarser soils. However, $TN_{cum}(\theta)$ and $TN_{max}(\theta)$ possessed good sensitivity for finer soil texture (sandy loam and silty clay) over the full range of θ, and similarly for the coarse sand and fine sand at low θ (Fig. 4.1B and C). When θ was low, the added water formed the wedge films in macro pores between the coarse sand and fine sand soil particles and then gradually filled the pores; therefore, λ increased and TN_{cum} and TN_{max} decreased rapidly within increasing θ. This increase slowed down when the field capacity exceeded, as most of the voids were filled and further increase in θ had less effect on λ (Sepaskhah and Boersma, 1979; Nikolaev et al., 2013; Lu et al., 2014). Therefore, relative low sensitivities were observed for $\lambda(\theta)$, $TN_{cum}(\theta)$, and $TN_{max}(\theta)$ curves of coarse sand and fine sand at high θ.

To quantitatively evaluate the measurement error σ_θ of θ determinations, not only the sensitivities of λ, TN_{cum}, and TN_{max} to θ, but also the standard deviations of these three properties were considered based on Eq. 4.26. Figure 4.2a shows that σ_θ of coarse sand from the three methods increased with increasing θ. The three methods had similarly small errors (less than 0.01 m^3 m^{-3}) for the coarse sand when $\theta < 0.15$ m^3 m^{-3}. However, when $\theta > 0.15$ m^3 m^{-3}, σ_θ of the coarse sand from the $TN_{max}(\theta)$ method increased rapidly from 0.01 to 0.13 m^3 m^{-3} with increasing θ, and σ_θ from the $\lambda(\theta)$ and $TN_{cum}(\theta)$ methods increased to 0.06 m^3 m^{-3}. The σ_θ of the fine sand, sandy loam, and silty clay were all similar and less than 0.01 m^3 m^{-3}, although a large error was found for the $\lambda(\theta)$ method for the dry silty clay soil due to the flat local slope of the fitted curve (Fig. 4.2B, C, and D). This result differed from that of Sayde et al. (2010) with the AHFO-DTS method,

in which they showed that σ_θ of the $T_{cum}(\theta)$ method was smaller than that of the $T_{max}(\theta)$ method. Furthermore, the errors they obtained were 0.03 and 0.08 $m^3\ m^{-3}$ at a $\theta = 0.30\ m^3\ m^{-3}$ for the $T_{cum}(\theta)$ and $T_{max}(\theta)$ methods, respectively; which were much larger than that from our study for all soils except for the coarse sand.

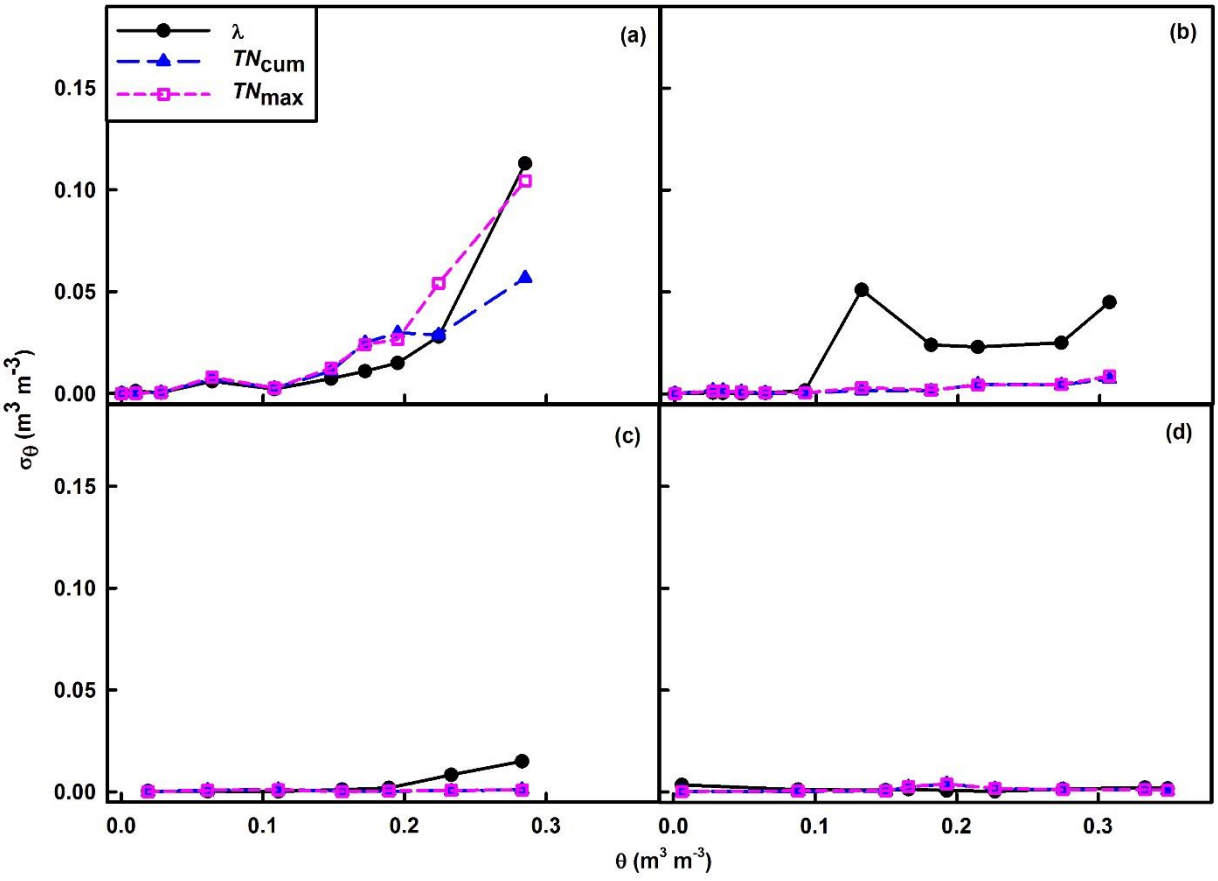

Fig. 4.2. Errors calculated from Equation 4.26 in soil water content (σ_θ) as a function of soil water content (θ) by thermal conductivity (λ)~θ relation, normalized cumulative temperature increase (TN_{cum})~θ relation, and normalized maximum temperature increase (TN_{max})~θ relation of coarse sand (A), fine sand (B), sandy loam (C), and silty clay (D), measured by the first probe with a heating duration of 600 s.

Aside from the coarse sand showing similar σ_θ to the AHFO-DTS method (Sayde et al., 2010), σ_θ from both the $TN_{cum}(\theta)$ and $TN_{max}(\theta)$ methods using the SPHP here were similar to each other and much smaller than that of the AHFO-DTS method. Possible reasons for this may be twofold: (1) the stainless steel tube of the heat pulse probe had much higher λ than the soil, and thus had

minimum resistance to heat conduction as compared to the AHFO-DTS system; and (2) the heat pulse probe is in direct contact with soils, whereas the fibre optic cable of the AHFO-DTS system is surrounded by armoured sheathing with low λ which reduced the sensitivity of the measurements. Both results of Sayde et al. (2010) and this study show that errors in θ estimates increase with an increase in θ. However, the errors in our study fluctuated slightly as opposed to changing monotonically with an increasing θ as is shown in Sayde et al. (2010). This is likely because the fibre optic cable was buried in soil columns and provided repeated measurements at the same location, whereas the measurements in this study were obtained from independent soil samples packed at each θ. The repacking of each soil could introduce additional errors due to slightly different ρ_b and particle packing.

4.5.2 Effect of the heating duration

To calculate λ, it is important to choose an appropriate range of long-time (Manohar et al., 2000) for use in Eq. 4.6. Our data showed that all the ΔT~ln(t) curves of all tested soils became linear after 50 s, which satisfies the requirement $t \gg r^2/\alpha$ (r^2/α = 5 s). A smaller diameter probe was chosen in this study to allow the ΔT~ln(t) curves to reach linearity earlier. Therefore, 50 s was chosen as the start time of the long-time solution for λ estimation. The ending time of the heat pulse (t_{end}) was chosen to be 600 s because t_{end} should be long enough to obtain accurate λ values, but also short enough to avoid the boundary effects of the soil column on heat conduction. To examine the effect of heating duration on λ, the λ values with t_{end} ranging from 120 to 600 s for each temperature response curve were calculated. The results show that λ values with t_{end} from 120 to 600 s from the same temperature response curve were almost identical for all tested soils

at all ranges of θ (data not shown). Therefore, a 120 s heating duration is sufficiently long to obtain accurate λ values for the soils and probes used in this study.

The values and curves of $\lambda(\theta)$, $TN_{cum}(\theta)$, and $TN_{max}(\theta)$ differed with different heating duration. Figure 4.3 shows that σ_θ from the $\lambda(\theta)$ method was affected by t_{end} when $t_{end} < 200$ s for all soils. However, the effect of t_{end} on σ_θ from the $TN_{cum}(\theta)$, and $TN_{max}(\theta)$ methods was negligible when $t_{end} > 10$ s (data not shown). All the errors from both the $TN_{cum}(\theta)$ and $TN_{max}(\theta)$ methods were less than 0.01 $cm^3\ cm^{-3}$ for all tested soils at various θ with t_{end} ranging from 10 s to 600 s. Therefore, to eliminate the effect of t_{end} on σ_θ from the $\lambda(\theta)$ method, a minimum 200 s duration heat pulse should be applied in this case. However, a heating duration as short as 10 s can be used for the $TN_{cum}(\theta)$ and $TN_{max}(\theta)$ methods, which is helpful when performing in situ θ monitoring with rapidly changing θ.

4.5.3 Probe dependence of the three relationships

Probe construction, in addition to the selection of either $\lambda(\theta)$, $TN_{cum}(\theta)$, or $TN_{max}(\theta)$ methods, could affect the accuracy of θ measurements. Two additional single probes with the identical dimensions were used to measure the four soils at various θ with independently repacked soil samples. The results show that the three probes provided similar λ values (data not shown), but different TN_{cum} and TN_{max} values (Fig. 4.4). The difference in the TN_{cum} and TN_{max} values between the three probes, were nearly constant at different θ, which may be caused by the different H of the three probes with their surrounding soil particles. Despite the identical lengths and diameters of the three probes, the amount of epoxy filled in the needles and the position of the heating wires could be slightly different, which may affect the heat transfer from the probe body to the soils. Therefore, the temperature increases of each probe varied unavoidably. However, the probe

construction only affects the short-time temperature rise and the λ values obtained from the long-time temperature rise were not significantly affected. Furthermore, the differences of TN_{cum} and TN_{max} between probes can be easily eliminated by one point calibration in agar-stabilized water.

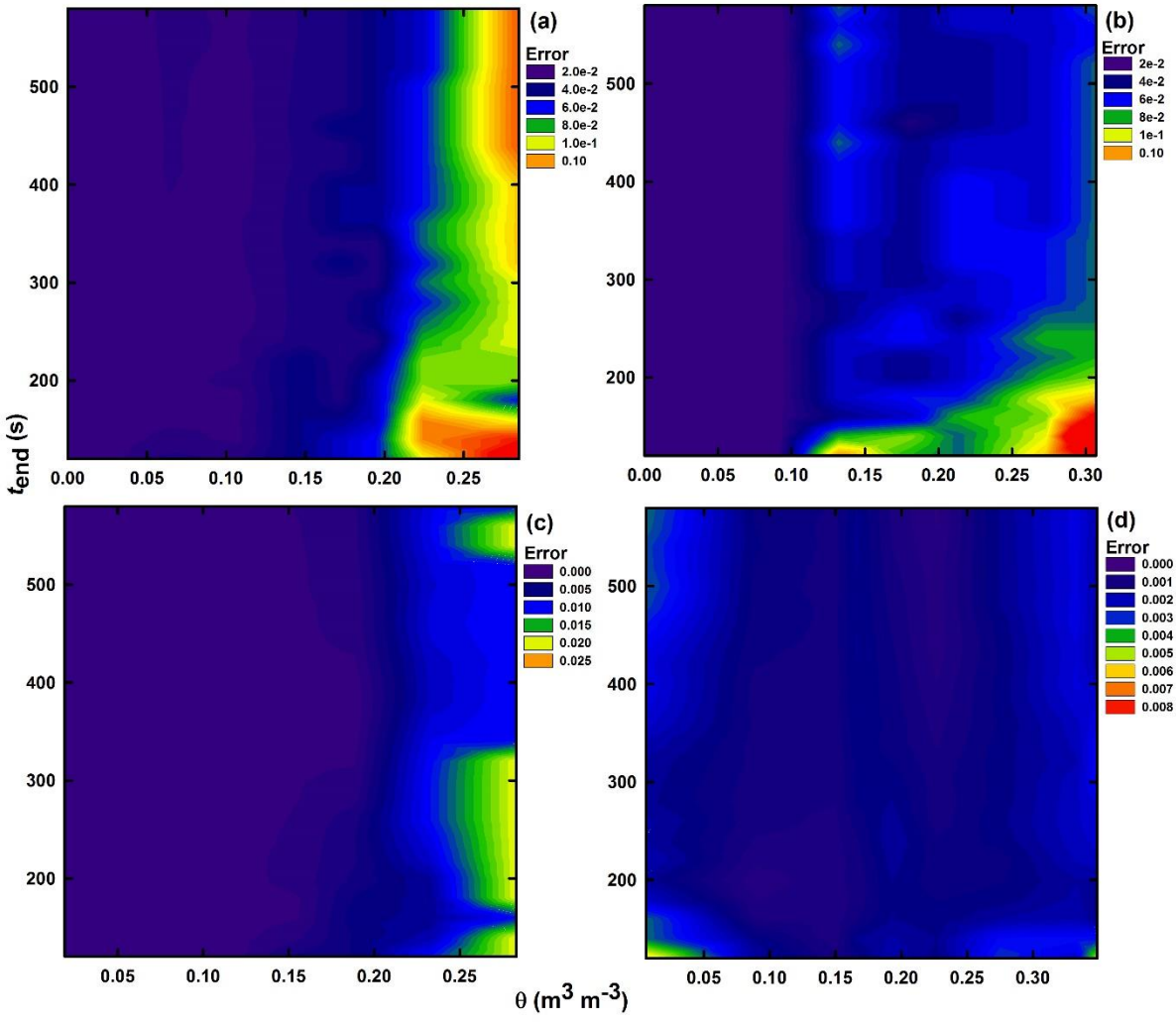

Fig. 4.3. Effect of ending time of heat pulse (t_{end}) on calculated errors in soil water content (σ_θ) as a function of soil water content (θ) by thermal conductivity~θ relation for coarse sand (A), fine sand (B), sandy loam (C), and silty clay (D) measured by the first probe.

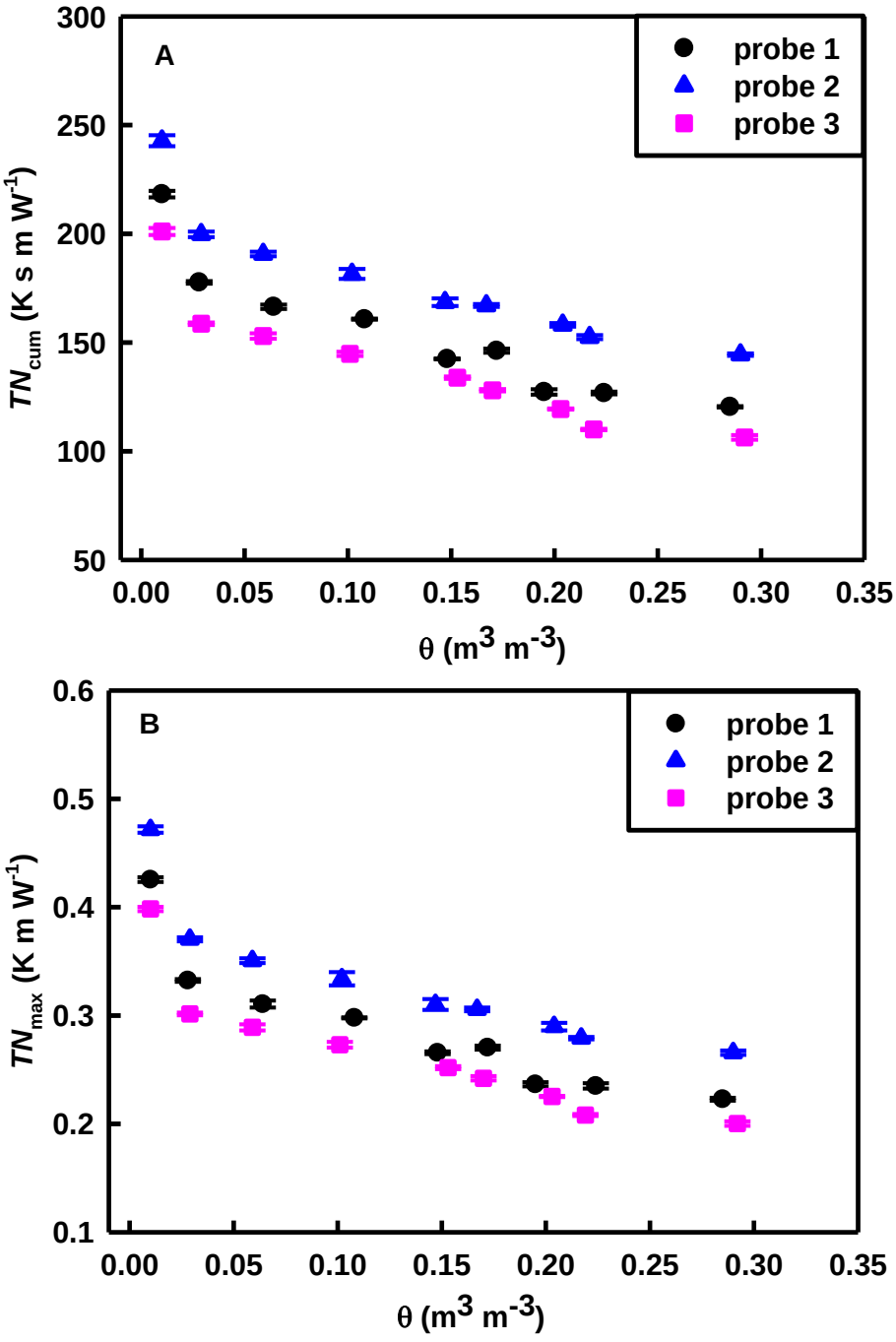

Fig. 4.4. Differences in normalized cumulative temperature increase (TN_{cum}) (A) and normalized maximum temperature increase (TN_{max}) (B) of wet coarse sand following a heating pulse of 600 s at various soil water contents (θ) between three heat pulse probes. Error bars indicate the standard deviation of four replications.

To obtain an accurate and standard calibration a priori, 5 kg m^{-3} agar-stabilized water solutions were measured by three probes. The water was stabilized by agar to avoid the convection of water caused by the temperature gradient. The results show that λ values of the agar solutions were 0.67 W m^{-1} K^{-1} from all three probes (Table 4.3). However, the TN_{cum} and TN_{max} values of the agar solutions from the second probe were 21.7 K s m W^{-1} and 0.04 K m W^{-1} higher than that from the first probe, and the TN_{cum} and TN_{max} values from the third probe were 14.2 K s m W^{-1} and 0.02 K m W^{-1} lower than that from the first probe, respectively (Table 4.3). By deducting 21.7 K s m W^{-1} from the TN_{cum} of the second probe at various θ, the calibrated TN_{cum} values as a function of θ were obtained for the second probe. Similarly, the calibrated TN_{cum} and TN_{max} values were obtained for the second and third probe.

Table 4.3. Thermal conductivity (λ), normalized cumulative temperature increase (TN_{cum}), and normalized maximum temperature increase (TN_{max}) of agar-stabilized water solution measured by three heat pulse probes with a heating duration of 600 s.

Probe	λ	TN_{cum}	TN_{max}
	W m^{-1} K^{-1}	K s m W^{-1}	K m W^{-1}
1	0.67 (0.006†)	338.9 (0.9)	0.68 (0.003)
2	0.67 (0.003)	360.6 (1.3)	0.72 (0.003)
3	0.67 (0.003)	324.7 (0.7)	0.66 (0.001)

† Numbers in parentheses are standard deviations of four replicates.

4.5.4 Soil water content determination

By inputting the λ, calibrated TN_{cum}, and calibrated TN_{max}, values of the second and third probe into the fitted models in Table 4.2, the heat pulse probe predicted θ values were obtained and compared with the measured θ values obtained by the oven-dry method. The second probe had similar θ predictions as the third probe (Fig. 4.5), which demonstrated good reproducibility between probes. For the coarse sand, the λ(θ) method provided accurate θ predictions throughout the entire range of θ, whereas the TN_{cum}(θ) and TN_{max}(θ) methods could not predict θ when θ >

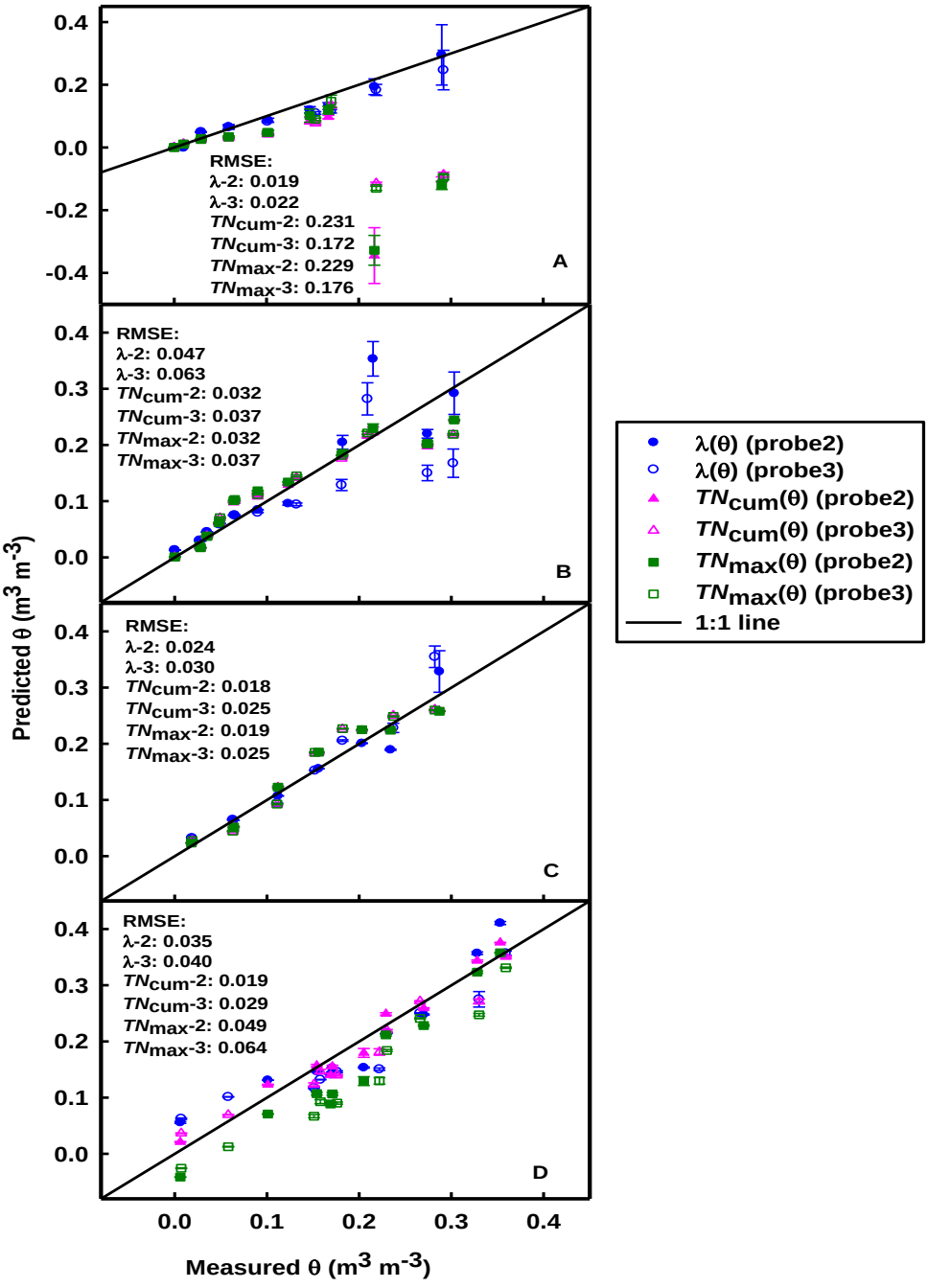

Fig. 4.5. The prediction of soil water content (θ) of coarse sand (A), fine sand (B), sandy loam (C), and silty clay (D) by the second and third probes using three methods: thermal conductivity (λ)~θ method, normalized cumulative temperature increase (TN_{cum})~θ method, and normalized maximum temperature increase (TN_{max})~θ method measured with a heating duration of 600 s. Error bars indicate the standard deviation of four replications.

0.2 m^3 m^{-3}. This is caused by the limited sensitivity (flat slopes in Fig. 4.1B and C) of TN_{cum} and TN_{max} to θ when θ > 0.2 m^3 m^{-3}, which is consistent with the result of the error analysis that the λ(θ) method had smaller errors than that of the $TN_{cum}(\theta)$ and $TN_{max}(\theta)$ methods for the coarse sand when θ > 0.2 m^3 m^{-3} (Fig. 4.2A). For the other three soils, the predicted θ from all three methods agreed well with the θ from the oven-dry method, indicated by the small and similar root mean square errors (RMSE) (RMSE < 0.063). For the fine sand, the θ predictions from the λ(θ) method at high θ departed from the 1:1 line more obviously than other methods (Fig. 4.2B), which is also due to the relatively flat local slope of the fitting (Fig. 4.2A).

As can be seen from Fig. 4.1, the TN_{cum}~θ and TN_{max}~θ relations were inversely related to the λ~θ relation. If we use the thermal resistance (1/λ) to interpret the data, the shapes and trends of the 1/λ(θ) curves of four soils were very similar to the $TN_{cum}(\theta)$ and $TN_{max}(\theta)$ curves, and the differences are in the values of the properties. Surprisingly, fitting the 1/λ(θ) curves using the rational model for the $TN_{cum}(\theta)$ and $TN_{max}(\theta)$ relations resulted in very similar measurement errors and θ predictions as the $TN_{cum}(\theta)$ and $TN_{max}(\theta)$ methods (data not shown). Similarly, the $1/TN_{cum}(\theta)$ and $1/TN_{max}(\theta)$ methods provided similar measurement errors and θ predictions as the λ(θ) method. Thus, with each SPHP measurement, a total of six properties (λ, TN_{cum}, TN_{max}, 1/λ, $1/TN_{cum}$, and $1/TN_{max}$) can be obtained.

Though the above six relationships can be obtained simultaneously from each temperature response curve, not all six relationships are suitable for all soils. Therefore, the most suitable or combination of the most suitable relationships for θ estimation must be investigated through soil-specific calibration as demonstrated in this paper. The λ(θ) combined with $1/TN_{cum}(\theta)$ or $1/TN_{max}(\theta)$ methods can be used for coarse textured soils, and the 1/λ(θ) combined with $TN_{cum}(\theta)$ or $TN_{max}(\theta)$ methods can be used for fine textured soils. In most situations, the λ(θ) and 1/λ(θ) methods are

preferred as probe-dependent calibration is not needed, which is especially convenient when more than one probe is used. It also has important implications for the state-of-the-art AHFO-DTS systems, where a heated fibre optic cable of a few kilometres long may not be identical in each 1 m segment. Furthermore, the obtained thermal property λ is needed in many other applications.

Nevertheless, the possibility of short (i.e., 10 s) heating durations for the $TN_{cum}(\theta)$, $TN_{max}(\theta)$, $1/TN_{cum}(\theta)$, and $1/TN_{max}(\theta)$ methods has practical advantages, when the heat pulse probe (either the fibre optic cable or the single heat pulse probe) is buried at a shallow depth. In that case, a short heating duration would be required to avoid the influence of the finite medium, and be useful to monitor the fast soil θ changes during precipitation. The above four methods with short heating durations are also of value when the power supply is a limitation, which is especially useful for applications at remote sites on Earth and extra-terrestrial bodies (Zent et al., 2010) or the AHFO-DTS system where a large amount of energy is needed during each measurement for a kilometres-long fibre optical cable.

4.6 Conclusions

The advantages of the SPHP over the DPHP are the larger measuring scale and free of needle deflection error. This study is the first comprehensive comparison of the $\lambda(\theta)$, $T_{cum}(\theta)$, and $T_{max}(\theta)$ methods for θ estimation using the SPHP. The $\lambda(\theta)$, $TN_{cum}(\theta)$, and $TN_{max}(\theta)$ curves differed with the tested soils. Error analyses and θ predictions from two additional probes verified that SPHP is an accurate method for measuring θ. The effect of the heating duration was examined and the result showed that it had a negligible effect on the precision and accuracy of θ determinations from all the methods for all four soils, except for the $\lambda(\theta)$ method when the heat pulse < 200 s. Different probes with identical dimensions and materials provided the same λ values, but different

TN_{cum} and TN_{max} values, which can be compensated for by calibration in agar-stabilized water. The θ values obtained from all the methods were accurate for all soils with exception given to the $TN_{cum}(\theta)$ and $TN_{max}(\theta)$ methods for the coarse sand when $\theta > 0.20$ m^3 m^{-3}. The reciprocals of λ, TN_{cum}, and TN_{max} were also examined and it showed that the $1/\lambda(\theta)$ method had similar performance as the $TN_{cum}(\theta)$ and $TN_{max}(\theta)$ methods, and the $1/TN_{cum}(\theta)$ and $1/TN_{max}(\theta)$ methods had similar performance as the $\lambda(\theta)$ method.

We improved the $T_{cum}(\theta)$ and $T_{max}(\theta)$ methods through normalization and one point calibration, and presented and validated the reciprocals of λ, TN_{cum}, and $TN_{max,}$ so that they are only soil-specific, but not *q* and probe dependent. The combination of different methods may also improve θ estimation with the SPHP. More research is needed to quantitatively establish the calibration relationships and consider the effect of soil organic matter.

5 DETERMINATION OF THERMAL CONTACT CONDUCTIVITY BETWEEN SINGLE HEAT PULSE PROBE AND SOIL

5.1 Preface

The feasibility of using the single-probe heat pulse (SPHP) method to measure soil water content (θ, $m^3\ m^{-3}$) was shown in the previous chapter. However, those methods need soil specific calibrations. In order to obtain θ and all three soil thermal properties from the SPHP method without soil specific information, the thermal contact conductivity (H, $W\ m^{-2}\ K^{-1}$) between soil and probe has to be known. However, little is known about the values of H. In this chapter, H values were inversely obtained by measuring soil samples with known θ. The effects of soil properties on H were discussed, and the possibility of θ determination by the $H(\theta)$ relationships were shown.

5.2 Abstract

The single-probe heat pulse (SPHP) method has been only used to measure soil thermal conductivity (λ, W m^{-1} K^{-1}). If thermal contact conductivity (H, W m^{-2} K^{-1}) between the single probe and soil can be accurately obtained, then the SPHP can also determine soil thermal diffusivity (α, m^2 s^{-1}), heat capacity (C, J m^{-3} K^{-1}) and soil water content (θ, m^3 m^{-3}). This study experimentally determined H of the single probe by fitting the Blackwell equation to the temperature response curve with known oven-dried θ, and explored the feasibility of θ estimation from the $H(\theta)$ relations. Four soils (the coarse sand, fine sand, sandy loam, and silty clay) packed at fixed bulk densities (ρ_b, kg m^{-3}) over a wide range of θ were measured by three single probes. The temperature response curves were recorded following a 400 s continuous heat pulse with the heating strength (q, W m^{-1}) of 5 W m^{-1}. The results showed that H values of the four soils ranged between 180 and 5400 W m^{-2} K^{-1} and H of the same soil increased with increasing θ. At the same θ, H values decreased as soil texture became finer. The $H(\theta)$ relations were linearly fitted; however, the slopes and intercepts of three probes for the same soil were different. By unifying these differences, probes 2 and 3 provided satisfactory θ estimates for all soils ($\pm$ 0.04 m^3 m^{-3}) except for the coarse sand. The probe body and ρ_b also influence H values and more research is needed to quantify the difference of H between different probes and to relate the $H(\theta)$ relation parameters to soil physical properties.

5.3 Introduction

Accurate in situ determination of soil thermal properties is important in soil physics, hydrology, and environmental science, as soil thermal properties control the energy balance of the Earth's surface and the temperature regime of the root zone (de Vries and Peck, 1958a; C. et al.,

1998; Nikolaev et al., 2013). Soil thermal properties, including λ, *C* and α, vary mainly with θ in the field. Changes in θ result in changes in soil thermal properties; and conversely, soil thermal properties affect soil energy balance and latent and sensible heat fluxes, which in turn affect the soil water balance (Liu and Si, 2011b; Trautz et al., 2014). Furthermore, soil temperature regime and θ are two of the most important factors that influence the plant growth, nutrient cycling, and microbiological activities in soils (Song et al., 1999; Abu-Hamdeh, 2001). Knowledge of soil temperature and θ in agricultural land, which are affected by soil thermal properties, helps determine the optimum time for seeding and irrigation (Wierenga et al., 1969). Therefore, it is important to measure soil thermal properties and θ simultaneously at the same measuring scale and by a single instrument.

Popular methods for measuring soil thermal properties are the heat pulse methods (hot needle/plate method), including the steady-state method and transient method. Due to the stringent boundary condition requirement and usually long equilibrium time, the steady-state hot plate method is not suitable for in situ soil thermal property measurement (de Vries, 1952; de Vries and Peck, 1958a). The transient heat pulse probe methods, including the SPHP and dual-probe heat pulse (DPHP), are the only available method that can be appropriately used to measure soil thermal properties in situ (Bristow et al., 1994b). The advantages of the heat pulse probe methods include low cost, automated and continuous data acquisition, and minor disturbance to the soil (Zhang et al., 2011).

However, the existence of thermal contact resistance between the probe body and soil, which is caused by the limited actual contact areas at the soil-probe interface (Cooper et al., 1969), limited the applications of both the SPHP and DPHP,. It has been shown that the interface between two lightly-touched, flat surfaces is rough when viewed through a microscope (Lorenzini et al.,

2016), causing a heat flux resistance at the interface. This resistance is defined as the ratio of the temperature drop at the probe-soil interface to the average heat flux across the interface, and is more frequently quantitatively described by its inverse, *H* (Fletcher, 1988; Sauer et al., 2007).

Thermal contact conductivity is intensively investigated in engineering because of its importance in many heating related applications, such as: the heat flux between the rocket surface insulation material and atmosphere, or between two metallic materials, the heat management of solid oxide fuel cell, and the cooling system design of the electronic devices (Wang et al., 2012; Ghalambor et al., 2013; Goodarzi et al., 2014; Dillig et al., 2015). Nonetheless, it is difficult to access *H* analytically in most studies because of difficulty in measuring the contact area, and therefore the empirical corrections from experimental studies are generally used. Even though many models have been built to investigate *H* between two flat/rough surfaces for different materials (Bahrami et al., 2004a; b; Jeng et al., 2006; Cui et al., 2014; Lorenzini et al., 2016), these models have limited applications in determining *H* between the heat pulse probe and soil particles, because soil is a porous medium (Fletcher, 1988). Furthermore, *H* is affected by soil particle dimensions, shape, and arrangement, which are difficult to characterize in the field soils (Sauer et al., 2007).

The unknown *H* limited the application of the SPHP in determining all the three soil thermal properties. The SPHP method has been used to measure λ of liquids (Van Der Held and Van Drunen, 1949; Nagasaka, 1981), dry and wet soils (Blackwell, 1954; de Vries and Peck, 1958b), frozen soils (Penner, 1970; Slusarchuk and Watson, 1975), rocks (Woodside and Messmer, 1961b; Cull, 1974), and snow (Jaafar and Picot, 1970); however, α and *C* cannot be obtained from the SPHP due to the unknown *H* values. Blackwell (1954) devised the simple approximations for both the short-time and long-time solutions. The long-time solution is used to determine λ, and the

short-time solution is used to determine H, thus α, C and θ. However, accurate determination of H remained difficult due to the insufficient data points to fit the short-time temperature response curve. Recently, the use of high-frequency (20 Hz) dataloggers made it possible to obtain α and H values of methane hydrate from the short-time solution (Waite et al., 2006), but showed large uncertainties. Accurate H values of dry soils were obtained (Liu and Si, 2011a) with the same method; however, it is problematic when applied on wet soils.

The DPHP method is relatively less affected by H. The temperature sensor needle of a dual probe is usually located 5 to 10 mm away from the heater needle, and α and C can be calculated without knowing H from the time and the value of the maximum temperature increase of the temperature sensor following a short period of heat pulse (Bristow et al., 1994a). Then λ and θ can be obtained from α and C. Therefore, by assuming zero thermal contact resistance (infinite large H value) and using the pulsed infinite line source approximation (Noborio et al., 1996; Hopmans et al., 2002; Liu and Si, 2010; Knight et al., 2012), all the three soil thermal properties and θ can be obtained simultaneously by the DPHP method (Campbell et al., 1991; Kluitenberg et al., 1993; Bristow et al., 1994a). However, the finite H values and probe length, and the existence of probe radius (r) and probe heat capacity (C_p) may cause an underestimation of λ and overestimation of C for the DPHP method (Baker and Goodrich, 1987; Tarnawski et al., 2009; Liu et al., 2012; Macher et al., 2014).

Compared to the dual probe, the single probe needle is more robust in the field and has a large zone of influence. Besides, the single probe method is not affected by needle deflections which can cause large errors on soil thermal properties measured by the DPHP (Liu et al., 2008a). Therefore, a better understanding of H for the single probes may improve the SPHP for simultaneous soil thermal properties and θ measurement. It also helps improve another advanced

technique – the active heated fibre optic-distributed temperature sensing (AHFO-DTS), which utilizes similar principles as the SPHP, but extends the measuring scale from conventional point scale to kilometers scale (Sayde et al., 2010). Also due to unknown *H* values, the AHFO-DTS can only estimate θ from the empirical relationships between θ and cumulative temperature increase (Sayde et al., 2010), maximum temperature increase (Striegl and Loheide, 2012), or λ (Ciocca et al., 2012). The dependence on soil texture and ρ_b of the above mentioned relationships limit the applications in practice.

To date, little is known about the accurate values of *H* between the heat pulse probe and soils (Goto and Matsubayashi, 2008; Liu and Si, 2011a; Macher et al., 2013, 2014; Dang and Leong, 2015). The objective of this paper was to experimentally determine *H* between the single probe and different textured soils over a wide range of θ, and to evaluate the possibility of estimating θ from obtained *H*(θ) relations. With known *C* calculated from oven-dried θ and λ obtained by the long-time solution of the Blackwell (1954) equation, *H* was obtained by fitting the Blackwell equation to the temperature response curves. The issues of obtaining *H* from the conventional short-time solution of Blackwell equation, as well as the effects of soil textures, θ, ρ_b and probe body on *H* values were discussed.

5.4 Materials and methods

5.4.1 Theory

For an infinite cylindrical heat source of radius *r* (m) that is surrounded by homogeneous infinite soil, if the heat is liberated continuously at a constant heating strength *q* (W m^{-1}), the radial heat flow equations are given as (Blackwell, 1954)

$$\frac{\partial^2 \Delta T_2}{\partial \rho^2} + \frac{1}{\rho}\frac{\partial \Delta T_2}{\partial \rho} = \frac{1}{\alpha}\frac{\partial \Delta T_2}{\partial t} \quad r < \rho < \infty \quad t > 0 \tag{Eq. 5.1}$$

$$\Delta T_1 = \Delta T_2 = 0 \quad t = 0 \tag{Eq. 5.2}$$

$$-\lambda \frac{\partial \Delta T_2}{\partial \rho} = H(\Delta T_1 - \Delta T_2) \quad \rho = r \quad t > 0 \tag{Eq. 5.3}$$

$$-\lambda \frac{\partial \Delta T_2}{\partial \rho} = \frac{q}{2\pi r} - \frac{r C_p}{2}\frac{\partial \Delta T_1}{\partial t} \quad \rho = r \quad t > 0 \tag{Eq. 5.4}$$

$$\Delta T_2 \text{ is bounded as } \rho \to \infty \tag{Eq. 5.5}$$

where H (W m^{-2} K^{-1}) is the thermal contact conductivity, ΔT_1 and ΔT_2 are the temperature changes from the initial temperature of the probe and soil (˚C), respectively; ρ is the radial coordinate, λ and α are thermal conductivity (W m^{-1} K^{-1}) and thermal diffusivity (m^2 s^{-1}) of soil, respectively; C_p is the heat capacity of probe (J m^{-3} K^{-1}), and t is time (s).

Laplace transformation of the above differential equations and boundary conditions with respect to t results in

$$\frac{\partial^2 \textcircled{T}_2}{\partial \rho^2} + \frac{1}{\rho}\frac{\partial \textcircled{T}_2}{\partial \rho} = \frac{p}{\alpha}\textcircled{T}_2 \quad r < \rho < \infty \tag{Eq. 5.6}$$

$$-\lambda \frac{\partial \textcircled{T}_2}{\partial \rho} = H(\textcircled{T}_1 - \textcircled{T}_2) \quad \rho = r \tag{Eq. 5.7}$$

$$-\lambda \frac{\partial \textcircled{T}_2}{\partial \rho} = \frac{q}{2\pi r p} - \frac{r C_p p}{2}\textcircled{T}_1 \quad \rho = r \tag{Eq. 5.8}$$

$$\textcircled{T}_2 \text{ is bounded as } \rho \to \infty \tag{Eq. 5.9}$$

where p is the Laplace transformation variable; $\textcircled{T}_1$ and $\textcircled{T}_2$ are the Laplace transforms of ΔT_1 and ΔT_2, respectively. Solution of Eq. 5.6 subject to Eq. 5.7, 5.8, and 5.9 gives

$$\textcircled{T}_1 = \frac{q\Gamma}{\pi p\left[r^2 C_p p\Gamma + 2\lambda K_1\left(\sqrt{\frac{p}{\alpha}}r\right)\right]} \quad \text{(Eq. 5.10)}$$

where $\Gamma = \frac{Y_0\left(\sqrt{\frac{p}{\alpha}}r\right)}{\sqrt{\frac{p}{\alpha}}r} + \frac{\lambda Y_1\left(\sqrt{\frac{p}{\alpha}}r\right)}{rH}$, $Y_0(x)$ and $Y_1(x)$ are modified Bessel functions of the second kind, zero and first orders, respectively. The Gaver-Stehfest (Stehfest, 1970) inverse Laplace transform algorithm were used in Mathcad 15.0 (PTC Inc., Needham, MA) software to solve Eq. 5.10.

This solution can be simplified to calculate λ using the long-time approximation (Blackwell, 1954):

$$\Delta T_1(t) = A\ln(t) + B \quad t \gg \frac{r^2}{\alpha} \quad \text{(Eq. 5.11)}$$

where

$$A = \frac{q}{4\pi\lambda} \quad \text{(Eq. 5.12)}$$

$$B = \frac{q}{4\pi\lambda}\left[\ln(\alpha) - 2\ln(r) + \ln(4) - \gamma + \frac{2\lambda}{rH}\right] \quad \text{(Eq. 5.13)}$$

where γ is Euler's constant = 0.5772. The A and B can be obtained by linear fitting ΔT_1~ln(t) curve at the long-time range to Eq. 5.11, and then λ can be calculated by Eq. 5.12.

The Blackwell short-time solution can be expressed as (Blackwell, 1954; Liu et al., 2012)

$$\Delta T_1(t) = Z_1 t - Z_1 Z_2 t^2 + Z_1 Z_2 Z_3 t^{2.5} \quad t \ll \frac{r^2}{\alpha} \qquad \text{(Eq. 5.14)}$$

where Z_1, Z_2, and Z_3 are the fitting parameters, and H can be obtained by

$$H = \frac{q}{\pi r}\frac{Z_2}{Z_1} \quad t \ll \frac{r^2}{\alpha} \qquad \text{(Eq. 5.15)}$$

If H is known, α can be obtained from Eq. 5.13. Then C can be calculated by $C = \lambda / \alpha$, and θ can be obtained by

$$\theta = \frac{C - \rho_b c_s}{\rho_w c_w} \qquad \text{(Eq. 5.16)}$$

where c_s and c_w are the specific heat capacity of soil mineral and water ($c_w = 4.18 \times 10^3$ J kg^{-1} K^{-1} at 20 ˚C), ρ_w is the density of water (ρ_w = 1000 kg m^{-3} at 20 ˚C).

As H value from the Blackwell short-time solution is subjected to large errors depending on the selection of the short-time range, we obtained H in the following way with known θ as follows: The value of C was calculated from Eq. 5.16 for a given θ and ρ_b, and λ was obtained from the long-time solution. Then α was obtained from $\alpha = \lambda / C$, and H was obtained by fitting the inverse Laplace transform of Eq. 5.10 to the temperature response curve.

The linear regression was used to fit the $H(\theta)$ relations of four soils measured by three probes with the same sizes and materials. As the $H(\theta)$ relations from three probes may be different for the same soil at the same θ, the following calibration method was used to eliminate the difference between probes. Suppose the $H(\theta)$ relations of the same soil at the same θ measured by probes 1 and 2 were

$$H_1 = a_1\theta + b_1 \quad \text{(Eq. 5.17)}$$

$$H_2 = a_2\theta + b_2 \quad \text{(Eq. 5.18)}$$

respectively. Combining Eq. 5.17 and 5.18, we get

$$H_1 = \frac{a_1}{a_2}H_2 + b_1 - \frac{a_1}{a_2}b_2 \quad \text{(Eq. 5.19)}$$

Taking H_1 as the benchmark, Eq. 5.19 can be used to adjust H values from probes 2 and 3. Then the adjusted values of H from probes 2 and 3 were treated as two replicates to evaluate the θ predictions based on the $H(\theta)$ linear relationships obtained from probe 1 for the four soils. The root mean square error (RMSE) and bias of the estimations were calculated to evaluate the performance of θ estimations:

$$RMSE = \sqrt{\frac{\sum(\theta_m - \theta_e)^2}{n}} \quad \text{(Eq. 5.20)}$$

$$bias = \frac{\sum(\theta_m - \theta_e)}{n} \quad \text{(Eq. 5.21)}$$

where n is the number of data points, θ_m and θ_e are the measured and estimated θ (m^3 m^{-3}), respectively.

5.4.2 Soil column setup and soil sample preparation

Three single heat pulse probes with the same dimensions and construction were built as three replicates. Each probe is made of stainless steel needle (Penn Stainless Products, Quakertown, PA) and is 11 cm in length with an outer and inner diameters of 2.108 mm and 1.240 mm, respectively. A thermistor (10 KΩ at 25 ˚C, Model 10K3MCD1, BetaTHERM Corp., Shrewsbury, MA) was

placed in the center of the hollow needle. A one-loop nichrome wire (Nichrome A, electrical resistance is 69.06 Ω m^{-1}, Pelican Wire Co., Naples, FL) was inserted into the needle and the needle was subsequently filled with Omegabond 101 epoxy (Omega Engineering, Stamford, CT), which has a relatively high λ and is an excellent electrical insulator. The needle was secured into a predrilled hole in a 32-mm-diameter and 32-mm-thick plastic plug. The plug was then installed at the bottom of a cylindrical PVC container (13 cm in height and 10 cm in diameter) which was used to house the soil sample. The ends of the heating wires and thermistors were soldered to 18 AWG electrical wires and connected to a datalogger (Model CR9000XC, Campbell Scientific, Logan, UT) for data collection.

The datalogger was used to control the heat input, to monitor the electric current through the heater, and to measure the temperatures of the sensor as a function of time. Three adjustable resistors and a heater-control relay circuit were used to control and measure the amount of heat released from the three probes. A continuous heating duration of 400 s ($q \approx 5$ W m^{-1}) was applied and the temperature was recorded with a frequency of 20 Hz for each probe. The heat pulses were executed four hours after the soil samples were packed into the columns to permit enough time for the ambient temperature to reach equilibrium. The temperatures five minutes before each heat pulse were recorded to double check the equilibrium. In the cases of non-equilibrium during our measurement, corrections were conducted using the linear interpolation method presented by Jury and Bellantuoni (1976).

Four different textured soils were tested: the coarse sand (Industrial quartz sand, Unimin, New Canaan, CT), fine sand (collected from the Great Sand Hills, Saskatchewan), sandy loam (collected in Central Butte, Saskatchewan) and silty clay (collected in Saskatoon, Saskatchewan). All soils were air-dried and then passed through a 2 mm sieve to remove roots and other debris.

Soil texture was determined by the pipette method (Dane and Topp, 2002) and was classified based on the U.S. Department of Agriculture Classification (Table 5.1). Each soil was measured at θ ranging from air-dry to around 0.30 m^3 m^{-3}. There were four replicates of measurement at each θ. The pre-determined amount of water was spread on to soil sample, mixed in a plastic bag, shaken to distribute water uniformly and then packed into soil column. The actual θ was double checked by the standard oven-dry method after each heat pulse measurement. Because of the abundance of macro-pores in the coarse sand (all soil particle sizes larger than 1 mm) and the effect of gravity, the soil could not be packed to obtain uniform θ at the middle range of water contents. Therefore, the coarse sand were only tested at lower θ and higher θ. At the middle range of θ, we used 5 kg m^{-3} agar stabilized water instead of liquid water for the coarse sand measurement at θ from 0.03 m^3 m^{-3} to 0.30 m^3 m^{-3}. The dry ρ_b of each soil packed in the soil columns were shown in Table 5.1.

Table 5.1. Sand, silt, and clay contents, specific heat of solids (c_s) and dry bulk densities (ρ_b) of four soils.

Soil texture	Clay content (%)	Silt content (%)	Sand content (%)	c_s at 20 °C (J kg^{-1} K^{-1})	ρ_b (kg m^{-3})
Coarse sand	0 (0†)	0 (0)	100 (0)	721	1.75×10^3
Fine sand	2.3 (0.3)	0.3 (0.01)	97.4 (0.3)	848	1.56×10^3
Sandy loam	12.3 (0.3)	22.3 (0.8)	65.5 (0.6)	897	1.43×10^3
Silty clay	43.6 (1.2)	41.9 (0.2)	14.5 (1.0)	867	1.25×10^3

† Numbers in parentheses are standard deviations of the replications.

The value of c_s was measured by a modulated differential scanning calorimetry (MDSC) technique (Model Q2000, TA instruments, New Castle, DE) (Kozlowski, 2012). The soil dry solids ($m_{soil} \approx 10$ mg) were compressed into a hermetic aluminum pan ($m \approx 55$ mg). All the samples were put in the MDSC machine and equilibrated initially at 20 ˚C for five minutes, followed by the application of modulated temperature at ± 0.5 ˚C every 120 s for 10 min. The MDSC was

calibrated by using a standard sample with a known specific heat capacity (sapphire, in this study). The temperature change of the samples versus time under a heat flow signal was recorded by the MDSC machine, and the specific heat capacity was obtained directly through the TA Universal Analysis software (TA instruments, New Castle, DE). Details about the MDSC method used here refers to Li et al. (2015) and the results of c_s are shown in Table 5.1.

To obtain H, C_p of the three probes in Eq. 5.10 need to be known. The single probe bodies were not only made of stainless steel, but also contained a mounted loop of heating wire, temperature sensor and epoxy. The small differences in C_p of each of the components and in the heating wire's installation may cause the C_p of the three probes to be different from each other and from that of stainless steel. To solve this problem, C_p of each probe was calibrated in an agar-stabilized water solutions, with known thermal properties. The measured values of C_p for the three probes were 3.2 (±0.3)×10^6, 2.8 (±0.3)×10^6, and 4.5 (±0.3)×10^6 J m^{-3} K^{-1}, respectively.

5.5 Results and Discussion

5.5.1 Soil thermal conductivity and thermal diffusivity

A typical temperature increase ΔT in the single probe as a function of ln(t) curve is shown in Fig. 5.1A and seemed to be linear after 50 s. The residuals showed no obvious trends with time, indicating adequate fit by a linear regression in the time range of 50 to 400 s (Fig. 5.1B), and this behavior applied to all the measured ΔT~ln(t) curves (data not shown for brevity). Furthermore, the use of Eq. 5.11 requires $t \gg r^2/\alpha$, where r = 0.0011 m and the smallest $\alpha = 3\times10^{-7}$ m^2 s^{-1} from the four soils (Fig. 5.2A). As a result, the largest r^2/α value was 4 s, which was 10 times smaller than 50 s. Therefore, 50 s was considered as the beginning of the long-time and data points from 50 to 400 s were chosen to calculate λ using Eq. 5.11.

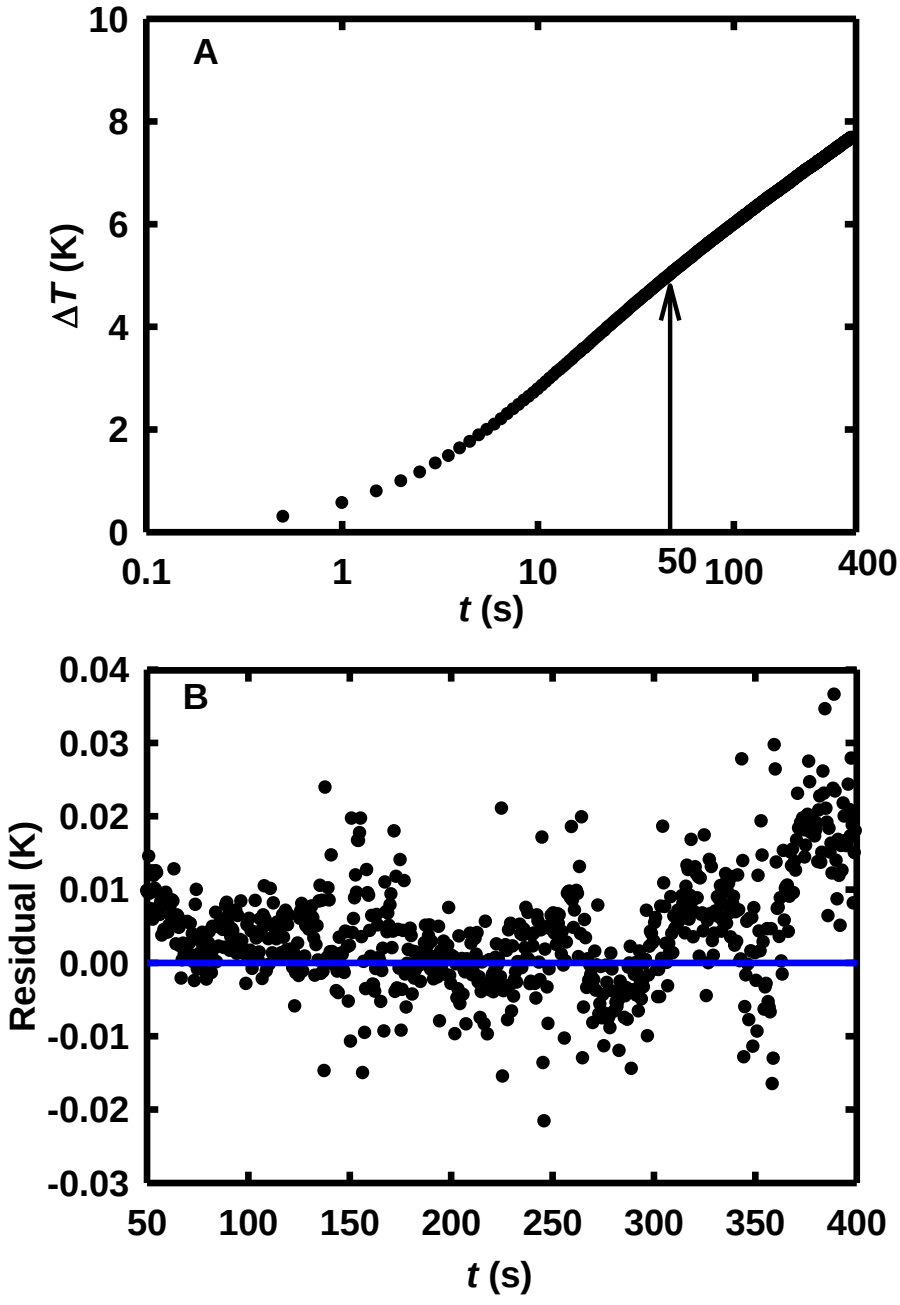

Fig. 5.1. (A) Typical temperature increases (Δ*T*) as a function of logarithmic time (*t*) curve measured by a single heat pulse probe with measuring frequency of 2 Hz and (B) the residual plot of its linear regression of the Δ*T*~ln(*t*) relation at 50 to 400 s time range.

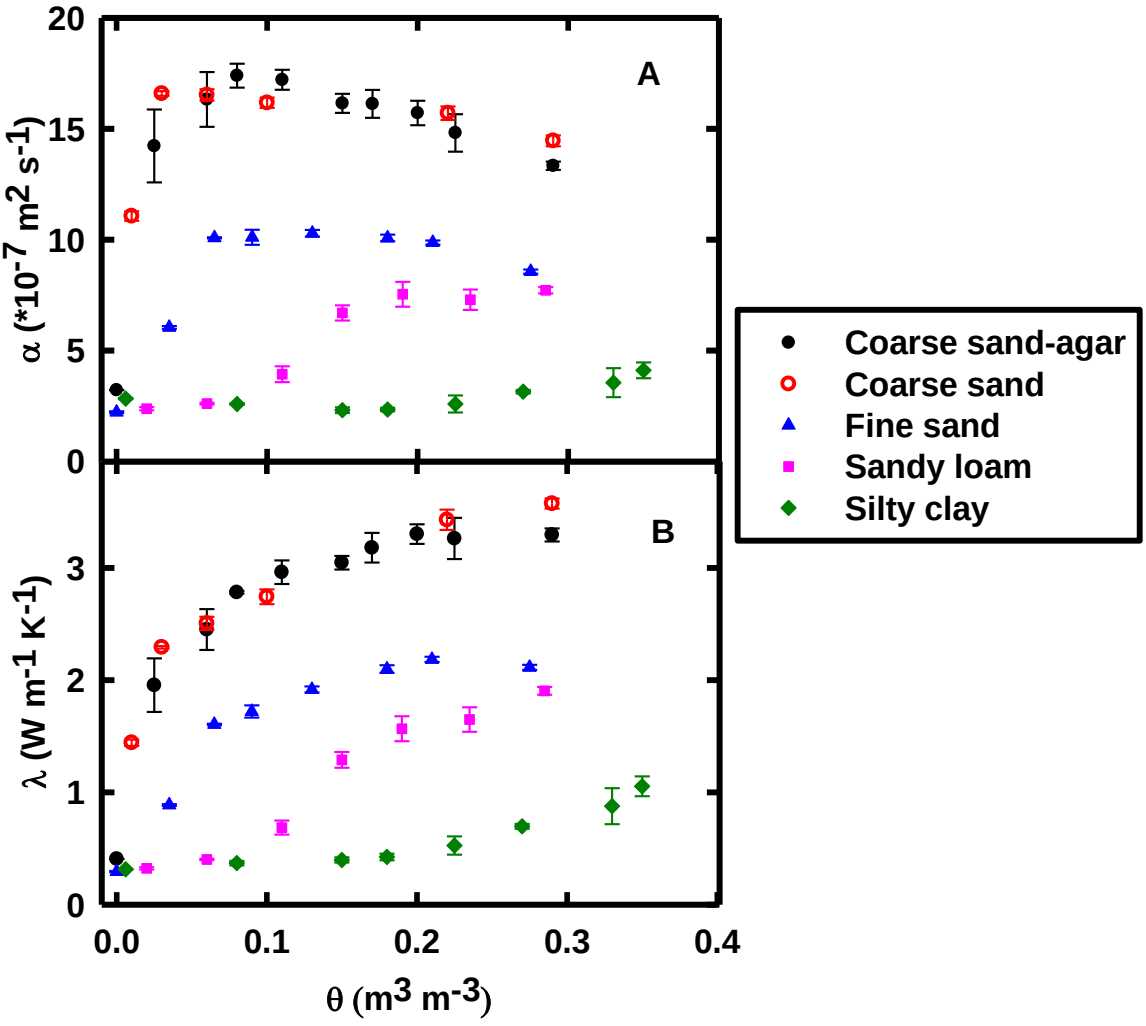

Fig. 5.2. (A) Thermal diffusivity α and (B) thermal conductivity λ of soils at various water contents θ. Error bars indicate the standard deviations in λ or α values of the three probes.

As shown in Fig. 5.2B, λ values were between 0.3 and 0.5 W m^{-1} K^{-1} for the dry soils, and λ increased with increasing θ. For the coarse sand and fine sand, there was a rapid increase of λ with increasing θ when θ < 0.10 m^3 m^{-3} and slightly afterwards; whereas for the sandy loam and silty clay, λ increased slightly when θ increased from 0 to 0.10 m^3 m^{-3}, and then increased more rapidly from 0.10 to 0.20 m^3 m^{-3}. When the soils were at the same θ, λ values were lower for the finer textured soil. As a note, both λ and α of the coarse sand obtained from the agar-stabilized water and liquid water were similar (Fig. 5.2), suggesting the agar-solution did not affect thermal

properties of the coarse sand even though the status of water was changed from liquid to gel. This result was consistent with that obtained by Liu and Si (2010).

When the soils were dry, α of all the four soils were around 3×10^{-7} m^2 s^{-1} (Fig. 5.2A). As θ increased, α increased sharply to 1.6×10^{-6} m^2 s^{-1} for the coarse sand and to 1.0×10^{-6} m^2 s^{-1} for the fine sand at $\theta = 0.05$ m^3 m^{-3}, and then decreased gradually as θ continued to increase. Thermal diffusivities of the sandy loam increased to a peak value of 7×10^{-7} m^2 s^{-1} at $\theta = 0.2$ m^3 m^{-3}, and that of silty clay increased to only 4×10^{-7} m^2 s^{-1} at $\theta = 0.35$ m^3 m^{-3}. Most of the standard deviations of λ and α were smaller than 0.1 W m^{-1} K^{-1} and 6×10^{-8} m^2 s^{-1}, respectively, indicating that the three probes provided very similar λ and α values. There were several exceptions with higher standard deviations (Fig. 5.2); however, they were still small compared to the λ and α values. For example, λ and α had the largest standard deviations at $\theta = 0.03$ m^3 m^{-3}, but they were only 12% of the λ and α values. Therefore, the λ and α values were soil dependent, but were probe independent. This result is consistent with that of Macher et al (2013), who showed that the difference between heat pulse probes due to the existence of H only causes a shift of the $\Delta T \sim \ln(t)$ curve, but does not affect the slope of the curve from where λ is calculated. Therefore, the effect of H on λ determined from the slope of the $\Delta T \sim \ln(t)$ curve is negligible. Note that λ and α had low sensitivity to θ change for finer materials, suggesting inferring θ from the λ~θ relation as indicated by Ciocca et al. (2012) may be problematic with the SPHP or the AHFO-DTS method.

5.5.2 Thermal contact conductivity

5.5.2.1 Issue with the short-time solution of Blackwell equation

Obtaining H from the short-time solution was benefited by the recent development of high-frequency dataloggers that allows for more data points collected (Waite et al., 2006); however,

large errors may be caused by the selection of the short-time range. For example, Liu and Si (2011b) used the data points collected at a as high as 20 Hz frequency during the initial 1.2 s for the short-time solution. The range of short-time should be $t \ll r^2/\alpha$ where r is a constant for a probe, and the obtained α values of all dry soils were around 2.7×10^{-7} m^2 s^{-1}, which was similar to that of our results (Fig. 5.2A). However, when the soils are wet, α varies as θ and soil texture change, which means that a suitable short-time range may be different from soil to soil and vary with θ.

To examine the errors on H due to the different selection of the short-time range, the CR9000XC datalogger (Campbell Scientific, Logan, UT) with an even higher measuring frequency (100 Hz) was used here. Another advantage of the high frequency is that more accurate value of the time-lag of the thermistor's temperature response can be detected. It shows that the temperature of the thermistor increased immediately (Fig. 5.3A), indicating the time-lag was smaller than 0.01 s. This result was different from that observed by others, such as 0.08 s by Liu and Si (2011b) and 0.2 s by Waite et al. (2006). Nevertheless, fitting data points in 0 to 0.9 s time range may cause more than 70% relative error in the estimated H as compared to fitting data in 0 to 1.2 s time range (Fig. 5.3A), even with such high-frequency and high-precision temperature data (Fig. 5.3B). Different time range would result in substantially different α, indicating the short-time approximation may not be valid. Therefore, the short-time solution of the Blackwell equation was not suitable for the wet soils in practice.

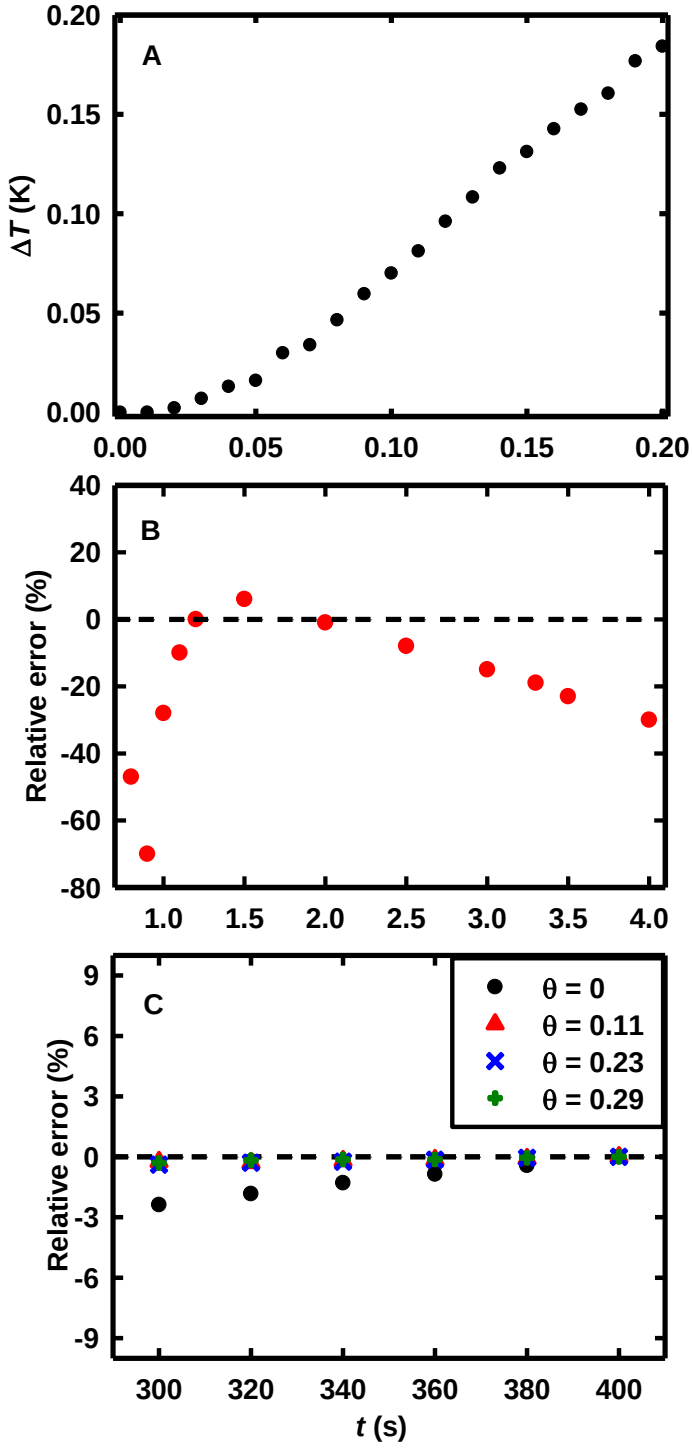

Fig. 5.3. (A) Typical temperature increase (ΔT) as a function of time (t) curve at the first 0.2 s with measuring frequency of 100 Hz; and (B) relative errors of thermal contact conductivity between the dry coarse sand and probe 1 obtained from the short-time solution using different time ranges (0 to 0.8-2.5 s) as compared to 0 to 1.2 s; and (C) relative errors of thermal contact conductivity between the coarse sand and probe 1 at various water contents (θ, $m^3\ m^{-3}$) obtained by curve fitting the inverse Laplace transform of Equation 5.10 using different time ranges from 0 to 300-400 s as compared to 0 to 400 s.

5.5.2.2 Full time range solution of inverse Laplace transform of Blackwell equation

Instead of using the short-time solution, we obtained *H* by fitting the inverse Laplace transform of Eq. 5.10 to the temperature data for the full time range from 0 to 400 s. It shows that the obtained *H* was not affected by the time range selection as compared to the short-time solution (Fig. 5.3C). For example, fitting data points from 0 to 300 s instead of from 0 to 400 s only caused less than 2.5% and 0.5% relative errors on *H* for dry and wet soils, respectively (Fig. 5.3C). The time range independence is a great advantage for the full time range curve fitting using the inverse Laplace transform method as compared to the short-time solution. The *H* values of four soils at various θ from the curve fitting method were presented in Fig. 5.4. The effects of θ, ρ_b, and soil texture on *H* values will be discussed below.

For a specific in situ soil, θ is the dominant factor that control *H*. Similar to λ, *H* of the coarse sand with agar-stabilized water did not show obvious differences from that with the liquid water (Fig. 5.4A). The *H* value of the coarse sand increased with increasing θ. When soil was dry, there was only a small portion of the soil particle surface touching the probe body; consequently, *H* was very small with around 600 W m^{-2} K^{-1} for all three probes. When the soils were wet, the water occupied some of the void space between probe and soil, thus there was increased contact areas between soil and the probe through the water films. As a result, *H* increased sharply for all three probes; however, the absolute *H* values of these three probes were different. The increasing trend of *H* with θ also showed in the fine sand, sandy loam, and silty clay soils (Fig. 5.4B, C, and D). It was interesting to see that *H* of the coarse sand at very low θ were abnormally high, which is unexplainable and should be studied further.

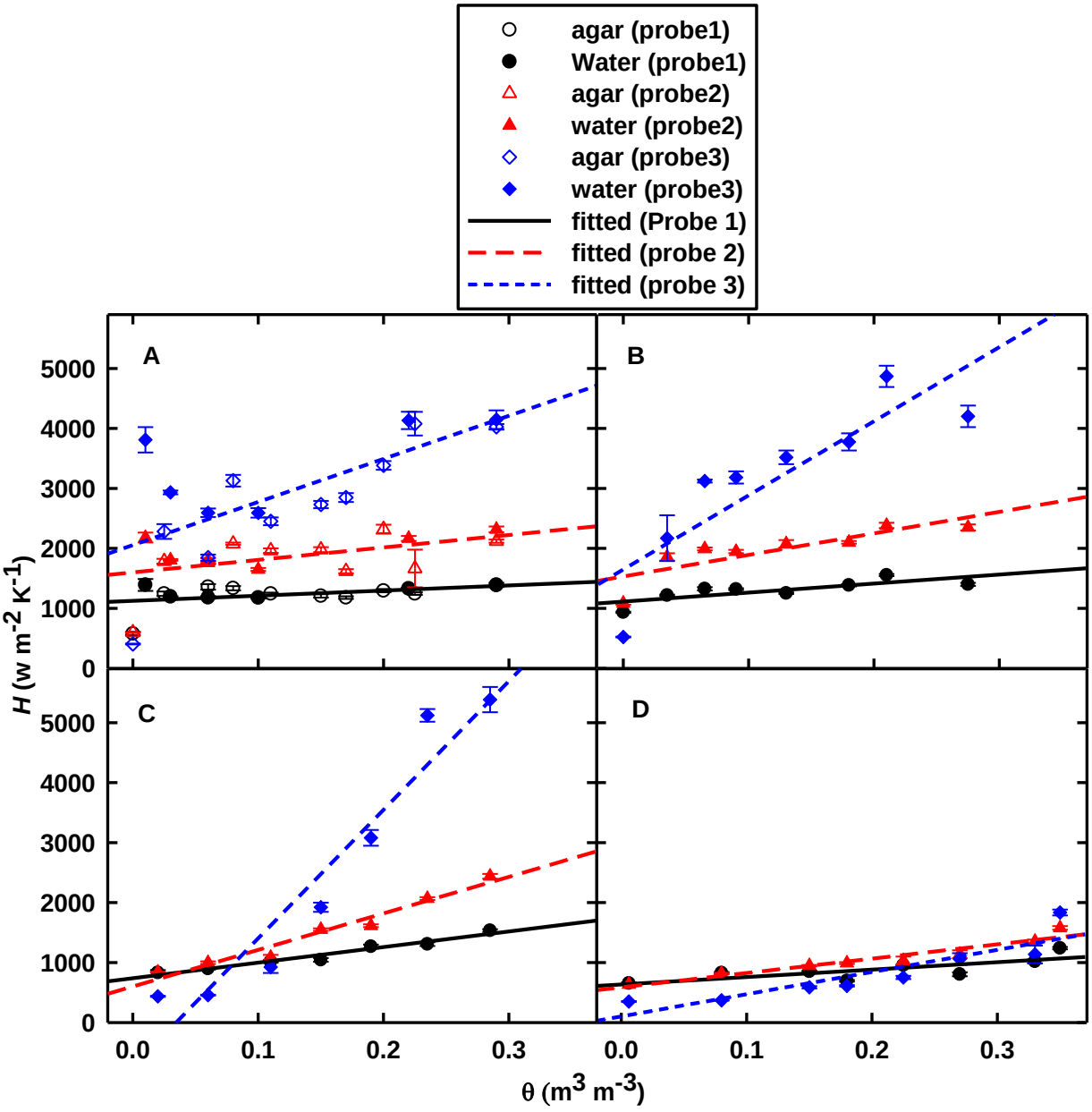

Fig. 5.4. Thermal contact conductivities (*H*) of coarse sand (A), fine sand (B), sandy loam (C), and silty clay (D) at various water contents (θ). The lines are fitted *H*(θ) relations by the linear regression. Error bars indicate the standard deviations of four measurement replicates.

To investigate the effect of ρ_b on *H* values, it is important to maintain the same ρ_b during the experiment; however, it was difficult to pack different textured soils at the same ρ_b in practice. In this study, ρ_b decreased as soil texture became finer (Table 5.1). Nonetheless, we maintained the same ρ_b for the same soil at different θ. There were two main effects of ρ_b on *H*. Firstly, the coarser soils with the higher ρ_b resulted in higher *H* values when they were at the same θ. This may be because higher ρ_b is associated with higher contact pressure between two materials' contact interface, which contributes to the increased actual contact area and increases in *H* (Cooper et al., 1969; Bahrami et al., 2004b; Wang et al., 2012). Secondly, as shown in the standard Proctor compaction test, with the same amount of packing power, ρ_b increased as θ increased, and reaches a maximum at a certain mid-range of θ, and then decreased with further increase in θ (Penner et al., 1975). Our experiments showed that the coarse sand and fine sand had a relative constant ρ_b at different θ. However, with the same amount of packing power, ρ_b became higher at the mid-range of θ for the sandy loam and silty clay. To keep a constant ρ_b for the same soil, we had to reduce the power to pack the sandy loam and silty clay soils at the middle range of θ, which may resulted in lower contact pressure and less contact area between soil particles and the probe than that at the lower and higher θ. This may be the reason for the smaller *H* increase in the sandy loam and silty clay soils than in sand soils at the mid-range of θ.

Soil texture affects *H* in two ways. First, the typical ranges of ρ_b values of different textured soils are different, which resulted in different *H* values as discussed above. Second, different textured soils are composed of different percentage of the sand, silt, and clay particles, and have different characterizations of surface deformation, soil particle shape and arrangement at the soil-probe interface (Bahrami et al., 2004b; Sauer et al., 2007; Cui et al., 2014). However, more

detailed studies at smaller scales with the aid of microscope are needed to have clearer views on the actual contact situation and to better explain those factors in the future.

5.5.2.3 Soil water content prediction

Even though *H* from the three probes showed a similar trend with increasing θ, the absolute *H* values of three probes were quite different. As shown in Fig. 5.4, the *H* values of probe 1 were consistently higher than that of probe 2; however, *H* of probe 3 for the two sandy soils were lower than probes 1 and 2 when soils were dry, and higher than them when soils were wet. For the sandy loam and silty clay soils, the *H* values of probe 3 were lower than probes 1 and 2 at lower θ, and higher than them when θ were higher than 0.12 $m^3\ m^{-3}$ and 0.32 $m^3\ m^{-3}$, respectively. In order to eliminate or reduce the differences of *H* between the three probes, we measured the *H* values in 5 $kg\ m^{-3}$ agar-stabilized water, and the ratios of the *H* values in soils to the *H* values in agar solutions of the three probes were taken (Results not shown). However, there were still substantial differences in the ratio of *H* between probes after this treatment. The difficulty in unifying the differences of *H* values between the three probes indicated that *H* may not only be affected by the probe properties, but also affected by the interactions between the probes, soil and water, and more research is needed.

The $H(\theta)$ relationships of four soils measured by the three probes were well fitted with high coefficient of determinations ($r^2 > 0.61$), except for the coarse sand (Table 5.2, Fig. 5.4). As *H* not only changed with θ but also was soil specific, it was important to quantitatively relate soil properties to $H(\theta)$ relationships. The relations between ρ_b and the slopes and the intercepts of $H(\theta)$ relationships were shown in Fig. 5.5. The slopes of $H(\theta)$ relations for the three probes decreased with increasing ρ_b, except for the silty clay. The intercepts of $H(\theta)$ relations for the three probes

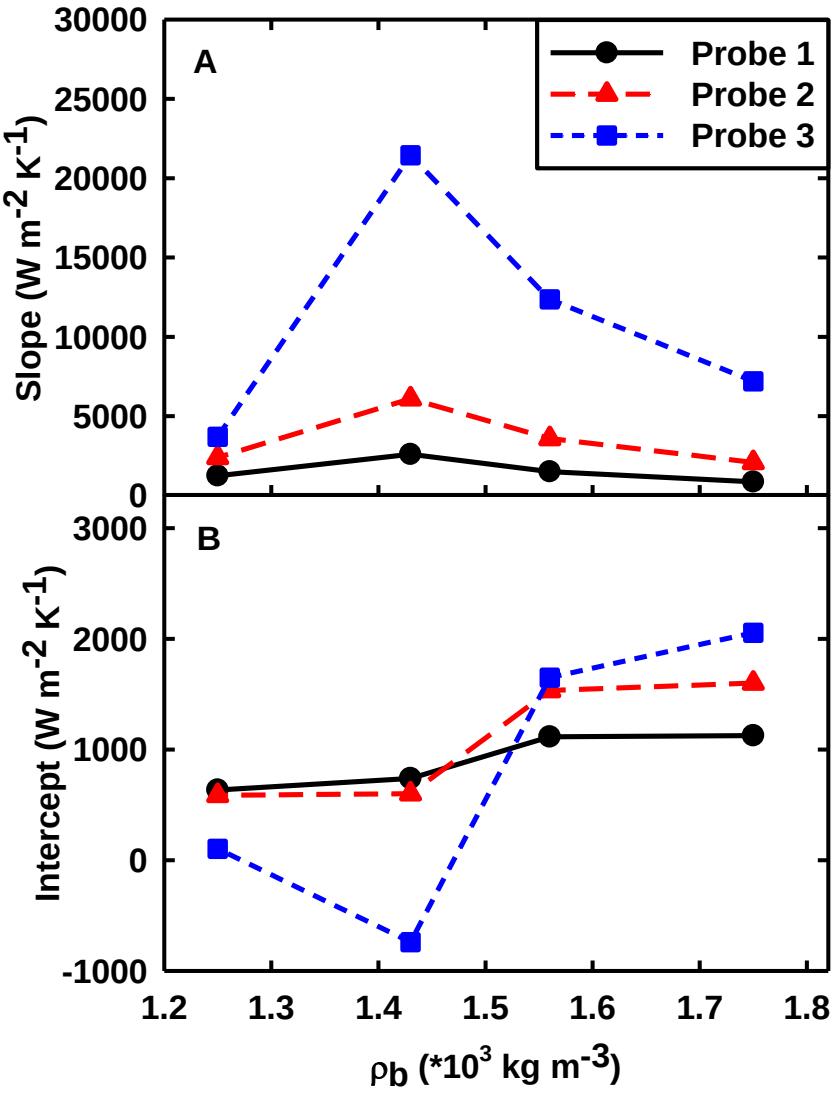

Fig. 5.5. Effects of soil bulk density (ρ_b) on the (A) slope and (B) intercept of the thermal contact conductivity-soil water content relations.

increased with increasing ρ_b, except for probe 3 of the sandy loam. Therefore, although there was a trend between the slope and intercept of $H(\theta)$ relations and ρ_b, it was still challenging to quantitatively describe their relationship.

Given the probe dependence of H, and if we unify the differences between three probes using the fitted linear $H(\theta)$ relations, we may obtain accurate θ predictions from probes 2 and 3 based on the $H(\theta)$ relations of probe 1. To do this, the H values of probes 2 and 3 were calibrated through Eq. 5.19, and then the predicted θ values of probes 2 and 3 were obtained from the $H(\theta)$ relations of probe 1, and were compared with that measured by the oven-dry method (Fig. 5.6).

Table 5.2. Slope (a), intercept (b) and coefficient of determination (r^2) between the thermal contact conductivity (H) and soil water content (θ) ($H=a\theta+b$) for four soils measured by three probes.

	Coarse sand			Fine sand			Sandy loam			Silty clay		
Probe	1	2	3	1	2	3	1	2	3	1	2	3
a (W m^{-2} K^{-1})	858	2078	7193	1503	3589	12358	2599	6095	21446	1240	2392	3700
b (W m^{-2} K^{-1})	1126	1600	2054	1114	1532	1649	739	600	-741	635	586	102
r^2	0.19	0.24	0.49	0.61	0.69	0.75	0.96	0.96	0.92	0.62	0.93	0.80

Probes 2 and 3 provided accurate θ predictions for all soils except for the coarse sand with the errors < 0.04 m^3 m^{-3}. The estimate accuracies were indicated by the RMSE and bias (Fig. 5.6). The RMSE for probe 2 were smaller than 0.038 m^3 m^{-3} for all soils, except for the coarse sand with RMSE = 0.114 m^3 m^{-3}. The RMSE were smaller than 0.056 m^3 m^{-3} for all soils, except for the probe 3 for the coarse sand with RMSE = 0.075 m^3 m^{-3}. The negative or positive bias values indicate the over- or underestimations of θ. Both probes provided unbiased θ predictions (< 0.03 m^3 m^{-3}). The bias values of the coarse sand and fine sand were ranged -3.02×10^{-2} ~ -1.14×10^{-2} m^3 m^{-3}, and that of sandy loam and silty clay were even smaller (ranged -1.63×10^{-6} ~ 1.62×10^{-6} m^3 m^{-3}). The RMSE and bias values of the same soil from both probes 2 and 3 were similar, indicating small variability between probes.

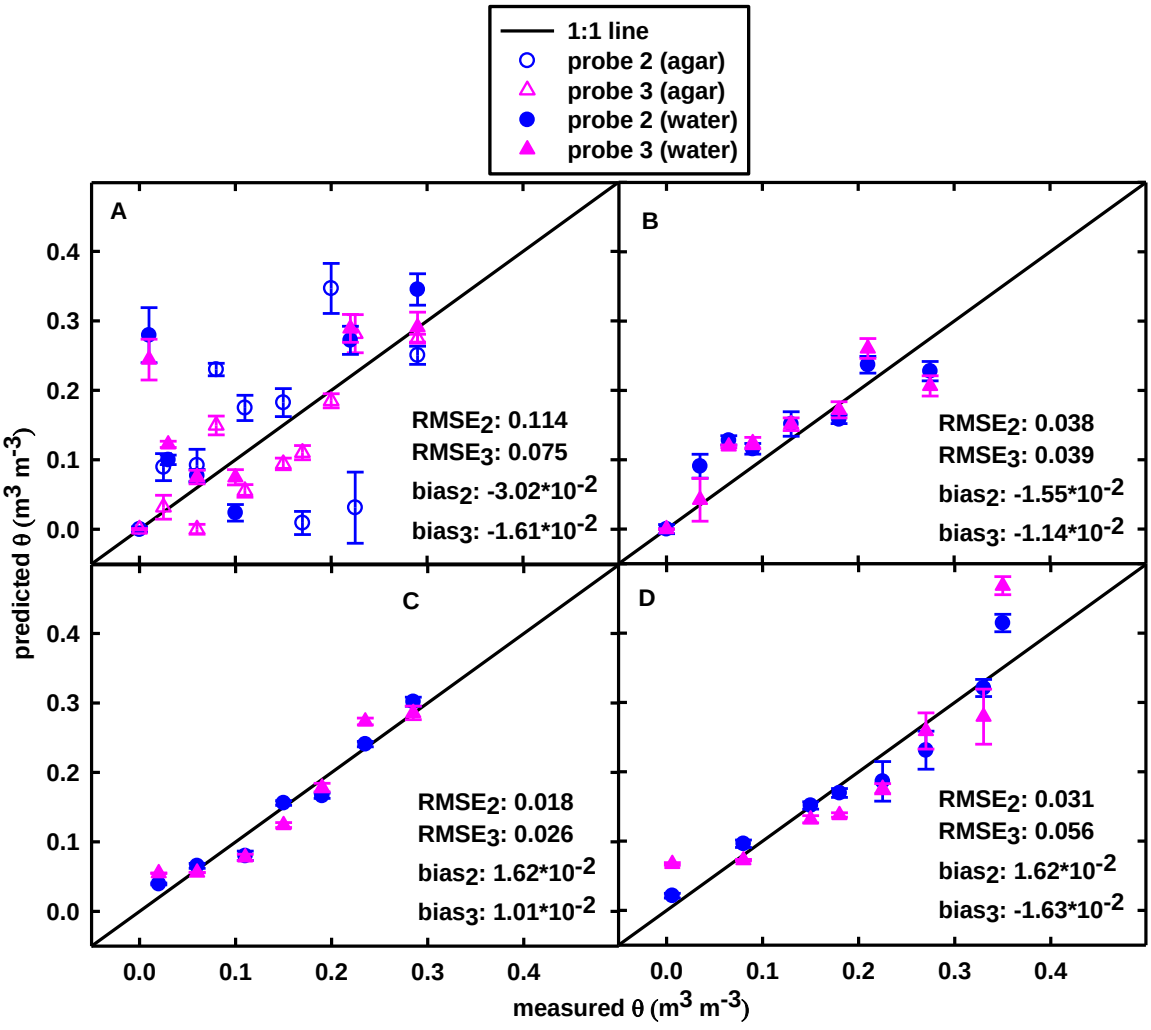

Fig. 5.6. Soil water content (θ) of coarse sand (A), fine sand (B), sandy loam (C), and silty clay (D) predicted by probe 2 and 3 based on the linear relations of thermal contact conductivity (*H*) as a function of θ obtained from probe 1, compared to θ measured by the oven-dry method. Error bars indicate the standard deviations of four measurement replicates.

The poor θ predictions of the coarse sand may be caused by the inaccurate *H* values determined by the single probes. The fine sand, sandy loam, and silty clay soils collected in the field contained well mixed soil particles with different sizes; however, the coarse silica sand only contained sand particles with diameter > 1 mm (Table 5.1). The lack of silt and clay particles in the coarse sand may lead to different ρ_b and contact changes during each packing of soil, which resulted in inaccurate *H* values.

5.6 Conclusions

By using high frequency temperature data points, we proved that the accuracy of *H* between the single heat pulse probe and soil from the short-time solution of Blackwell equation were highly depends on the selection of the short-time range. Therefore, an alternative method to obtain *H* from the known θ by fitting the inverse Laplace transform of Blackwell equation were conducted on four soils at a wide range of θ. The results showed that the new full time range curve fitting method was better than the Blackwell short-time solution as it was independent of time range selection. The main factors that influence the *H* values include θ, the probe body, soil texture and ρ_b. The *H* values increased with increasing θ, decreased as soil texture became finer, and decreased as ρ_b became smaller. Quantitative description of $H(\theta)$ relations as a function of soil physical properties is challenging and need further studies. After unifying the differences of *H* values between the three probes, probes 2 and 3 provided accurate θ predictions based on the linear $H(\theta)$ relations from probe 1 for all the field soils except the coarse silica sand. This study presented the potential of the SPHP method in determining in situ θ and a better understanding in *H* values.

6 SYNTHESIS AND CONCLUSIONS

The heat pulse probe method can be used to measure thermal properties and the water content of soils and rocks, as well as soil water flux, sap flow, soil ice content, and snow density. Based on the principles of the heat pulse probe, the AHFO-DTS system extended the soil thermal properties and θ measurement scale from one point to the intermediate scale. The interactions between soil thermal properties and θ indicates the importance to measure soil thermal properties and θ at the same time, location, and scale by one single instrument. Currently, the SPHP method can only measure soil λ. The DPHP method can measure all three soil thermal properties and θ; however, it has not been applied in saturated media, such as bogs, lake bottoms, and oil sands MFT. Based on the SPHP principle, the AHFO-DTS system can measure λ and θ of soils; whereas based on the DPHP principle, it can measure all three soil thermal properties and θ. Therefore, it is important to extend the DPHP method to other materials, and develop the SPHP method to enable it to measure all three thermal properties and θ, allowing the AHFO-DTS method to also be improved.

Canada has the largest oil sands reserves in the world, subsequently generating a large volume of MFT. The characterization of the spatial and temporal distribution of MFT consolidation is critical for the management of the MFT reclamation. The DPHP method has the potential to be a useful tool to monitor the MFT solidification process by measuring MFT's solid percentage. Therefore, the first objective of this research was to examine the feasibility of the DPHP method to measure the solid percentage of MFT.

The DPHP method is subject to large errors due to needle deflections when the dual probe is inserted into hard soils, especially in dry clay soils and in soils with rocks. This issue can be

avoided by the SPHP method. Therefore, developing the SPHP method for simultaneous soil thermal properties and θ measurement would be beneficial. Therefore, the second objective of this research was to test the possibility of determining θ with the SPHP method by comparing three different methods of data interpretation developed from the AHFO-DTS method.

Accurate determination of θ by the SPHP method was obtained by the AHFO-DTS methods; however, those methods need soil-specific calibrations. In order to obtain θ and all three soil thermal properties from the SPHP method without soil-specific information, H between the soil and the probe has to be known. Therefore, the final objective was to determine H, examine the effects of soil properties on H, and explore the possibility of θ determination by $H(\theta)$ relationships.

In the previous three research chapters (Chapter 3-5), developments of both the DPHP and SPHP methods were presented for soil and oil sands MFT measurements of thermal properties, θ, and solid percentage.

6.1 Summary of Findings

Chapter 3 demonstrated that the DPHP method can be used to monitor the consolidation process of oil sands MFT in situ. The DPHP measured solid percentages agreed well with the standard oven-dry measurements. The accuracy of DPHP measured MFT solid percentage can be further improved by the independently measuring actual specific heat of each MFT sample using the MDSC method. Since the DPHP method is accurate, inexpensive, and can be automated, it can be easily adapted to monitor the energy flux and balance and consolidation process of MFT in oil sand tailing ponds.

Chapter 4 compared the $\lambda(\theta)$, $TN_{cum}(\theta)$, and $TN_{max}(\theta)$ methods for θ determination using the SPHP soil column experiments. The results showed that the $\lambda(\theta)$, $TN_{cum}(\theta)$, and $TN_{max}(\theta)$ curves from a single probe differed with the tested soils. Error analyses and θ predictions from two additional probes verified that the SPHP method is accurate to determine θ. However, each of the three methods was only suitable for certain soil types. Within the commonly used time range, the choice of heating time had a negligible effect on the precision and accuracy of θ determinations from all three methods for all four soils (the coarse sand, fine sand, sandy loam, and silty clay soils). One drawback of the three methods is that a soil-specific calibration is required and more research is needed to quantitatively establish the calibration relationships. The $TN_{cum}(\theta)$ and $TN_{max}(\theta)$ methods required shorter heating time, thus providing fast measurements. However, the $\lambda(\theta)$ method does not require probe specific calibration. The choice of three methods ultimately depends on the users requirements.

Chapter 5 presented a new way to calculate H and predicted θ from the $H(\theta)$ relationships. The problem associated with the traditional Blackwell short-time scale solution to calculate H between the single probe and soil were discussed, and a new method to obtain H from a known θ by fitting the inverse Laplace transform of Blackwell equation was conducted on four soils over a wide range of θ values. The results showed that the new method is not affected by the time range selection. Soil thermal contact conductivity is affected by many factors, such as θ, probe body, soil texture and ρ_b. A quantitative description of the $H(\theta)$ relationships as a function of soil physical properties is currently challenging and need future studies. Results from three probes with the same dimensions and materials showed that accurate θ predictions based on the probe specific linear $H(\theta)$ relations can be obtained for all soils except the coarse sand. This study showed the potential of monitoring θ in situ using the SPHP method.

6.2 Future Research Directions

This research extended the application of the DPHP method to oil sands MFT. It is also the first study on ρ_b measurement by the DPHP method without additional θ measurements. This study enhanced our understanding on soil *H* and θ measurement using the SPHP method. The dual probe study results provide a improved option for the oil sands industries to monitor the MFT solidification process, and to understand the temperature regime and heat balance of MFT. The results of *H* between single probe and soils improve the current understanding of the probe-soil contact effects, and how it changes with water, soil, and the probe. Finally, the knowledge about *H* allows better θ measurement with the SPHP method and the AHFO-DTS system.

To further improve the heat pulse probe method, the following research topics are suggested for future studies:

1. Multiple dual probes can be installed in oil sands MFT ponds at different depths and locations to evaluate the in situ performance and long-term monitoring of solid percentage measurements.

2. The DPHP method can be used in the future to study the flux and balance of coupled energy and water of MFT reclamation sites for an improved re-vegetation management. It also can be used in other saturated soil medium, such as the bottom of bogs, rivers, lakes, and deltas, if studies on the water, temperature, and heat regimes are needed.

3. The effect of ρ_b on the *H* values between the single probe and soil should be further studied. Different ρ_b values of the same soil at the same θ should be measured and compared in the future.

4. The study on the SPHP method showed that the $\lambda(\theta)$, $TN_{max}(\theta)$, $TN_{cum}(\theta)$, and $H(\theta)$ relations were soil-specific, and unifying the difference using the non-empirical relationships is difficult. One possible solution to this issue was addressed by Nakshabandi and Kohnke (1965). For different textured soils, the thickness and geometric arrangement of the water layer around the soil particles influence the conductivity of the system. Since the arrangement of water molecules in the soil is linked with water tension, substituting θ with soil matric potential in these four relationships may eliminate the difference between different textured soils. However, this treatment involves additional measurement of soil water retention.

5. The effect of temperature on the soil thermal properties of unfrozen and frozen soils has been previously studied. Temperature has less of an effect on soil thermal properties compared to θ in unfrozen soils; however, the appearance of both water and ice and the differences in thermal properties between water and ice make soil thermal properties and ice content measurements in frozen soils complex. A better methodology should be built to allow the measurement of soil ice content using the heat pulse probe method and to solve the problems associated with the latent heat flux and phase change caused by probe heating when the soil temperature is near 0 ˚C.

6. Soil thermal contact conductivity *H* between the fibre optic cable and soil should be further studied to explore the potential of the AHFO-DTS system for simultaneous λ, *C*, α, and θ measurements at an intermediate scale.

7. The dependence of soil thermal properties on temperature is well known. However, *H* was only measured in room temperature in this study. Therefore more studies are needed to explore the temperature effect on *H*.

8. This study assumed that the soil and MFT systems measured by the heat pulse probes were homogeneous and isotropic. However, the needle deflection of the dual probe caused by the shrink and swell should be considered or solved for a long-term in situ monitoring. The presents of cracks and macro pores will cause more resistance on heat transport; therefore, the effect of the size, shape, and other configurations of the cracks on heat pulse probe measurement should be studies in the future. In addition, the forced convection of heat can happen as a result of water flow in soil, which violates the assumption of an isotropic soil medium, especially during the rainfall events. Therefore, the effects of soil water flux density and direction on heat pulse probe measurement accuracy should be evaluated.

7 REFERENCES

Abu-Hamdeh, N.H. 2001. Measurement of the thermal conductivity of sandy loam and clay loam soils using single and dual probes. J. Agric. Eng. Res. 80(2): 209–216.

Abu-Hamdeh, N.H., A.I. Khdair, and R.C. Reeder. 2001. A comparison of two methods used to evaluate thermal conductivity for some soils. Int. J. Heat Mass Transf. 44(5): 1073–1078.

Abu-Hamdeh, N.H., and R.C. Reeder. 2000. Soil thermal conductivity effects of density, moisture, salt concentration, and organic matter. Soil Sci. Soc. Am. J. 64: 1285–1290.

Alexander, E.B. 2014. Soils in natural landscapes. CRC Press, Boca Raton, FL.

Allen, E.W. 2008. Process water treatment in Canada's oil sands industry: II. A review of emerging technologies. J. Environ. Eng. Sci. 7(5): 499–524.

Anderson, S., and J.W. Hopmans. 2013. Soil-water-root processes : Advances in tomography and imaging (SSSA special publication ; no. 61). Soil Science Society of America, Inc, Madison, WI.

Baatz, R., H.R. Bogena, H.-J. Hendricks Franssen, J.A. Huisman, C. Montzka, and H. Vereecken. 2015. An empirical vegetation correction for soil water content quantification using cosmic ray probes. J. Hydrol. 51: 2030–2046.

Bahrami, M., J.R. Culham, M.M. Yovanovich, and G.E. Schneider. 2004a. Thermal Contact Resistance of NonConforming Rough Surfaces, Part 1: Contact Mechanics Model. J. Thermophys. Heat Transf. 18(2): 209–217.

Bahrami, M., J.R. Culham, M.M. Yovanovich, and G.E. Schneider. 2004b. Thermal Contact Resistance of Non-Conforming Rough Surfaces, Part 1: Contact Mechanics Model. J. Thermophys. Heat Transf. 18(2): 218–227.

Baker, T.H.W., and L.E. Goodrich. 1987. Measurement of soil water content using the combined time-domain reflectometry-thermal conductivity probe. Can. Geotech. J. 24(1982): 160–163.

Barry-Macaulay, D., A. Bouazza, B. Wang, and R.M. Singh. 2015. Evaluation of soil thermal conductivity models. Can. Geotech. J. 52: 1892–1900.

Basinger, J.M., G.J. Kluitenberg, J.M. Ham, J.M. Frank, P.L. Barnes, and M.B. Kirkham. 2003. Laboratory evaluation of the dual-probe heat-pulse method for measuring soil water content. Vadose Zo. J. 2: 389–399.

Baver, L.D. 1956. Soil physics. 3rd ed. Wiley, New York.

Beck, A.E. 1976. An improved method of computing the thermal conductivity of fluid-filled sedimentary rocks. Geophysics 41(I): 133–144.

Beck, A.E., F.M. Anglin, and J.H. Sass. 1971. Analysis of heat flow data-in situ thermal conductivity measurements. Can. J. Earth Sci. 8(1): 1–19.

Benítez-Buelga, J., C. Sayde, L. Rodríguez-Sinobas, and J.S. Selker. 2014. Heated Fiber Optic Distributed Temperature Sensing: A Dual-Probe Heat-Pulse Approach. Vadose Zo. J. 13(11).

Bird, N.R.A., A.R. Preston, E.W. Randall, W.R. Whalley, and A.P. Whitmore. 2005.

Measurement of the size distribution of water-filled pores at different matric potentials by stray field nuclear magnetic resonance. Eur. J. Soil Sci. 56(1): 135–143.

Blackwell, J.H. 1954. A transient-flow method for determination of thermal constants of insulating materials in bulk Part Ⅰ-Theory. J. Appl. Phys. 25(2): 137–144.

Blackwell, J.H. 1956. The axial-flow error in the thermal-conductivity probe. Can. J. Phys.: 412–417.

Brady, N.C., and R.R. Weil. 2008. The nature and properties of soils. 14th ed. Prentice Hall, Upper Saddle River, NJ.

Bristow, K.L. 1998. Measurement of thermal properties and water content of unsaturated sandy soil using dual-probe heat-pulse probes. Agric. For. Meteorol. 89: 75–84.

Bristow, K.L. 2002a. 5.3 Thermal conductivity. p. 222–225. *In* Dane, J.H., Topp, G.C. (eds.), Methods of Soil analysis: Part 4-Physical Methods. 1st ed. SSSA, Inc, Madison, Wisconsin, USA.

Bristow, K.L. 2002b. 5.3 Thermal Conductivity. p. 1216–1224. *In* Dane, J.H., Topp, G.C. (eds.), Methods of Soil analysis: Part 4-Physical Methods. 1st ed. Soil Science Society of America, Inc, Madison, Wisconsin, USA.

Bristow, K.L., J.R. Bilskie, G.J. Kluitenberg, and R. Horton. 1995. Comparison of techniques for extracting soil thermal properties from dual-probe heat-pulse data. Soil Sci. 160(1): 1–7.

Bristow, K.L., G.S. Campbell, and K. Calissendorff. 1993. Test of a heat-pulse probe for measuring changes in soil water content. Soil Sci. Soc. Am. J. 57: 930–934.

Bristow, K.L., G.J. Kluitenberg, C.J. Goding, and T.S. Fitzgerald. 2001. A small multi-needle probe for measuring soil thermal properties, water content and electrical conductivity. Comput. Electron. Agric. 31(3): 265–280.

Bristow, K.L., G.J. Kluitenberg, and R. Horton. 1994a. Measurement of Soil Thermal Properties with a Dual-Probe Heat-Pulse Technique. Soil Sci. Soc. Am. J. 58(5): 1288–1294.

Bristow, K.L., R.D. White, and G.J. Kluitenberg. 1994b. Comparison of single and dual probes for measuring soil thermal properties with transient heating. Soil Res. 32: 447–464.

C., P.-L.D., E. Blackburn, X. Liang, and W.F. E. 1998. The Effect of Soil Thermal Conductivity Parameterization on Surface Energy Fluxes and Temperatures. J. Atmos. Sci. 55(7): 1209–1224.

Campbell, G.S. 1985. Soil physics with BASIC. Elsevier, New York.

Campbell, G.S., C. Calissendorff, and J.H. Williams. 1991. Probe for measuring soil specific heat using a heat-pulse method. Soil Sci. Soc. Am. J. 55: 291–293.

Campbell, G.S., J.D. Jungbauer, W.R. Bidlake, and R.D. Hungerford. 1994. Predicting the effect of temperature on soil thermal conductivity. Soil Sci. 158(5): 307–313.

Campbell, D.I., C.E. Laybourne, and I.J. Blair. 2002. Measuring peat moisture content using the dual-probe heat pulse technique. Soil Res. 40: 177–190.

Canarache, A., I. Vintilă, and I. Munteanu. 2006. Elsevier's Dictionary of Soil Science : In English (with Definitions), French, German and Spanish. Boston: Elsevier, Amsterdam.

Carslaw, H.S., and J.C. Jaeger. 1946. Conduction of heat in solids. 1st ed. Oxford University Press, Oxford.

Carter, M.R., and E.G. Gregorich. 2008. Soil Sampling and Methods of Analysis. 2nd ed. CRC Press, Pinawa, Manitoba : Boca Raton, FL: Canadian Society of Soil Science.

Chalaturnyk, R.J., J. Don Scott, and B. Özüm. 2002. Management of Oil Sands Tailings. Pet. Sci. Technol. 20(9-10): 1025–1046.

Chen, M., G. Walshe, E. Chi Fru, J.J.H. Ciborowski, and C.G. Weisener. 2013. Microcosm assessment of the biogeochemical development of sulfur and oxygen in oil sands fluid fine tailings. Appl. Geochemistry 37: 1–11.

Ciocca, F., I. Lunati, N. Van de Giesen, and M.B. Parlange. 2012. Heated Optical Fiber for Distributed Soil-Moisture Measurements: A Lysimeter Experiment. Vadose Zo. J. 11(4).

Cobos, D.R., and J.M. Baker. 2003. In Situ Measurement of Soil Heat Flux with the Gradient Method. Vadose Zo. J. 2(4): 589–594.

Cooper, M.G., B.B. Mikic, and M.M. Yovanovich. 1969. Thermal contact conductance. Int. J. Heat Mass Transf. 12: 279–300.

Corey, J.C., S.F. Peterson, and M.A. Wakat. 1971. Measurement of attenuation of Cs-137 and Am-241 gamma rays for soil density and water content determinations. Soil Sci. Soc. Am. Procedings 35(2): 215–219.

Costa, J.C., J.A.R. Borges, and L.F. Pires. 2013. Soil bulk density evaluated by gamma-ray attenuation: Analysis of system geometry. Soil Tillage Res. 129: 23–31.

Costabel, S., and U. Yaramanci. 2013. Estimation of water retention parameters from nuclear magnetic resonance relaxation time distributions. Water Resour. Res. 49(4): 2068–2079.

Côté, J., and J. Konrad. 2005. A generalized thermal conductivity model for soils and construction materials. Can. Geotech. J. 42: 443–458.

Coulter, B. 2011. Coulter LS series product manual. Beckman Coulter, Inc., Miami, FL.

Cui, T., Q. Li, Y. Xuan, and P. Zhang. 2014. Multiscale simulation of thermal contact resistance in electronic packaging. Int. J. Therm. Sci. 83(1): 16–24.

Cull, J.P. 1974. Thermal conductivity probes for rapid measurements in rock. J. Phys. E. 7: 771–774.

Dane, J.H., and G.C. Topp. 2002. Methods of Soil Analysis. Part 4-Physical methods. Soil Science Society of America, Inc, Madison, Wisconsin, USA.

Dang, L., and W.H. Leong. 2015. Thermal conductivity probe – Part II – An experimental analysis. Int. J. Heat Mass Transf. 86: 1004–1014.

de Vries, D.A. 1952. A nonstationary method for determining thermal conductivity of soil in situ. Soil Sci. 73(2): 83–89.

de Vries, D.A., and A.J. Peck. 1958a. On the cylindrical probe method of measuring thermal conductivity with special reference to soils. I. Extension of theory and discussion of probe characteristics. Aust. J. Phys.: 255–271.

de Vries, D.A., and A.J. Peck. 1958b. On the cylindrical probe method of measuring thermal

conductivity with special reference to soils. II. Analysis of moisture effects. Aust. J. Phys.: 409–423.

Dias, P.C., W. Roque, E.C. Ferreira, and J. a. Siqueira Dias. 2013. A high sensitivity single-probe heat pulse soil moisture sensor based on a single npn junction transistor. Comput. Electron. Agric. 96: 139–147.

Dillig, M., T. Biedermann, and J. Karl. 2015. Thermal contact resistance in solid oxide fuel cell stacks. J. Power Sources 300: 69–76.

Dirksen, C. 1999. Soil Physics Measurements. Catena, Reiskirchen, Germany.

Dobchuk, B.S., R.E. Shurniak, S.L. Barbour, M. a. O'Kane, and Q. Song. 2013. Long-term monitoring and modelling of a reclaimed watershed cover on oil sands tailings. Int. J. Mining, Reclam. Environ. 27(3): 180–201.

Dong, Y., J.S. Mccartney, and N. Lu. 2015. Critical review of thermal conductivity models for unsaturated soils. Geotech. Geol. Eng. 33: 207–221.

Dubois, S., and F. Lebeau. 2013. Design, construction and validation of a guarded hot plate apparatus for thermal conductivity measurement of high thickness crop-based specimens. Mater. Struct.

Ewen, J., and H.R. Thomas. 1987. The thermal probe—a new method and its use on an unsaturated sand. Geotechnique 37(1): 91–105.

Ewing, R.P., and R. Horton. 2007. Thermal conductivity of a cubic lattice of spheres with capillary bridges. J. Phys. D. Appl. Phys. 40(16): 4959–4965.

Farkish, A., and M. Fall. 2013. Rapid dewatering of oil sand mature fine tailings using super absorbent polymer (SAP). Miner. Eng. 50-51: 38–47.

Farkish, a, and M. Fall. 2014. Consolidation and Hydraulic Conductivity of Oil Sand Mature Fine Tailings Dewatered by Using Super Absorbent Polymer. J. Geotech. Geoenvironmental Eng. 140: 06014006:1–6.

Faybishenko, B.A. 1995. Hydraulic Behavior of Quasi-Saturated Soils in the Presence of Entrapped Air: Laboratory Experiments. Water Resour. Res. 31(10): 2421–2435.

Fletcher, L.S. 1988. Recent developments in contact conductance heat transfer. J. Heat Transfer 110: 1059–1070.

Foth, H.D. 1990. Fundamentals of soil science. 8th ed. Wiley, New York.

Freifeld, B.M., S. Finsterle, T.C. Onstott, P. Toole, and L.M. Pratt. 2008. Ground surface temperature reconstructions: Using in situ estimates for thermal conductivity acquired with a fiber-optic distributed thermal perturbation sensor. Geophys. Res. Lett. 35(14): L14309.

Galagedara, L.W., G.W. Parkin, J.D. Redman, P. Von Bertoldi, and A.L. Endres. 2005. Field studies of the GPR ground wave method for estimating soil water content during irrigation and drainage. J. Hydrol. 301(1-4): 182–197.

Gangadhara Rao, M.V.B.B., and D.N. Singh. 1999. A generalized relationship to estimate thermal resistivity of soils. Can. Geotech. J. 36(4): 767–773.

Gardiner, D.T., and R.W. Miller. 2004. Soils in our environment. 10th ed. Pearson/Prentice Hall,

Upper Saddle River, N.J.

Garven, G. 1989. A hydrogeologic model for the formation of the giant oil sands deposits of the Western Canada sedimentary basin. Am. J. Sci. 289: 105–166.

Ghalambor, S., D. Agonafer, and a. Haji-Sheikh. 2013. Analytical Thermal Solution to a Nonuniformly Powered Stack Package With Contact Resistance. J. Heat Transfer 135(11): 111015.

Ghildyal, B.P., and R.P. Tripathi. 1987. Soil Physics. J. Wiley & Sons, New York.

Ghuman, B.S., and R. Lal. 1985. Thermal conductivity, thermal diffusivity, and thermal capacity of some Nigerian soils. Soil Sci. 139(1): 74–80.

Gil-Rodríguez, M., L. Rodríguez-Sinobas, J. Benítez-Buelga, and R. Sánchez-Calvo. 2013. Application of active heat pulse method with fiber optic temperature sensing for estimation of wetting bulbs and water distribution in drip emitters. Agric. Water Manag. 120: 72–78.

Goodarzi, K., S.R. Ramezani, and S. Hajati. 2014. Reducing thermal contact resistance using nanocoating. Appl. Therm. Eng. 70(1): 641–646.

Gori, F., and S. Corasaniti. 2003. Experimental measurements and theoretical prediction of the thermal conductivity of two-and three-phase water/olivine systems. Int. J. Thermophys. 24(5): 1339–1353.

Goto, S., and O. Matsubayashi. 2008. Inversion of needle-probe data for sediment thermal properties of the eastern flank of the Juan de Fuca Ridge. J. Geophys. Res. 113(B8): B08105.

Hadas, A. 1974. Problems involved in measuring the soil thermal conductivity and diffusivity in a moist soil. Agric. Meteorol. 13: 105–113.

Ham, J.M., and E.J. Benson. 2004. On the construction and calibration of dual-probe heat capacity sensors. Soil Sci. Soc. Am. J. 68: 1185–1190.

Han, X., M.D. MacKinnon, and J.W. Martin. 2009. Estimating the in situ biodegradation of naphthenic acids in oil sands process waters by HPLC/HRMS. Chemosphere 76(1): 63–70.

Hanks, R.J. 1992. Applied Soil Physics : Soil Water and Temperature Applications. 2nd ed. Springer-Verlag, New York.

Heitman, J.L., J.M. Basinger, G.J. Kluitenberg, J.M. Ham, J.M. Frank, and P.L. Barnes. 2003. Field evaluation of the dual-probe heat-pulse method for measuring soil water content. Vadose Zo. J. 2: 552–560.

Van Der Held, E.F.M., and F.G. Van Drunen. 1949. A method of measuring the thermal conductivity of liquids. Physica (10): 865–881.

Herman, D.C., P.M. Fedorak, M.D. MacKinnon, and J.W. Costerton. 1994. Biodegradation of naphthenic acids by microbial populations indigenous to oil sands tailings. Can. J. Microbiol. 40(6): 467–477.

Hillel, D. 1998. Introduction to Environmental soil physics. Academic Press, San Diego, CA.

Hiraiwa, Y., and T. Kasubuchi. 2000. Temperature dependence of thermal conductivity of soil over a wide range of temperature (5–75 C). Eur. J. Soil Sci. 51: 211–218.

Hopmans, J.W., and J.H. Dane. 1986. Thermal conductivity of two porous media as a function of

water content, temperature, and density. Soil Sci. 142(4): 187–195.

Hopmans, J.W., J. Šimunek, and K.L. Bristow. 2002. Indirect estimation of soil thermal properties and water flux using heat pulse probe measurements: Geometry and dispersion effects. Water Resour. Res. 38(1): 7–1–7–14.

Horton, R., and P.J. Wierenga. 1984. The Effect of Column Wetting on Soil Thermal Conductivity. Soil Sci.: 102–108.

Huang, P.M., Y. Li, and M.E. Sumner. 2012. Handbook of soil sciences. Taylor & Francis, Boca Raton, Fla. : London: CRC.

Huisman, J.A., S.S. Hubbard, J.D. Redman, and A.P. Annan. 2003. Measuring Soil Water Content with Ground Penetrating Radar. Vadose Zo. J. 2(4): 476.

Huisman, J. a., C. Sperl, W. Bouten, and J.M. Verstraten. 2001. Soil water content measurements at different scales: Accuracy of time domain reflectometry and ground-penetrating radar. J. Hydrol. 245(1-4): 48–58.

Jaafar, H., and J.J.C. Picot. 1970. Thermal conductivity of snow by a transient state probe method. Water Resour. Res. 6(1): 333–335.

Jaeger, J.C. 1956. Conduction of heat in an infinite region bounded internally by a circular cylinder of a perfect conductor. Aust. J. Phys.: 167–179.

Jeng, Y.-R., J.-T. Chen, and C.-Y. Cheng. 2006. Thermal contact conductance of coated surfaces. Wear 260: 159–167.

Johnson, M.D., and B. Lowery. 1985. Effect of three conservation tillage practices on soil temperature and thermal properties. Soil Sci. Soc. Am. J. 49(6): 1547–1552.

Jones, B.W. 1988a. Thermal conductivity probe: Development of method and application to a coarse granular medium. J. Phys. E. 21: 832–839.

Jones, B.W. 1988b. Thermal conductivity probe: development of method and application to a coarse granular medium. J. Phys. E. 21: 832–839.

Jury, W.A., and B. Bellantuoni. 1976. A background temperature correction for thermal conductivity probes. Soil Sci. Soc. Am. J. 40: 608–610.

Kamai, T., G.J. Kluitenberg, and J.W. Hopmans. 2009. Design and Numerical Analysis of a Button Heat Pulse Probe for Soil Water Content Measurement. Vadose Zo. J. 8(1): 167.

Kasubuchi, T. 1977. Twin transient-state cylindrical-probe method for the determination of the thermal conductivity of soil. Soil Sci. 124(5): 255–258.

Kasubuchi, T. 1992. Development of in-situ soil water measurement by heat-probe method. Japan Agric. Res. Q. 26: 178–181.

Kelleners, T.J., R.W.O. Soppe, J.E. Ayars, and T.H. Skaggs. 2004. Calibration of Capacitance Probe Sensors in a Saline Silty Clay Soil. Soil Sci. Soc. Am. J. 68(3): 770.

Kettridge, N., and A. Baird. 2007. In situ measurements of the thermal properties of a northern peatland: Implications for peatland temperature models. J. Geophys. Res. 112: F02019 1–12.

Kirkham, D., and w. L. Powers. 1972. Advanced soil physics. J. Wiley & Sons, New York, London, Sydney, Toronto.

Kluitenberg, G.J., K.L. Bristow, and B.S. Das. 1995. Error analysis of heat pulse method for measuring soil heat capacity, diffusivity, and conductivity. Soil Sci. Soc. Am. J. 59: 719–726.

Kluitenberg, G.J., J.M. Ham, and K.L. Bristow. 1993. Error analysis of the heat pulse method for measuring soil volumetric heat capacity. Soil Sci. Soc. Am. J. 57: 1444–1451.

Kluitenberg, G.J., T. Kamai, J.A. Vrugt, and J.W. Hopmans. 2010. Effect of probe deflection on dual-probe heat-pulse thermal conductivity measurements. Soil Sci. Soc. Am. J. 74(5): 1537–1540.

Kluitenberg, G.J., T.E. Ochsner, and R. Horton. 2007. Improved analysis of heat pulse signals for soil water flux determination. Soil Sci. Soc. Am. J. 71(1): 53–55.

Kluitenberg, G.J., and J.R. Philip. 1999. Dual thermal probes near plane interfaces. Soil Sci. Soc. Am. J. 63: 1585–1591.

Kluitenberg, G.J., and A.W. Warrick. 2001. Improved Evaluation Procedure for Heat-Pulse Soil Water Flux Density Method. Soil Sci. Soc. Am. J. 65: 320–323.

Knight, J.H., W. Jin, and G.J. Kluitenberg. 2007. Sensitivity of the dual-probe heat-pulse method to spatial variations in heat capacity and water content. Vadose Zo. J. 6(4): 746–758.

Knight, J.H., and G.J. Kluitenberg. 2004. Simplified computational approach for dual-probe heat-pulse method. Soil Sci. Soc. Am. J. 68: 447–449.

Knight, J.H., G.J. Kluitenberg, T. Kamai, and J.W. Hopmans. 2012. Semianalytical Solution for Dual-Probe Heat-Pulse Applications that Accounts for Probe Radius and Heat Capacity. Vadose Zo. J. 11(2).

Kojima, Y., J.L. Heitman, G.N. Flerchinger, T. Ren, R.P. Ewing, and R. Horton. 2014. Field Test and Sensitivity Analysis of a Sensible Heat Balance Method to Determine Soil Ice Contents. Vadose Zo. J. 13(9).

Koorevaar, P., G. Menelik, and C. Dirksen. 1983. Elements of soil physics (Elsevier, Ed.). New York.

Kozlowski, T. 2012. Modulated Differential Scanning Calorimetry (MDSC) studies on low-temperature freezing of water adsorbed on clays, apparent specific heat of soil water and specific heat of dry soil. Cold Reg. Sci. Technol. 78: 89–96.

Krause, S., L. Rose, and N.J. Cassidy. 2014. Reply to comment by J. S. Selker et al. on "Capabilities and limitations of tracing spatial temperature patterns by fiber-optic distributed temperature sensing." Water Resour. Res. 50: 5375–5377.

Larson, T.H. 1988. Thermal measurement of soils using a multineedle probe with a pulsed-point source. Geophysics 53(2): 266–270.

Li, M., S.L. Barbour, and B.C. Si. 2015. Measuring Solid Percentage of Oil Sands Mature Fine Tailings Using the Dual Probe Heat Pulse Method. J. Environ. Qual. 44(1): 293–298.

Liu, G., B. Li, T. Ren, and R. Horton. 2007. Analytical solution of the heat pulse method in a parallelepiped sample space. Soil Sci. Soc. Am. J. 71(5): 1607–1619.

Liu, G., B. Li, T. Ren, R. Horton, and B.C. Si. 2008a. Analytical solution of heat pulse method in a parallelepiped sample space with inclined needles. Soil Sci. Soc. Am. J. 72(5): 1208–1216.

Liu, X., S. Lu, R. Horton, and T. Ren. 2014. In Situ Monitoring of Soil Bulk Density with a Thermo-TDR Sensor. Soil Sci. Soc. Am. J. 78(2): 400.

Liu, X.N., T. Ren, and R. Horton. 2008b. Determination of soil bulk density with thermo-time domain reflectometry sensors. Soil Sci. Soc. Am. J. 72: 1000–1005.

Liu, G., and B.C. Si. 2008. Dual-probe heat pulse method for snow density and thermal properties measurement. Geophys. Res. Lett. 35: L16404 1–5.

Liu, G., and B.C. Si. 2010. Errors analysis of heat pulse probe methods: Experiments and simulations. Soil Sci. Soc. Am. J. 74(3): 797–803.

Liu, G., and B.C. Si. 2011a. Single-and dual-probe heat pulse probe for determining thermal properties of dry soils. Soil Sci. Soc. Am. J. 75(3): 787–794.

Liu, G., and B.C. Si. 2011b. Soil ice content measurement using a heat pulse probe method. Can. J. Soil Sci. 91: 235–246.

Liu, G., B.C. Si, A.X. Jiang, B.G. Li, T.S. Ren, and K.L. Hu. 2012. Probe Body and Thermal Contact Conductivity Affect Error of Heat Pulse Method Based on Infi nite Line Pulsed Infi nite Line Source Model of Dual Probe. Soil Sci. Soc. Am. J. 76(2): 370–374.

Liu, G., M. Wen, X. Chang, T. Ren, and R. Horton. 2013a. A Self-Calibrated Dual Probe Heat Pulse Sensor for In Situ Calibrating the Probe Spacing. Soil Sci. Soc. Am. J. 77(2): 417–421.

Liu, G., L. Zhao, M. Wen, X. Chang, and K. Hu. 2013b. An Adiabatic Boundary Condition Solution for Improved Accuracy of Heat-Pulse Measurement Analysis Near the Soil–Atmosphere Interface. Soil Sci. Soc. Am. J. 77: 422–426.

van Loon, W.K.P., I.A. van Haneghem, and J. Schenk. 1989. A new model for the non-steady-state probe method to measure thermal properties of porous media. Int. J. Heat Mass Transf. 32(8): 1473–1481.

Lorenzini, G., E.X. Barreto, C.C. Beckel, P.S. Schneider, L.A. Isoldi, E.D. dos Santos, and L.A.O. Rocha. 2016. Constructal design of I-shaped high conductive pathway for cooling a heat-generating medium considering the thermal contact resistance. Int. J. Heat Mass Transf. 93: 770–777.

Lu, Y., S. Lu, R. Horton, and T. Ren. 2014. An Empirical Model for Estimating Soil Thermal Conductivity from Texture, Water Content, and Bulk Density. Soil Sci. Soc. Am. J.

Lu, Y., Y. Wang, and T. Ren. 2013. Using Late Time Data Improves the Heat-Pulse Method for Estimating Soil Thermal Properties with the Pulsed Infinite Line Source Theory. Vadose Zo. J. 12(4).

Luna Wolter, G.L., and M.A. Naeth. 2014. Dry Mature Fine Tailings as Oil Sands Reclamation Substrates for Three Native Grasses. J. Environ. Qual. 43(4): 1510–1516.

Lv, L., T.E. Franz, D.A. Robinson, and S.B. Jones. 2014. Measured and Modeled Soil Moisture Compared with Cosmic-Ray Neutron Probe Estimates in a Mixed Forest. Vadose Zo. J. 13(12).

Macher, W., N.I. Kömle, M.S. Bentley, and G. Kargl. 2013. The heated infinite cylinder with sheath and two thermal surface resistance layers. Int. J. Heat Mass Transf. 57(2): 528–534.

Macher, W., N.I. Kömle, M.S. Bentley, and G. Kargl. 2014. Temperature evolution of two parallel

composite cylinders with contact resistances and application to thermal dual-probes. Int. J. Heat Mass Transf. 69: 481–492.

Madill, R.E., M.T. Orzechowski, G. Chen, B.G. Brownlee, and N.J. Bunce. 2001. Preliminary risk assessment of the wet landscape option for reclamation of oil sands mine tailings: bioassays with mature fine tailings pore water. Environ. Toxicol. 16(3): 197–208.

Manoel, C., P. Vaz, and J.W. Hopmans. 2001. with a Combined Penetrometer – TDR Moisture Probe. (iii): 4–12.

Manohar, K., D.W. Yarbrough, and J.R. Booth. 2000. Measurement of apparent thermal conductivity by the thermal probe method. J. Test. Eval.: 345–351.

Miyazaki, T., S. Hasegawa, and T. Kasubuchi. 1993. Water Flow in Soils. Books in Soils, Plants, and the Environment. Marcel Dekker, New York.

Moench, A.F., and D.D. Evans. 1970. Thermal conductivity and diffusivity of soil using a cylindrical heat source. Soil Sci. Soc. Am. Procedings 34: 377–381.

Momose, T., and T. Kasubuchi. 2002. Effect of reduced air pressure on soil thermal conductivity over a wide range of water content and temperature. Eur. J. Soil Sci. 53: 599–606.

Mori, Y., J.W. Hopmans, A.P. Mortensen, and G.J. Kluitenberg. 2003. Multi-functional heat pulse probe for the simultaneous measurement of soil water content, solute concentration, and heat transport parameters. Vadose Zo. J. 2: 561–571.

Nadler, A., A. Gamliel, and I. Peretz. 1999. Practical aspects of salinity effect on TDR-measured water content: A field study. Soil Sci. Soc. Am. J. 63(5): 1070–1076.

Nagasaka, Y. 1981. Simultaneous measurement of the thermal conductivity and the thermal diffusivity of liquids by the transient hot-wire method. Rev. Sci. Instrum. 52(2): 229–232.

Nakshabandi, G.A. l., and H. Kohnke. 1965. Thermal conductivity and diffusivity of soils as related to moisture tension and other physical properties. Agric. Meteorol. 2(1965): 271–279.

Nikolaev, I. V., W.H. Leong, and M.A. Rosen. 2013. Experimental Investigation of Soil Thermal Conductivity Over a Wide Temperature Range. Int. J. Thermophys. 34(6): 1110–1129.

Njoku, E.G., and D. Entekhabi. 1996. Passive microwave remote sensing of soil moisture. J. Hydrol. 184: 101–129.

Noborio, K. 2001. Measurement of soil water content and electrical conductivity by time domain reflectometry : a review. Comput. Electron. Agric. 31: 213–237.

Noborio, K., K.J. McInnes, and J.L. Heitman. 1996. Measurements of Soil Water Content, Heat Capacity, and Thermal Conductivity With A Single TDR Probe. Soil Sci. 161(1): 22–28.

Ochsner, T.E., and J.M. Baker. 2008. In situ monitoring of soil thermal properties and heat flux during freezing and thawing. Soil Sci. Soc. Am. J. 72: 1025–1032.

Ochsner, T.E., R. Horton, G.J. Kluitenberg, and Q. Wang. 2005. Evaluation of the Heat Pulse Ratio Method for Measuring Soil Water Flux. Soil Sci. Soc. Am. J. 69(3): 757–765.

Ochsner, T.E., R. Horton, and T. Ren. 2001a. A new perspective on soil thermal properties. Soil Sci. Soc. Am. J. 65: 1641–1647.

Ochsner, T.E., R. Horton, and T. Ren. 2001b. Simultaneous water content, air-filled porosity, and

bulk density measurements with thermo-time domain reflectometry. Soil Sci. Soc. Am. J. 65(6): 1618–1622.

Ochsner, T.E., R. Horton, and T. Ren. 2003. Use of the Dual-Probe Heat-Pulse Technique to Monitor Soil Water Content in the Vadose Zone. Vadose Zo. J. 2(4): 572–579.

Oliveira, J.C.M., K. Reichardt, C.M.P. Vaz, and D. Swartzendruber. 1997. Improved soil particle-size analysis by gamma-ray attenuation. Soil Sci. Soc. Am. J. 61(1): 23–26.

Olmanson, O.K., and T.E. Ochsner. 2006. Comparing ambient temperature effects on heat pulse and time domain reflectometry soil water content measurements. Vadose Zo. J. 5: 751–756.

Olmanson, O.K., and T.E. Ochsner. 2008. A partial cylindrical thermo-time domain reflectometry sensor. Soil Sci. Soc. Am. J. 72: 571–577.

Penner, E. 1970. Thermal conductivity of frozen soils. Can. J. Earth Sci. 7(3): 982–987.

Penner, T.J., and J.M. Foght. 2010. Mature fine tailings from oil sands processing harbour diverse methanogenic communities. Can. J. Microbiol. 56: 459–470.

Penner, E., G.H. Johnston, and L.E. Goodrich. 1975. Thermal conductivity laboratory studies of some Mackenzie Highway soils. Can. Geotech. J. 12(3): 271–288.

Peron, H., L. Laloui, L.-B. Hu, and T. Hueckel. 2012. Formation of drying crack patterns in soils: a deterministic approach. Acta Geotech. 8(2): 215–221.

Philip, J., and G. Kluitenberg. 1999. Errors of dual thermal probes due to soil heterogeneity across a plane interface. Soil Sci. Soc. Am. J. 63: 1579–1585.

Pires, L.F., O.O.S. Bacchi, and K. Reichardt. 2005. Soil water retention curve determined by gamma-ray beam attenuation. Soil Tillage Res. 82(1): 89–97.

Plaster, E.J., and H.E. Reiley. 1992. Soil science & management. 2nd ed. Delmar Publishers, Albany, N.Y.

Proskin, S., D. Sego, and M. Alostaz. 2010. Freeze-thaw and consolidation tests on Suncor mature fine tailings (MFT). Cold Reg. Sci. Technol. 63(3): 110–120.

Putkonen, J. 2003. Determination of frozen soil thermal properties by heated needle probe. Permafr. Periglac. Process. 14(4): 343–347.

Ramos-Padrón, E., S. Bordenave, S. Lin, I.M. Bhaskar, X. Dong, C.W. Sensen, J. Fournier, G. Voordouw, and L.M. Gieg. 2011. Carbon and sulfur cycling by microbial communities in a gypsum-treated oil sands tailings pond. Environ. Sci. Technol. 45(2): 439–46.

Read, T., O. Bour, J.S. Selker, V.F. Bense, T.L. Borgne, R. Hochreutener, and N. Lavenant. 2014. Active-distributed temperature sensing to continuously quantify vertical flow in boreholes. Water Resour. Res. 50: 3706–3713.

Reading, M., A. Luget, and R. Wilson. 1994. Modulated differential scanning calorimetry. Thermochim. Acta 238: 295–307.

Redfield, E., C. Croser, J.J. Zwiazek, M.D. MacKinnon, and C. Qualizza. 2003. Responses of red-osier dogwood to oil sands tailings treated with gypsum or alum. J. Environ. Qual. 32(3): 1008–14.

Reedy, R.C., and B.R. Scanlon. 2003. Soil Water Content Monitoring Using Electromagnetic

Induction. J. Geotech. Geoenvironmental Eng. 129(11): 1028–1039.

Ren, T., G.J. Kluitenberg, and R. Horton. 2000. Determining soil water flux and pore water velocity by a heat pulse technique. Soil Sci. Soc. Am. J. 64: 552–560.

Ren, T., K. Noborio, and R. Horton. 1999. Measuring soil water content, electrical conductivity, and thermal properties with a thermo-time domain reflectometry probe. Soil Sci. Soc. Am. J. 63: 450–457.

Ren, T., T.E. Ochsner, and R. Horton. 2003a. Development of thermo-time domain reflectometry for vadose zone measurements. Vadose Zo. J. 2: 544–551.

Ren, T., T.E. Ochsner, R. Horton, and Z. Ju. 2003b. Heat-pulse method for soil water content measurement: influence of the specific heat of the soil solids. Soil Sci. Soc. Am. J. 67(6): 1631–1634.

Renault, S. 2003. Barley, a potential species for initial reclamation of saline composite tailings of oil sands. J. Environ. Qual. 32(6): 2245–2253.

Riha, S.J., K.J. McInnes, S.W. Childs, and G.S. Campbell. 1980. A finite element calculation for determining thermal conductivity. Soil Sci. Soc. Am. J. 44: 1323–1325.

Rose, L., S. Krause, and N.J. Cassidy. 2013. Capabilities and limitations of tracing spatial temperature patterns by fiber-optic distributed temperature sensing. Water Resour. Res. 49(3): 1741–1745.

Rowland, S.M., C.E. Prescott, S.J. Grayston, S.A. Quideau, and G.E. Bradfield. 2009. Recreating a functioning forest soil in reclaimed oil sands in northern alberta: an approach for measuring success in ecological restoration. J. Environ. Qual. 38(4): 1580–90.

Saito, H., J. Šimůnek, J.W. Hopmans, and A. Tuli. 2007. Numerical evaluation of alternative heat pulse probe designs and analyses. Water Resour. Res. 43: W07408 1–14.

Sakaguchi, A., T. Nishimura, and M. Kato. 2005. The Effect of Entrapped Air on the Quasi-Saturated Soil Hydraulic Conductivity and Comparison with the Unsaturated Hydraulic Conductivity. Vadose Zo. J 4(1): 139–144.

Sauer, T.J., T.E. Ochsner, and R. Horton. 2007. Soil heat flux plates: heat flow distortion and thermal contact resistance. Agron. J. 99: 304–310.

Sayde, C., J.B. Buelga, L. Rodriguez-Sinobas, L.E.I. Khoury, M. English, N. van de Giesen, and J.S. Selker. 2014. Mapping variability of soil water content and flux across 1–1000 m scales using the actively heated fiber optic method. Water Resour. Res. 50: 7302–7317.

Sayde, C., C. Gregory, M. Gil-Rodriguez, N. Tufillaro, S. Tyler, N. van de Giesen, M. English, R. Cuenca, and J.S. Selker. 2010. Feasibility of soil moisture monitoring with heated fiber optics. Water Resour. Res. 46(6): W06201.

Selker, J., N. van de Giesen, M. Westhoff, W. Luxemburg, and M.B. Parlange. 2006a. Fiber optics opens window on stream dynamics. Geophys. Res. Lett. 33(24): L24401.

Selker, J.S., L. Thévenaz, H. Huwald, A. Mallet, W. Luxemburg, N. van de Giesen, M. Stejskal, J. Zeman, M. Westhoff, and M.B. Parlange. 2006b. Distributed fiber-optic temperature sensing for hydrologic systems. Water Resour. Res. 42(12): W12202.

Sepaskhah, A.R., and L. Boersma. 1979. Thermal conductivity of soils as a function of

temperature and water content. Soil Sci. Soc. Am. J. 43: 439–444.

Shaw, B., and L.D. Baver. 1939. An electrothermal method for following moisture changes on the soil in situ. Soil Sci. Soc. Am. Procedings 4: 78–83.

Sheets, K.R., and J.M.H. Hendrickx. 1995. Noninvasive Soil Water Content Measurement Using Electromagnetic Induction. Water Resour. Res. 31(10): 2401.

Shiozawa, S., and G.S. Campbell. 1990. Soil thermal conductivity. Remote Sens. Rev. 5(1): 301–310.

Shiozawa, S., and G.S. Campbell. 1991. On the calculation of mean particle diameter and standard deviation from sand, silt, and clay fractions. Soil Sci. 152(6): 427–431.

Singh, D.N., and K. Devid. 2000. Generalized relationships for estimating soil thermal resistivity. Exp. Therm. Fluid Sci. 22(3-4): 133–143.

Slusarchuk, W.A., and G.H. Watson. 1975. Thermal conductivity of some ice-rich permafrost soils. Can. Geotech. J. 12: 413–424.

Smidt, E., and J. Tintner. 2007. Application of differential scanning calorimetry (DSC) to evaluate the quality of compost organic matter. Thermochim. Acta 459: 87–93.

Somerton, W.H., and M. Mossahebi. 1967. Ring Heat Source Probe for Rapid Determination of Thermal Conductivity of Rocks. Rev. Sci. Instrum. 38(10): 1368–1371.

Song, Y., and J.M. Ham. 1998. Measuring soil water content under turfgrass using the dual-probe heat-pulse technique. J. Am. Soc. Hortic. Sci. 123(5): 937–941.

Song, Y., M.B. Kirkham, J.M. Ham, and G.J. Kluitenberg. 1999. Dual probe heat pulse technique for measuring soil water content and sunflower water uptake. Soil Tillage Res. 50: 345–348.

Steele-Dunne, S.C., M.M. Rutten, D.M. Krzeminska, M. Hausner, S.W. Tyler, J. Selker, T.A. Bogaard, and N.C. van de Giesen. 2010. Feasibility of soil moisture estimation using passive distributed temperature sensing. Water Resour. Res. 46(3): W03534.

Stehfest, H. 1970. Algorithm 368: Numerical inversion of Laplace transform. Commun. ACM 13(1): 47–49.

Striegl, A.M., and S.P. Loheide. 2012. Heated distributed temperature sensing for field scale soil moisture monitoring. Ground Water 50(3): 340–347.

Sturm, M., and J.B. Johnson. 1992. Thermal conductivity measurements of depth hoar. J. Geophys. Res. 97: 2129–2139.

Suárez, F. 2014. Comment on "'Capabilities and limitations of tracing spatial temperature patterns by fiber-optic distributed temperature sensing'" by Liliana Rose et al. Water Resour. Res.: 9777–9779.

Tarara, J.M., and J.M. Ham. 1997. Measuring soil water content in the laboratory and field with dual-probe heat-capacity sensors. Agron. J. 89(4): 535–542.

Tarnawski, V.R., and W.H. Leong. 2012. A Series-Parallel Model for Estimating the Thermal Conductivity of Unsaturated Soils. Int. J. Thermophys. 33(7): 1191–1218.

Tarnawski, V.R., M.L. McCombie, T. Momose, I. Sakaguchi, and W.H. Leong. 2013. Thermal Conductivity of Standard Sands. Part III. Full Range of Saturation. Int. J. Thermophys. 34(6):

1130–1147.

Tarnawski, V.R., T. Momose, and W.H. Leong. 2011. Thermal Conductivity of Standard Sands II. Saturated Conditions. Int. J. Thermophys. 32(5): 984–1005.

Tarnawski, V.R., T. Momose, W.H. Leong, G. Bovesecchi, and P. Coppa. 2009. Thermal Conductivity of Standard Sands. Part I. Dry-State Conditions. Int. J. Thermophys. 30(3): 949–968.

Thomas, L.C. 2005. Modulated DSC paper #9: Measurement of accurate heat capacity values. TA instruments.

Tian, Z., J.L. Heitman, R. Horton, and T. Ren. 2015. Determining Soil Ice Contents during Freezing and Thawing with Thermo-Time Domain Reflectometry. Vadose Zo. J. 14(8).

Tindall, J.A., and J.R. Kunkel. 1999. Unsaturated zone hydrology for sicentists and engineers. 1st ed. Prentice Hall, Upper Saddle River, NJ.

Topp, G.C., and J.L. Davis. 1985. Measurement of soil water content using Time-Domain Reflectrometry (TDR)-a field evaluation. Soil Sci. Soc. Am. J. 49(1): 19–24.

Trautz, A.C., K.M. Smits, P. Schulte, and T.H. Illangasekare. 2014. Sensible Heat Balance and Heat-Pulse Method Applicability to In Situ Soil-Water Evaporation. Vadose Zo. J. 13(1).

Tyler, S.W., S.A. Burak, J.P. Mcnamara, A.L. Lamontagne, J.S. Selker, and J. Dozier. 2008. Spatially distributed temperatures at the base of two mountain snowpacks measured with fiber-optic sensors. J. Glaciol. 54(187): 1–7.

Tyler, S.W., J.S. Selker, M.B. Hausner, C.E. Hatch, T. Torgersen, C.E. Thodal, and S.G. Schladow. 2009. Environmental temperature sensing using Raman spectra DTS fiber-optic methods. Water Resour. Res. 45(4): W00D23.

Valente, A., R. Morais, A. Tuli, J.W. Hopmans, and G.J. Kluitenberg. 2006. Multi-functional probe for small-scale simultaneous measurements of soil thermal properties, water content, and electrical conductivity. Sensors Actuators A 132: 70–77.

Wagener, T., N. McIntyre, M.J. Lees, H.S. Wheater, and H. V. Gupta. 2003. Towards reduced uncertainty in conceptual rainfall-runoff modelling: Dynamic identifiability analysis. Hydrol. Process. 17(2): 455–476.

Waite, W.F., L.Y. Gilbert, W.J. Winters, and D.H. Mason. 2006. Estimating thermal diffusivity and specific heat from needle probe thermal conductivity data. Rev. Sci. Instrum. 77(4): 044904.

Waite, W.F., L. a. Stern, S.H. Kirby, W.J. Winters, and D.H. Mason. 2007. Simultaneous determination of thermal conductivity, thermal diffusivity and specific heat in sI methane hydrate. Geophys. J. Int. 169(2): 767–774.

Wang, Q., T.E. Ochsner, and R. Horton. 2002. Mathematical analysis of heat pulse signals for soil water flux determination. Water Resour. Res. 38(6): 27–1 – 27–7.

Wang, Z., J. Yang, M. Yang, and W. Zhang. 2012. Investigation on Thermal Contact Conductance Based on Data Analysis Method of Reliability. Chinese J. Aeronaut. 25(5): 791–795.

Warrick, A.W. 2002. Soil physics companion. CRC Press, Boca Raton, FL.

Weiss, J.D. 2003. Using Fiber Optics to Detect Moisture Intrusion into a Landfill Cap Consisting of a Vegetative Soil Barrier. J. Air Waste Manage. Assoc. 53(9): 1130–1148.

Wen, M., G. Liu, B. Li, B.C. Si, and R. Horton. 2015. Evaluation of a self-correcting dual probe heat pulse sensor. Agric. For. Meteorol. 200: 203–208.

Wierenga, P.J., D.R. Nielsen, and R.M. Hagan. 1969. Thermal properties of a soil based upon field and laboratory measurements. Soil Sci. Soc. Am. Procedings 33: 354–360.

Woodside, W., and J.H. Messmer. 1961a. Thermal conductivity of porous media. I. Unconsolidated sands. J. Appl. Phys. 32(9): 1688–1699.

Woodside, W., and J.H. Messmer. 1961b. Thermal conductivity of porous media. Ⅱ. Consolidated rocks. J. Appl. Phys. 32(9): 1699–1706.

Xiao, Z., S. Lu, J.L. Heitman, R. Horton, and T. Ren. 2012. Measuring subsurface soil-water evaporation with an improved heat-pulse probe. Soil Sci. Soc. Am. J. 76: 876–879.

Yeh, W.W.-G. 1986. Review of parameter identification procedures in groundwater hydrology: The inverse problem. Water Resour. Res. 22(2): 95–108.

Young, M.H., G.S. Campbell, and J. Yin. 2008. Correcting dual-probe heat-pulse readings for changes in ambient temperature. Vadose Zo. J. 7: 22–30.

Zent, A.P., M.H. Hecht, D.R. Cobos, S.E. Wood, T.L. Hudson, S.M. Milkovich, L.P. DeFlores, and M.T. Mellon. 2010. Initial results from the thermal and electrical conductivity probe (TECP) on Phoenix. J. Geophys. Res. 115: E00E14: 1–23.

Zhang, X., J.L. Heitman, R. Horton, and T. Ren. 2014. Measuring Near-Surface Soil Thermal Properties with the Heat-Pulse Method: Correction of Ambient Temperature and Soil–Air Interface Effects. Soil Sci. Soc. Am. J. 78(5): 1575–1583.

Zhang, Y., M. Treberg, and S.K. Carey. 2011. Evaluation of the heat pulse probe method for determining frozen soil moisture content. Water Resour. Res. 47: W05544 1–11.

Zhu, Z., L. Tan, S. Gao, and Q. Jiao. 2015. Observation on Soil Moisture of Irrigation Cropland by Cosmic-Ray Probe. IEEE Geosci. Remote Sens. Lett. 12(3): 472–476.

Zreda, M., D. Desilets, T.P. a Ferré, and R.L. Scott. 2008. Measuring soil moisture content non-invasively at intermediate spatial scale using cosmic-ray neutrons. Geophys. Res. Lett. 35(21): 1–5.

Zreda, M., W.J. Shuttleworth, X. Zeng, C. Zweck, D. Desilets, T. Franz, and R. Rosolem. 2012. COSMOS: The cosmic-ray soil moisture observing system. Hydrol. Earth Syst. Sci. 16(11): 4079–4099.

APPENDICES

Appendix 1 Heat Pulse Probe Fabrication Guide

Table A.1 Specialty materials for the heat pulse probe fabrication used in this study

Item	Manufacture	Single probe	Dual probe
Stainless steel hypodermic tubes	Penn Stainless Products, Quakertown, PA	Length: 115 mm Outer diameter: 2.108 mm Inner diameter: 1.240 mm	Length: 33 mm Outer diameter: 2.108 mm Inner diameter: 1.240 mm
Thermistors	BetaTHERM Corp., Shrewsbury, MA	10 kΩ at 25 ^{o}C, Model 10K3MCD1	
Heating wires	Pelican Wire Co., Naples, FL	69.06 Ω m^{-1}	205 Ω m^{-1}
Epoxy	Omega Engineering, Stamford, CT	Omegabond® 101 high thermal conductivity epoxy	
Plastic plug cups		Outer diameter: 32 mm Length: 32 mm Wall thickness: 5 mm With predrilled holes	
Glue for plug		LePage® speed set epoxy	
Solder		Lead free acid flux cored silver solder	
Electric cables		14 AWG	

Other consumables: cardboard, Scotch transparent removable tape, fine-grit sandpaper, heat-shrink rubber tubes, stirring sticks, thin hypodermic rubber tube, 6 mL syringe with needle.

Tools: caliper, cut off tool, heat gun, magnifying glass, ohmmeter, pen, razor blade, scissor, soldering iron, wire cutter and stripper.

Important tips:

1. **Be patient and gentle**. Because the thermistors and the wires are very tiny, make sure to be meticulous enough in each step, or they will be broken easily. It is worth to spend two whole days to build an accurate probe rather than two hours to build an inaccurate one.

2. **Check wire connections**. After sanding the ends of the heating wires and thermistors, be sure to use an ohmmeter to check if there are correct resistance readings. It is easy to break them, especially during the period after the soldering and before filling epoxy to the probe plug cup.

3. **Practice**. It is highly recommended to use the spare wires and tubes to practise your soldering and epoxy filling skills, which are the trickiest steps to build a heat pulse probe. As the heating wires need higher temperature for soldering than the thermistors, the heating wires may be more difficult to be soldered together with electrical cables.

Steps to fabricate a heat pulse probe:

1. **Cut off the stainless steel hypodermic tubes with the lengths needed**.

In this study, the needle lengths of the single probes are 110 mm, and a 5 mm additional length is needed to amount the tube into the probe body; therefore, in total of a 115 mm length is sufficient. For the dual probes, the needles are 33 mm long in total, with 5 mm in the wall of the probe body plug and 28 mm outside of the plug for measurement. Cut the needles needed with a drum tool, and then change the cutting tip with a sandpaper tip to smooth the cutting edges (Fig. A.1).

Fig. A.1 Stainless steel needles have been cut and the cut off tool with a sandpaper tip on.

2. **Cut off the thermistor wires and heating wires with the lengths needed and mark with the scotch removable tapes**.

Taking the single probe as an example, the heating wire will be threaded through the whole length of the needle in one loop. Therefore, first fold the heating wire and measure 115 mm with a caliper, put a tiny piece of removable tape to mark this spot. In this way, we have a sign to confirm that the heating wire is in the correct location when we insert the heating wire into the needle. An extra 10 mm length of the wire located outside of the needle and placed in the plug cup is needed to be soldered with the electrical cable later. Therefore, we should cut a total length of 250 mm for a loop of heating wire (Fig. A.2).

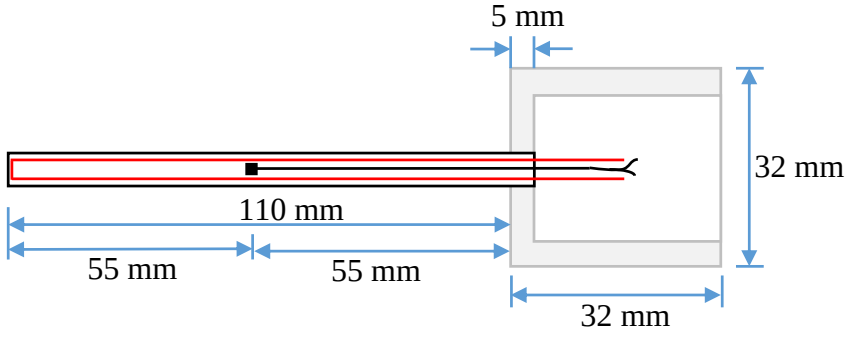

Fig. A.2 Schematic of the single probe sizes (not to scale).

For a thermistor, the tip of the thermistor should be placed a little over the centre of the needle, i.e. 55 mm distance from the tip of the needle as shown in Fig. A.2. This is because only 110 mm out of 115 mm of the needle is actually used as the probe for measurement, the rest of 5 mm needle is amounted in the plug cup. Therefore, we should mark 60 mm (55+5 mm) with the removable tape and cut it with a length of 70 mm (extra 10 mm for soldering).

The same method and calculations can be applied to the dual probes. As a much higher heating strength is needed for the dual probe, the heating wires should be two loops installed in the dual

needle to ensure enough heating power. Of course, the number of loops depends on the resistance per unit length of the heating wire you have. In conclusion, one loop of the heating wire and one thermistor are installed in the same needle for the single probe; whereas for the dual probe, two loops of the heating wire and one thermistor are installed in the heater needle and one thermistor is installed in the sensor needle. Note that the needle sizes and the heating wires are different between two kinds of probes (Table A.1).

3. **Glue the heating wire and thermistors in the needles with Omegabond® 101 epoxy**.

First, place the wires in the needles at the correct positons judged by the positions of the removable tapes. In Fig. A.3 you can see what I did was to make the wires a few cm longer than what is needed, and then cut the wires to the length I actually need after the wires were glued by the epoxy. You can choose do it in either way. Fix the needle and wires on a cardboard vertically with removable tapes and the tails of the wires should be at the top.

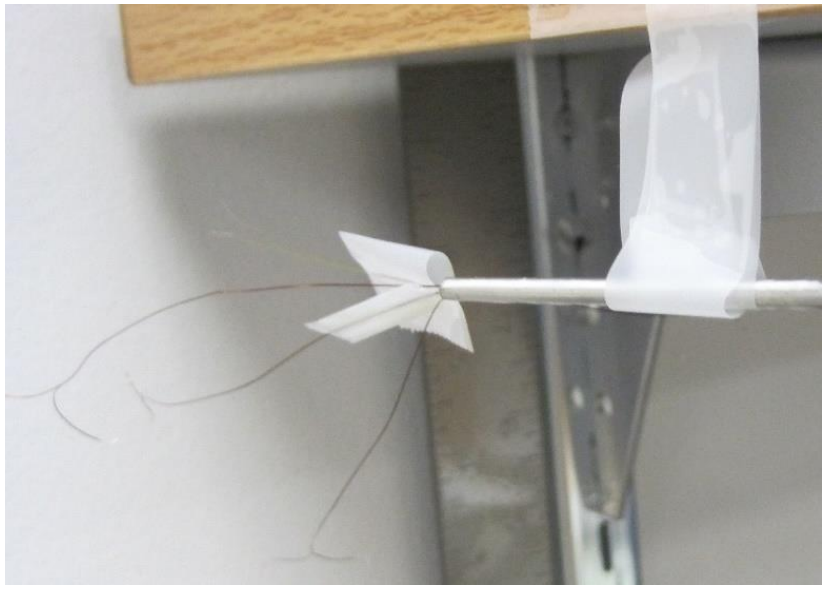

Fig. A.3 The single probe needle with one loop of heating wire and one thermistor installed.

Now take out the epoxy containers which should be kept in the refrigerator. There are two tins, one resin and another one catalyst (Fig. A.4). Mix them in a container around 1:1 volume with a stirring stick. The amount of epoxy needed for the needles is really tiny. The epoxy will become dry and sticky quickly, so be sure to use them as soon as possible. Load some epoxy in a 6mL or similar size syringe with a hypodermic needle.

The best way to squeeze the epoxy into the heat pulse probe needles may be to use a section of rubber tube that fits both the syringe needle tube and the heat pulse probe needles (Fig. A.4). It is recommended to practice this step with an empty needle. Do not push the syringe too fast, and give the epoxy enough time to fill up the whole the needle slowly without air entrapped. In addition, the heating wires and the thermistors may be pushed out when you fill the epoxy, because the epoxy is sticky. Please check the position of the tapes attached on the wires frequently and bring them back if they move. After finishing the filling, remove the rubber tube from the needle, and modify the tip of probe needle to a nice round shape with epoxy using a stick so the heating wire is not exposed out of the needle. Now put the probe needle horizontally and wait for 24 hours until the epoxy is try enough to continue next step.

4. **Solder the probe wires to the electric cables**.

When the epoxy is dry, remove the tapes on the wires. Use a fine-grit sandpaper to rub 3 mm of the tip ends of the wires to remove the enamel electric insulation coats. Using a magnifying glass to check if the coats at all sides of the wires have been removed. The two ends of the thermistor wires are tied together and need to be split all the way down to the base of the needle.

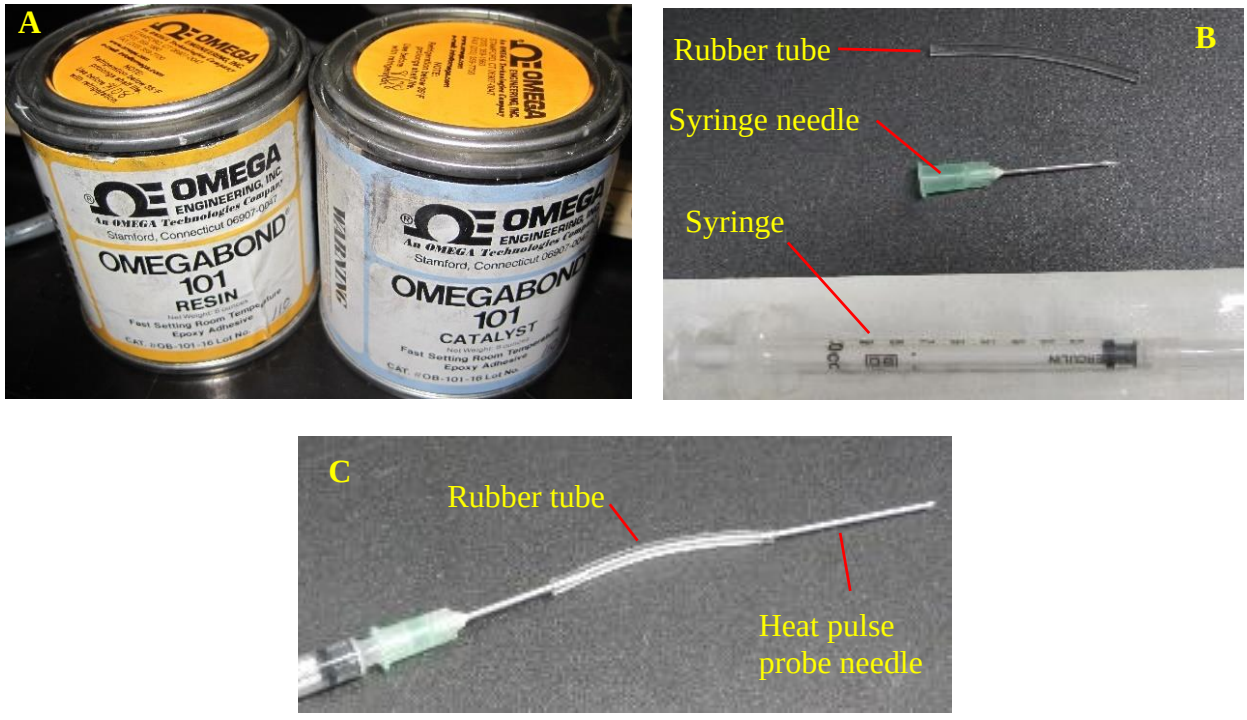

Fig. A.4 High thermal conductivity epoxy (A) and syringe items (B) and connections (C).

Choose the appropriate electric cable. Taking the single probe as example, each of the thermistor and the heating wire has two ends, therefore a 4-core electric cable can be used. Cut the electric cable to an appropriate length needed to connect the heat pulse probe to the datalogger. Strip 2 cm off two ends of the cable using a wire stripper to expose the four core wires, and then trim 3 mm off the two end of each core wire. One end for soldering to the probe and another for connecting to the datalogger (Fig. A.5).

Before the soldering, put a 2-cm long heat-shrink rubber tube on each end of the heating wire and thermistor, which will be used for thermal and water insulation. Place and fix the heating wires, the thermistors, and the probe needle on a cardboard using the removable tape, so that the tips of the wires needed to be soldered together touch each other. Heat up the soldering iron to 370 ^{o}C, and solder the wires using the flux-cored silver solder. A little bit of solder is enough, so try to avoid suing too much solder or soldering for too long. After finishing the soldering, check

the resistance of the wires at the end of the electric cable using an ohmmeter. Now adjust the positions of heat-shrink rubber tubes so they cover all naked wires around the soldering points, then use the heat gun to heat them to prevent short. Then label each core wire of the electric cable at your convenience so you know which wire is connected to which in the probe (Fig. A5).

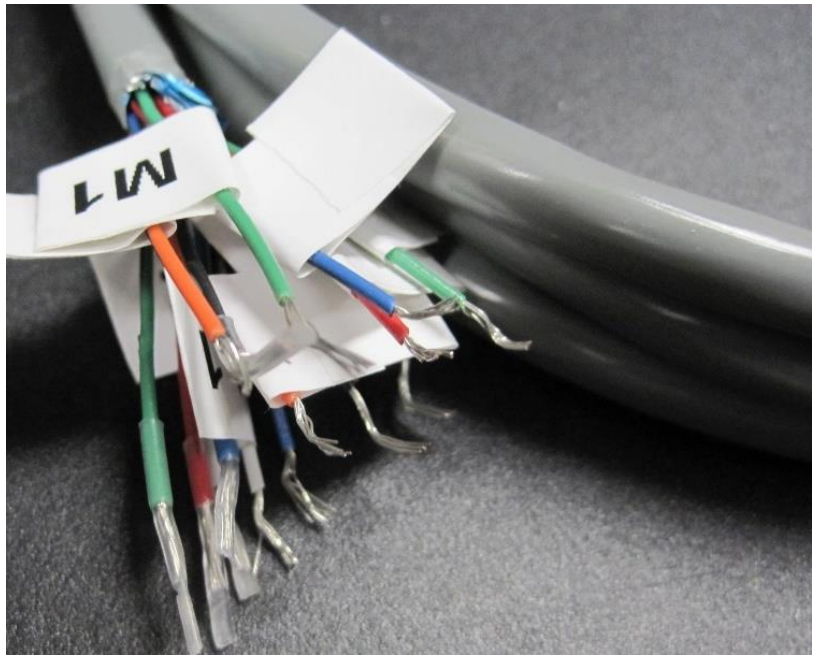

Fig. A.5 One end of the electric cable to be connected to a datalogger.

5. **Secure the needles in the probe body plug cup**.

This step needs your patient the most, as the soldered wires are very fragile. The Physics Shop, University of Saskatchewan, made the plastic plug cup with holes for us (Fig. A.6A), because a computer-assisted lathe is needed to drill a hole with such a small diameter of the heat pulse probe needles. Then coil up the cable and fix it on a cardboard, and then insert the probe needle slowly. Because the hole and the needle fits tightly, it is not easy to install. Be careful not to break the wires. After inserting the needle at the correct position in the cup, fix them on the cardboard with removable tapes, and then put the cardboard vertically for filling with epoxy.

Now it is ready to fill the cup with glue. We used the 5-minutes fast set epoxy glue to fill the cup following the product instructions; however, it takes several hours to be completely dry. One of the single probe we made is shown in Fig. A.6B.

Reference: E. Benson. 2004. A guide for the construction and operation of dual-probe heat-capacity sensors. Kansas State University.

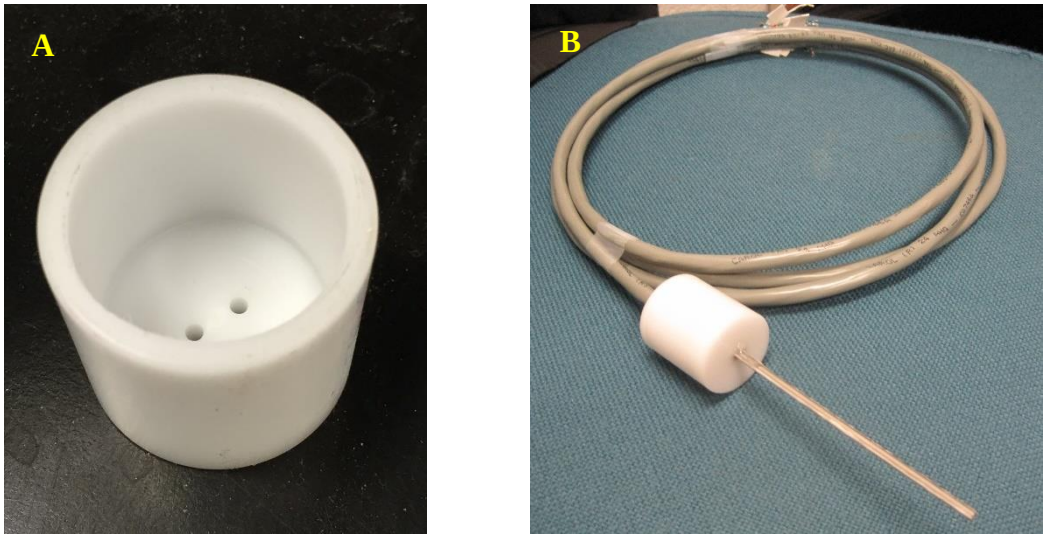

Fig. A.6 An example of the probe body plug cup (A) and a fabricated heat pulse single probe with electric cable (B).

Appendix 2 Wiring diagrams and pictures of the heat pulse probe setup

The heat pulse probe needs to be connected to a datalogger to conduct the automated soil property measurement. The commonly used dataloggers are CR10X, CR1000, and CR9000X from Campbell Scientific, Logan, UT. And the software to write, send, and receive programs to the datalogger and to download the measurement data is called LoggerNet (Campbell Scientific, Logan, UT).

The model CR10X is relative old and the program of CR10X is written in "Edlog", which is very difficult to read. The CR1000 and CR9000X are newer and use a much more friendly language - CRBasic - to write the programs. In addition, the internal data storage memories of CR1000 and CR9000X are larger and can be expended by an external memory. We mainly used the CR9000X datalogger in this study because it can measure as many as up to eight single probes at the same time, whereas the CR1000 has to use a multiplexer to hook up to more than two probes.

In this appendix we presented the wiring diagrams and pictures of the single probes with CR9000X datalogger connections to the readers. It will be the same way to connect a dual probe, and the only difference is that the dual probe does not need an adjustable resistor to control the heating strength. This is because a much higher heating strength is needed for the dual probe and the heating wires are installed two loops in the probe based on our calculation in advance to provide sufficient power. For the single probe; however, a much lower heating strength is required so the temperature of the probe increases slower. Therefore, an adjustable resistor is needed to limit the current. All the main equipment and materials needed to build up the system is listed in Table A.2.

Table A.2 Items used in this study for the single-probe heat pulse setup

Item	Manufacture	Notes	Picture
Datalogger	Campbell Scientific Logan, UT	Model CR9000X	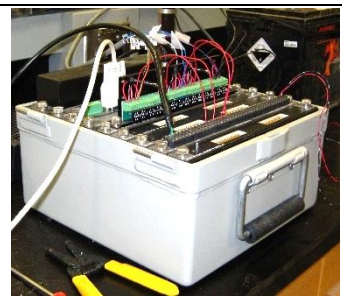
Resistor	Vishay Intertechnology Malvern, PA	Dale RH-25 25 W, 1 Ω, 1 % precision	
Precision resistor	Vishay Intertechnology Malvern, PA	5 kΩ, 0.01 % precision	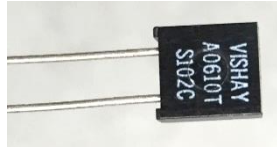
Adjustable resistor		0 - 100 Ω	
Relay	Crydom, San Diego, CA	Voltage: Control:3.5 - 32 V Load: 1 - 100 V	
Cylindrical PVC containers		Height: 13 cm Diameter: 10 cm Used as soil columns	
PVC container cover		Made of duck tapes filled with insulation batts	
Electrical wires		18 AWG	

Figure A.7 shows the CR9000X datalogger system with three single probes connected, which was used for soil measurement in Chapters 4 and 5. We used a vehicle battery to provide 12 V power for the datalogger. For the heaters of the probes; however, we used an independent AC to DC adapter for two reasons. First, the heater and datalogger sharing one power source can cause the datalogger system errors sometimes. Second, an AC to DC adapter can provide a constant heating input for the probes, whereas the voltage of the battery decrease after each measurement. A relay was used for the datalogger to turn on and off the heat pulses, and an adjustable resistor was used for each probe to control the single probe heating strength be around 5 W m^{-1} (Fig. A.8A). In order to reduce the ambient temperature change effect on the measurement, we made coat (Table A.2) for the PVC soil columns using the duck tapes with insulation batts inside.

The temperature data are calculated from the measured resistances of the thermistors through the Steinhart-Hart Equation, and the resistances are recorded by the datalogger through the four-wire half bridge measurements. Figure A.8B. To help the readers to connect their own probes, a wiring diagram (Fig. A.9A) is provided, with the wires in black for the sensor and those in red for the heater. As the most important wiring connection, a picture of the four-wire half bridge is shown in Fig. A. 9B.

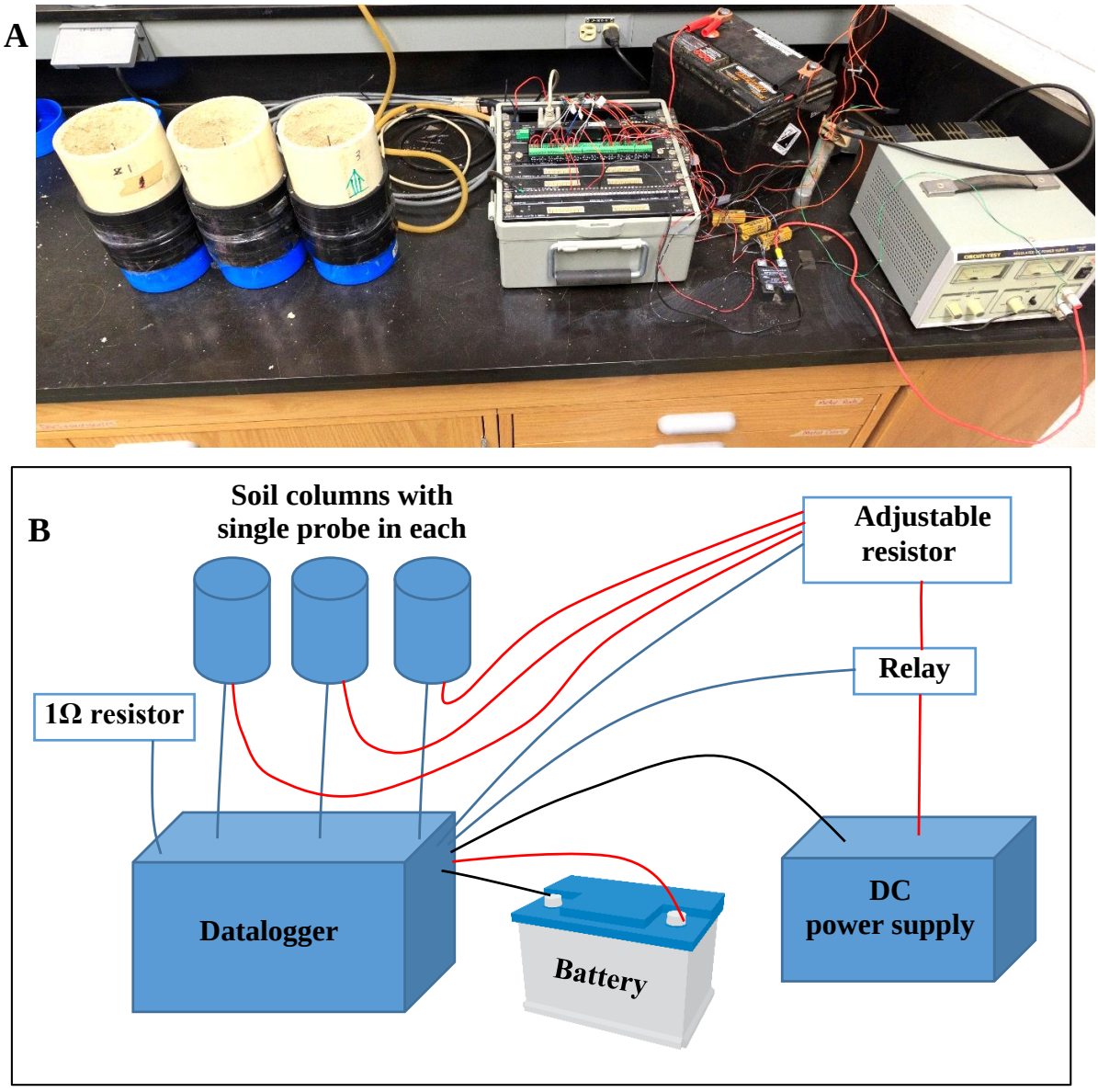

Fig. A.7 Picture (A) and schematic (B) of a CR9000X datalogger connected to three single probes.

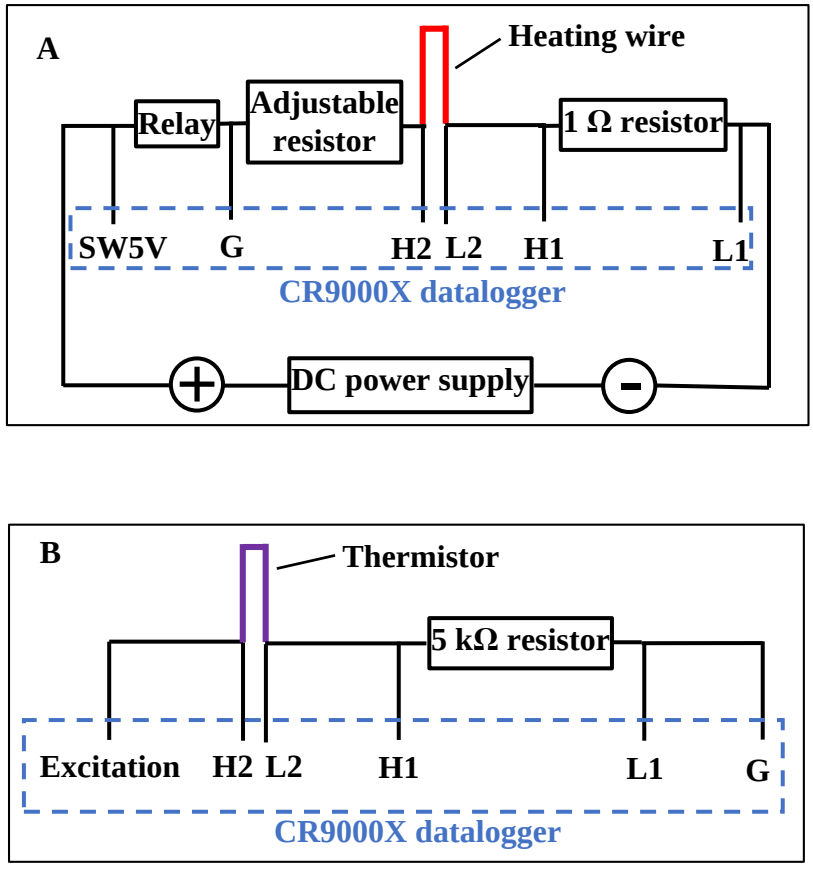

Fig. A.8 Electric diagrams of the four-wire half bridge connection of the sensor needle (A) and the connection of the heater needle (B).

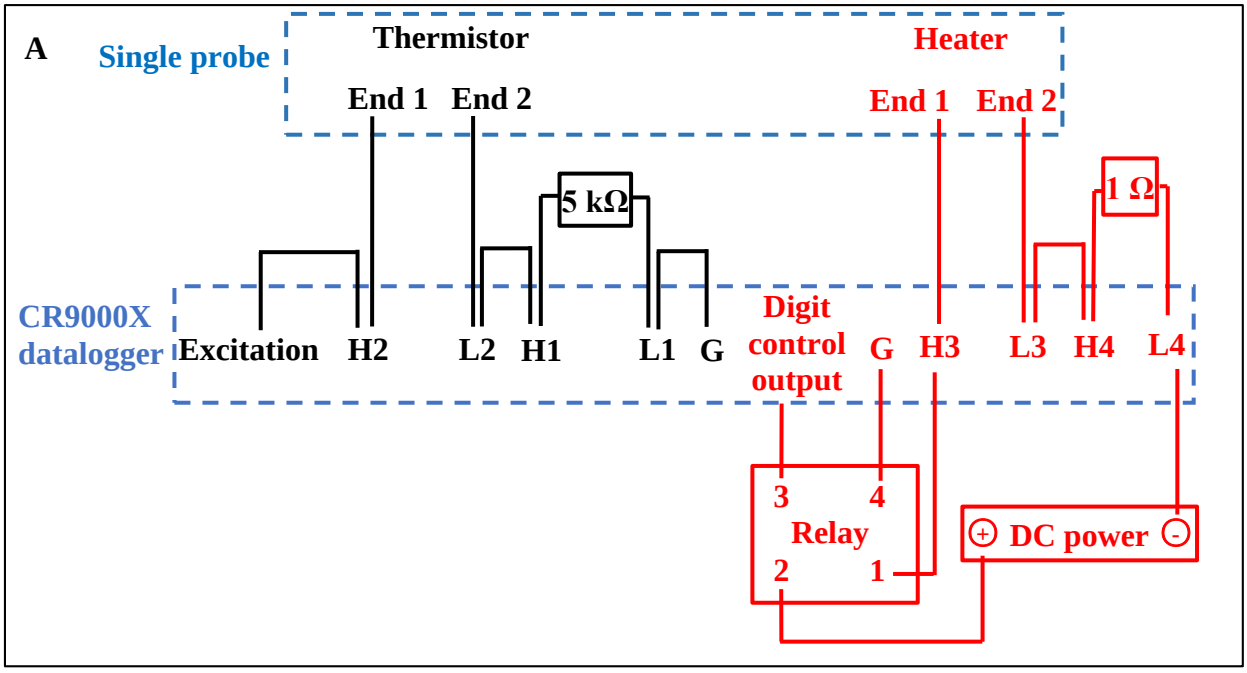

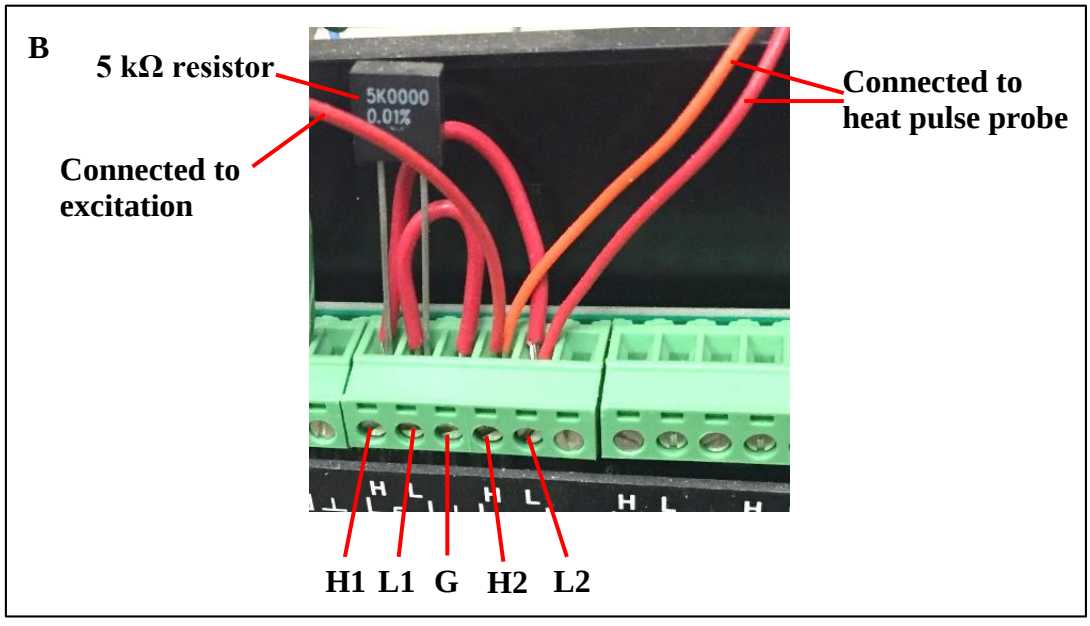

Fig. A.9 The wiring diagram of the single probe to the datalogger (A) and a picture of the four-wire half bridge connection of the thermistor (B).

Appendix 3 CRBasic program of the CR9000X datalogger for the single-probe heat pulse measurement

```
'                  Program name: MINLI.C9X
'                    Written by: minli
'                   I.D. number: 20110513
'                  Date written: 05-13-2011
'                  Time written: 18:26:21
'                PC9GEN Version: 5.3.0068
' This program was generated using Campbell Scientific's PC9GEN
' Program Generator for the CR9000 Measurement & Control System.
'        _____ Logger CONFIGURATION _____
'        Slot 1 = 9011     Slot 5 = 9050/51  Slot  9 = None
'        Slot 2 = 9032     Slot 6 = 9050/51  Slot 10 = None
'        Slot 3 = 9041     Slot 7 = 9060     Slot 11 = None
'        Slot 4 = 9050/51  Slot 8 = 9070/71  Slot 12 = None
'\\\\\\\\\\\\\\\\\\\\\\\\ SlotConfigure ////////////////////////
SlotConfigure(9050,9050,9050,9060,9070)
'\\\\\\\\\\\\\\\\\\\\\\ TIMING CONSTANTS //////////////////////
Const F = 138
Const SteinA = 1.1292E-3
Const SteinB = 2.3411E-4
Const SteinC = 8.7755E-8
'\\\\\\\\\\\\\\\\\ ALIASES & OTHER VARIABLES /////////////////
Public CumHeat1
Public CumHeat2
Public CumHeat3
Public CalcHeat1
Public CalcHeat2
Public CalcHeat3
Public CalcTemp11
Public CalcTemp1
Public CalcTemp22
Public CalcTemp2
Public CalcTemp33
Public CalcTemp3

Public elapsed
Public ExtraDelay
Public PortOn
Public Battery_V
Public Battery_mA

'\\\\\\\\\\\\\\\\\\\\\\\ OUTPUT SECTION ////////////////////////
```

```
    DataTable(TempData, True, -1)
    DataInterval(0,0,msec,1)
     CardOut (0,-1)
        Sample (1, CumHeat1, IEEE4)
        Sample (1, CalcHeat1, IEEE4)
        Sample (1, CalcTemp1, IEEE4)
        Sample (1, CumHeat2, IEEE4)
        Sample (1, CalcHeat2, IEEE4)
        Sample (1, CalcTemp2, IEEE4)
        Sample (1, CumHeat3, IEEE4)
        Sample (1, CalcHeat3, IEEE4)
        Sample (1, CalcTemp3, IEEE4)
        Sample (1, PortOn, IEEE4)
        Sample (1,Battery_V,IEEE4)
        Sample (1,Battery_mA,IEEE4)
    EndTable

    '\\\\\\\\\\\\\\\\\\\\\\\\\\\\ PROGRAM ////////////////////////////
BeginProg
    Dim StartTime( 6 )         'the first time to begin cycling power
    StartTime( 1 ) = 2012      'year
    StartTime( 2 ) = 6         'month
    StartTime( 3 ) = 1         'day
    StartTime( 4 ) = 3         'hour
    StartTime( 5 ) = 54        'minute
    StartTime( 6 ) = 00        'second

    Scan(50,mSec,1,19600)
        If IfTime(0,14400,sec) Then PortOn=1
        If IfTime(600,14400,sec) Then PortOn=0

        If IfTime(0,14400,sec) Then CumHeat1=0
        If IfTime(0,14400,sec) Then CumHeat2=0
        If IfTime(0,14400,sec) Then CumHeat3=0

        'set port1 high to turn on the heater, low to close.
        PortSet(7,8,PortOn,0)
        Timer(1000,uSec,2)

        SubScan (50,mSec,1)
        BrHalf4W (CalcTemp11,1,mV200,mV200,4,1,7,8,1,200,1,1,20,20,5000,0)
        CalcTemp11=SteinA+SteinB*LN(CalcTemp11)+SteinC*LN(CalcTemp11)*LN(CalcTe
mp11)*LN(CalcTemp11)
        CalcTemp11=1/CalcTemp11
        CalcTemp1=CalcTemp11-273.15
        CallTable(TempData)
```

```
        BrHalf4W (CalcTemp22,1,mV200,mV200,4,3,7,9,1,200,1,1,20,20,5000,0)
        CalcTemp22=SteinA+SteinB*LN(CalcTemp22)+SteinC*LN(CalcTemp22)*LN(CalcTe
mp22)*LN(CalcTemp22)
        CalcTemp22=1/CalcTemp22
        CalcTemp2=CalcTemp22-273.15
        CallTable(TempData)

        BrHalf4W (CalcTemp33,1,mV200,mV200,4,5,7,10,1,200,1,1,20,20,5000,0)
        CalcTemp33=SteinA+SteinB*LN(CalcTemp33)+SteinC*LN(CalcTemp33)*LN(CalcTe
mp33)*LN(CalcTemp33)
        CalcTemp33=1/CalcTemp33
        CalcTemp3=CalcTemp33-273.15
        CallTable(TempData)

        VoltDiff (CalcHeat1,1,mV5000,4,9,True,0,10,0.001,0)
        CumHeat1 = CumHeat1 + F * CalcHeat1 * CalcHeat1*0.05
        CallTable(TempData)
        VoltDiff (CalcHeat2,1,mV5000,4,11,True,0,10,0.001,0)
        CumHeat2 = CumHeat2 + F * CalcHeat2 * CalcHeat2*0.05
        CallTable(TempData)
        VoltDiff (CalcHeat3,1,mV5000,4,13,True,0,10,0.001,0)
        CumHeat3 = CumHeat3 + F * CalcHeat3 * CalcHeat3*0.05
        CallTable(TempData)

        Battery(Battery_mA,1)
        CallTable(TempData)

        Battery(Battery_V,0)
        CallTable(TempData)
        NextSubScan

        elapsed = Timer(1000,uSec,4)
    NextScan
    PowerOff (StartTime(),14400,Sec)
EndProg
'***** Program End *****
```

Appendix 4 Mathcad Program and import data for calibrating the dual probe needle spacing

Following is a program has been used in Chapter 3 to calculate the apparent needle spacing of a dual probe in agar-stabilized water with known thermal properties. Partial of an import data file is attached after the program for your reference.

Program:

Import the data from an excel file

Agar :=

.....\0. agar.xlsx

$$E11(x) := \begin{cases} \exp(-x)\cdot\dfrac{0.2677737343 + 8.6347608925\cdot x + 18.059016973\cdot x^2 + 8.5733287401\cdot x^3 + x^4}{x\cdot\left(x^4 + 9.5733223454\cdot x^3 + 25.6329561486\cdot x^2 + 21.0996530827\cdot x + 3.9584969228\right)} & \text{if } x > 1 \\ -\ln(x) - 0.57721566 + 0.99999193\cdot x - 0.24991055\cdot x^2 + 0.05519968\cdot x^3 - 0.00976004\cdot x^4 + 0.00107857\cdot x^5 & \text{otherwise} \end{cases}$$

Specific Heat, density, and thermal diffusivity as a function of temperature

$$cwater(T) := \left(-4.7115\cdot 10^{-11}\cdot T^5 + 1.5179\cdot 10^{-8}\cdot T^4 - 1.8610\cdot 10^{-6}\cdot T^3 + 1.1618\cdot 10^{-4}\cdot T^2 - 3.4918\cdot 10^{-3}\cdot T + 4.2175\right)\cdot 10^6$$

$$\rho water(T) := -1.34324\cdot 10^{-10}\cdot T^4 + 4.25544\cdot 10^{-8}\cdot T^3 - 7.59647\cdot 10^{-6}\cdot T^2 + 5.37877\cdot 10^{-5}\cdot T + 0.999853$$

$$\alpha water(T) := -2.089\cdot 10^{-12}\cdot T^2 + 5.586\cdot 10^{-10}\cdot T + 1.330\cdot 10^{-7}$$

Calibration using Agar solution

t0 := 8 frq := 20 r := 0.006

$$\Delta T(\alpha, C, q, r, t0, t) := \begin{cases} \dfrac{q}{4\cdot\pi\cdot\alpha\cdot C}\cdot\left(E11\left(\dfrac{r^2}{4\cdot\alpha\cdot t}\right)\right) & \text{if } t \le t0 \\ \dfrac{q}{4\cdot\pi\cdot\alpha\cdot C}\cdot\left[E11\left(\dfrac{r^2}{4\cdot\alpha\cdot t}\right) - E11\left[\dfrac{r^2}{4\cdot\alpha\cdot(t - t0)}\right]\right] & \text{otherwise} \end{cases}$$

$$Ag\_SSE(r, t, T, q, t0) := \sum_{i=1}^{length(t)-1}\left[\frac{\Delta T\left(\alpha water(18), cwater(18), q, r, t0, t_i\right) - \left(T_i - T_0\right)}{\sqrt{t_i + 1}}\right]^2$$

$$Ag\_parm(r, t, T, q, t0) := Minimize(Ag\_SSE, r)$$

```
Ag_parms(ii) := | N ← rows(Agar)
                | for i ∈ 0..1000
                |   M_i ← 1
                | j ← 0
                | for i ∈ 0..N − 1
                |   t_i ← Agar_{i,0}
                |   continue if i = 0
                |   M_j ← M_j + 1 if t_i > t_{i−1}
                |   j ← j + 1 otherwise
                | count ← 0
                | for iii ∈ 0..j
                |   k ← Σ_{i=0}^{iii} M_i − M_iii
                |   (time ← submatrix(Agar, k, k + M_iii − 1, 0, 0)  Temp ← submatrix(Agar, k, k + M_iii − 1, ii, ii))
                |   q ← Agar_{k+frq·t0·2,1} / t0
                |   rr_count ← Ag_parm(r, time, Temp, q, t0)
                |   count ← count + 1
                | rr
```

radius1 := Ag_parms(2) radius2 := Ag_parms(3)

$$r1 := \frac{\left(\sum_{i=0}^{8} radius1_{i,0}\right)}{9} = 5.999 \times 10^{-3} \qquad r2 := \frac{\left(\sum_{i=0}^{8} radius2_{i,0}\right)}{9} = 6.127 \times 10^{-3}$$

Example of the import data obtained from the dual probe heat pulse measurement in agar solution:

Time (s)	Total heat input (J m^{-1})	Temperature of sensor 1 (^{0}C)	Temperature of sensor 2 (^{0}C)
0.00	0.00	14.43	14.53
0.05	3.34	14.43	14.53
0.10	6.68	14.43	14.54
0.15	10.02	14.43	14.53
0.20	13.37	14.43	14.52
0.25	16.71	14.43	14.52
0.30	20.05	14.43	14.52

Appendix 5 Mathcad Program and import data to calculate the solid percentage of mature fine tailings

Following is a program has been used in Chapter 3 to calculate the thermal properties and solid percentages of mature fine tailings using the dual-probe heat pulse method. This program can calculate data from four sensors at the same time and can be revised and extended to as many as you need. Partial of an import data file is attached after the program for your reference.

Program:

$$E11(x) := \begin{cases} \exp(-x)\cdot\dfrac{0.2677737343 + 8.6347608925\cdot x + 18.059016973\cdot x^2 + 8.5733287401\cdot x^3 + x^4}{x\cdot\left(x^4 + 9.5733223454\cdot x^3 + 25.6329561486\cdot x^2 + 21.0996530827\cdot x + 3.9584969228\right)} & \text{if } x > 1 \\ -\ln(x) - 0.57721566 + 0.99999193\cdot x - 0.24991055\cdot x^2 + 0.05519968\cdot x^3 - 0.00976004\cdot x^4 + 0.00107857\cdot x^5 & \text{otherwise} \end{cases}$$

Specific Heat, density, and thermal diffusivity as a function of temperature

$$cwater(T) := \left(-4.7115\cdot10^{-11}\cdot T^5 + 1.5179\cdot10^{-8}\cdot T^4 - 1.8610\cdot10^{-6}\cdot T^3 + 1.1618\cdot10^{-4}\cdot T^2 - 3.4918\cdot10^{-3}\cdot T + 4.2175\right)\cdot10^6$$

$$\rho water(T) := -1.34324\cdot10^{-10}\cdot T^4 + 4.25544\cdot10^{-8}\cdot T^3 - 7.59647\cdot10^{-6}\cdot T^2 + 5.37877\cdot10^{-5}\cdot T + 0.999853$$

$$\alpha water(T) := -2.089\cdot10^{-12}\cdot T^2 + 5.586\cdot10^{-10}\cdot T + 1.330\cdot10^{-7}$$

$t0 := 8 \qquad frq := 1$

$$\Delta T(\alpha, C, q, r, t0, t) := \begin{cases} \dfrac{q}{4\cdot\pi\cdot\alpha\cdot C}\cdot\left(E11\left(\dfrac{r^2}{4\cdot\alpha\cdot t}\right)\right) & \text{if } t \le t0 \\ \dfrac{q}{4\cdot\pi\cdot\alpha\cdot C}\cdot\left[E11\left(\dfrac{r^2}{4\cdot\alpha\cdot t}\right) - E11\left[\dfrac{r^2}{4\cdot\alpha\cdot(t - t0)}\right]\right] & \text{otherwise} \end{cases}$$

$r1 := 0.005874 \quad r2 := 0.006164 \quad r3 := 0.006057 \quad r4 := 0.006100$

Dual Probe Heat Pulse method for estimating soil thermal properties

Import the data from an excel file

All :=

0. DPHP Data all in one.xlsx

Objective function

$$SSE(\alpha, C, t, T, r, q) := \sum_{i=1}^{length(t)-1} \left[\frac{\Delta T\left(\alpha \cdot 10^{-7}, C \cdot 10^{6}, q, r, t0, t_i\right) - \left(T_i - T_0\right)}{\sqrt{t_i + 1}} \right]^2$$

$$parm(\alpha, C, t, T, r, q) := Minimize(SSE, \alpha, C)$$

Smart method for obtaining initial parameter values

$$vg(t, T, r, q) := \left| \begin{array}{l} \left(m \leftarrow match(max(T), T)_0 \quad T_{max} \leftarrow T_m \quad T_i \leftarrow T_0\right) \\ \alpha \leftarrow \frac{r^2}{4} \cdot \left(\frac{\frac{1}{t_m - t0} - \frac{1}{t_m}}{\ln\left(\frac{t_m}{t_m - t0}\right)} \right) \\ C \leftarrow \frac{q}{4 \cdot \pi \cdot \alpha \cdot \left(T_{max} - T_i\right)} \cdot \left[E11\left(\frac{r^2}{4 \cdot \alpha \cdot t_m}\right) - E11\left[\frac{r^2}{4 \cdot \alpha \cdot \left(t_m - t0\right)}\right] \right] \\ stack\left(\alpha \cdot 10^{7}, C \cdot 10^{-6}\right) \end{array} \right.$$

Further minimize the sum of squared error by adjusting parameter values.

$$ThermParms(rr, ii) := \left| \begin{array}{l} N \leftarrow rows(All) \\ \text{for } i \in 0..1000 \\ \quad M_i \leftarrow 1 \\ j \leftarrow 0 \\ \text{for } i \in 0..N-1 \\ \quad \left| \begin{array}{l} t_i \leftarrow All_{i,0} \\ \text{continue if } i = 0 \\ M_j \leftarrow M_j + 1 \text{ if } t_i > t_{i-1} \\ j \leftarrow j + 1 \text{ otherwise} \end{array} \right. \\ count \leftarrow 0 \\ \text{for } iii \in 0..j \\ \quad \left| \begin{array}{l} k \leftarrow \sum_{i=0}^{iii} M_i - M_{iii} \\ \left(time \leftarrow submatrix\left(All, k, k + M_{iii} - 1, 0, 0\right) \quad Temp \leftarrow submatrix\left(All, k, k + M_{iii} - 1, ii, ii\right)\right) \\ \left(r \leftarrow rr \quad q_{count} \leftarrow \frac{All_{k+frq \cdot t0 \cdot 2, 1}}{t0}\right) \\ \begin{pmatrix} \alpha ini \\ Cini \end{pmatrix} \leftarrow vg\left(time, Temp, r, q_{count}\right) \\ \begin{pmatrix} \alpha_{count} \\ C_{count} \end{pmatrix} \leftarrow parm\left(\alpha ini, Cini, time, Temp, r, q_{count}\right) \\ \left(c_s \leftarrow 750000 \quad Cw \leftarrow cwater(24) \cdot \rho water(24) \quad \rho_p \leftarrow 2.65\right) \end{array} \right. \end{array} \right.$$

$$\lambda_{count} \leftarrow \alpha_{count} \cdot C_{count} \cdot 0.1$$

$$\theta_{count} \leftarrow \frac{C_{count} \cdot 10^{6} - c_s \cdot \rho_p}{Cw - c_s \cdot \rho_p}$$

$$solid_{count} \leftarrow \frac{(1 - \theta_{count}) \cdot \rho_p}{(1 - \theta_{count}) \cdot \rho_p + \theta_{count}}$$

$$sample_{count} \leftarrow All_{k,6}$$

$$count \leftarrow count + 1$$

$$augment\left(q, \alpha \cdot 10^{-7}, C \cdot 10^{6}, \lambda, \theta, solid, sample\right)$$

needle1 := ThermParms(r1 , 2)

needle2 := ThermParms(r2 , 3)

needle3 := ThermParms(r3 , 4)

needle4 := ThermParms(r4 , 5)

Alldata := augment(needle1 , needle2 , needle3 , needle4)

output-1.xls

Alldata

Example of the import data

Time (s)	Total heat input (J m^{-1})	Temperature increase (^{0}C)				Sample ID
		Sensor 1	Sensor 2	Sensor 3	Sensor 4	
0.75	0.00	0.00	0.00	0.00	0.00	1
1.875	0.00	0.00	0.00	0.01	0.00	1
2.875	41.62	0.00	0.00	0.01	0.00	1
3.875	83.49	0.00	0.00	0.01	-0.01	1
4.875	125.35	0.00	0.00	0.02	0.00	1
5.875	167.22	0.00	0.00	0.02	0.00	1
6.75	209.09	0.00	0.00	0.02	0.00	1
7.75	250.95	0.00	0.00	0.01	0.00	1
8.75	292.32	0.01	0.00	0.01	0.00	1
9.75	334.44	0.01	0.00	0.02	0.00	1
10.75	334.44	0.02	0.00	0.03	0.01	1
11.75	334.44	0.03	0.01	0.03	0.02	1
12.75	334.44	0.04	0.02	0.04	0.02	1
13.75	334.44	0.05	0.03	0.05	0.04	1

Appendix 6 Mathcad Program and import data for soil thermal contact conductivity calculations of the single-probe heat pulse measurement

Following is a program has been used in Chapter 5 to calculate the thermal properties of soil, which can calculate data from three single probes at the same time and can be revised and extended to as many as you need. Partial of an import data file is attached after the program for your reference.

Program:

Import the data from an excel file

All :=

5. silty clay.xlsx

frq := 2

n := 1

k := (n − 1)·600·frq

data := submatrix(All , k , 599·frq + k , 0 , 3)

$(data^{\langle 0 \rangle})_0 = 0 \quad (data^{\langle 0 \rangle})_{rows(data)-1} = 599$

t := $data^{\langle 0 \rangle}$ s T := $[data^{\langle 2 \rangle} - (data^{\langle 2 \rangle})_0]$·K

start := 50·frq = 100

end := 400·frq = 800

$$q := \frac{(data^{\langle 1 \rangle})_{end-1}}{\frac{end}{frq}} \cdot \frac{W}{m} = 5.972 \frac{1}{m} \cdot W$$

tt := submatrix(t , start , end , 0 , 0)

$$A := slope\left(ln\left(\frac{tt}{s}\right), submatrix\left(\frac{T}{K}, start, end, 0, 0\right)\right) = 1.524$$

$$\lambda := \frac{q}{4 \cdot \pi \cdot A \cdot K} = 0.31 \frac{1}{K \cdot m} \cdot W$$

$$\rho := 1250 \frac{kg}{m^3} \quad r := \frac{2.108}{2} mm \quad c := 867 \frac{J}{kg \cdot K}$$

$\theta := \text{data}_{10,3} = 6 \times 10^{-3}$

$C := c \cdot \rho + 4.186 \cdot 10^{6} \frac{J}{m^3 \cdot K} \cdot \theta = 1.109 \times 10^{6} \frac{1}{K \cdot m^3} \cdot J$

$\alpha := \frac{\lambda}{C} = 2.811 \times 10^{-7} \frac{m^2}{s}$

$L := 16$

$Cp := 3.2 \times 10^{6} \frac{1}{m^3 \cdot K} J$ $\qquad$ $Hguess := 800 \cdot \frac{W}{m^2 \cdot K}$

$$FBlackwell54(Q,R,C1,H,\alpha,\lambda,p) := \frac{Q}{\pi \cdot p} \cdot \frac{\left(\frac{1}{\sqrt{\frac{p}{\alpha}} \cdot R} K0\left(\sqrt{\frac{p}{\alpha}} \cdot R\right) + \frac{\lambda}{R \cdot H} \cdot K1\left(\sqrt{\frac{p}{\alpha}} \cdot R\right) \right)}{R^2 \cdot C1 \cdot p \cdot \left(\frac{1}{\sqrt{\frac{p}{\alpha}} \cdot R} K0\left(\sqrt{\frac{p}{\alpha}} \cdot R\right) + \frac{\lambda}{R \cdot H} \cdot K1\left(\sqrt{\frac{p}{\alpha}} \cdot R\right) \right) + 2 \cdot \lambda \cdot K1\left(\sqrt{\frac{p}{\alpha}} \cdot R\right)}$$

$Gavst\_Blackwell54(L,t,Q,R,C1,H,\alpha,\lambda) :=$

$nn2 \leftarrow \frac{L}{2}$

$nn21 \leftarrow nn2 + 1$

for $n \in 1..L$

  $z \leftarrow 0$

  for $k \in \text{floor}\left(\frac{n+1}{2}\right)..\min(n, nn2)$

    $z \leftarrow z + \frac{k^{nn2} \cdot (2 \cdot k)!}{(nn2 - k)! \cdot k! \cdot (k-1)! \cdot (n-k)! \cdot (2 \cdot k - n)!}$

  $v_n \leftarrow (-1)^{n+nn2} \cdot z$

$sum \leftarrow 0$

$ln2\_on\_t \leftarrow \frac{\ln(2.0)}{t}$

for $n \in 1..L$

  $p \leftarrow n \cdot ln2\_on\_t$

  $sum \leftarrow sum + v_n \cdot FBlackwell54(Q,R,C1,H,\alpha,\lambda,p)$

$ilt \leftarrow sum \cdot ln2\_on\_t$

$i := 1..799$

$tt_i := \frac{i+1}{800} \cdot 400s$

Objective functions

$$SSE1(H, tt, T, q, r, Cp, \alpha, \lambda) := \sum_{i=1}^{799} \left(\frac{Gavst\_Blackwell54(L, tt_i, q, r, Cp, H, \alpha, \lambda)}{K} - \frac{T_i}{K} \right)^2$$

Minimize the sum of squared error by adjusting parameter values.

$$parm1(tt, T, q, r, Cp, \alpha, \lambda) := Minimize(SSE1, Hguess)$$

$$Hfinal1 := parm1(tt, T, q, r, Cp, \alpha, \lambda)$$

$ThermParms(ii, Cp) :=$

$N \leftarrow rows(All)$

for $i \in 0..1000$

$M_i \leftarrow 1$

$j \leftarrow 0$

for $i \in 0..N-1$

$t_i \leftarrow All_{i,0}$

continue if $i = 0$

$M_j \leftarrow M_j + 1$ if $t_i > t_{i-1}$

$j \leftarrow j + 1$ otherwise

$count \leftarrow 0$

for $iii \in 0..j$

$k \leftarrow \sum_{i=0}^{iii} M_i - M_{iii}$

$(time \leftarrow submatrix(All, k, k + M_{iii} - 1, 0, 0) \quad Temp \leftarrow submatrix(All, k, k + M_{iii} - 1, ii, ii))$

$time \leftarrow time \cdot s$

$Temp \leftarrow (Temp - Temp_0) \cdot K$

$start \leftarrow 50 \cdot frq$

$end \leftarrow 400 \cdot frq$

$$A_{count} \leftarrow slope\left(ln\left(submatrix\left(\frac{time}{s}, start, end, 0, 0\right)\right), submatrix\left(\frac{Temp}{K}, start, end, 0, 0\right)\right)$$

$$B_{count} \leftarrow intercept\left(ln\left(submatrix\left(\frac{time}{s}, start, end, 0, 0\right)\right), submatrix\left(\frac{Temp}{K}, start, end, 0, 0\right)\right)$$

$$q_{count} \leftarrow \frac{All_{k+end-1, ii-1}}{\left(\frac{end}{frq}\right)} \cdot \frac{J}{m \cdot s}$$

$$\lambda_{count} \leftarrow \frac{q_{count}}{4 \cdot \pi \cdot A_{count}} \cdot \frac{1}{K}$$

$$theta_{count} \leftarrow All_{k+10 \cdot frq, ii+1}$$

$$C_{count} \leftarrow \left(1250 \cdot 867 + 4.186 \cdot 10^6 \cdot theta_{count}\right) \cdot \frac{J}{m^3 \cdot K}$$

$$\alpha_{count} \leftarrow \frac{\lambda_{count}}{C_{count}}$$

$$r \leftarrow \frac{2.108}{2000}\,m$$

$$Hintercep_{count} \leftarrow \frac{2\cdot\lambda_{count}}{r\cdot\left(\frac{B_{count}}{A_{count}} + 0.5772 - \ln\left(4\cdot\frac{\alpha_{count}}{r^2\cdot s^{-1}}\right)\right)}$$

$$H1_{count} \leftarrow parm1\left(submatrix(time,0,799,0,0), submatrix(Temp,0,799,0,0), q_{count}, r, Cp, \alpha_{count}, \lambda_{count}\right)$$

$$count \leftarrow count + 1$$

$$augment\left(theta, \frac{q}{J\cdot m^{-1}\cdot s^{-1}}, \frac{\lambda}{J\cdot K^{-1}\cdot m^{-1}\cdot s^{-1}}, \frac{C}{10^6\cdot J\cdot m^{-3}\cdot K^{-1}}, \frac{\alpha\cdot 10^7}{m^2\cdot s^{-1}}, \frac{Hintercep}{J\cdot m^{-2}\cdot K^{-1}\cdot s^{-1}}, \frac{H1}{J\cdot m^{-2}\cdot K^{-1}\cdot s^{-1}}\right)$$

$$AA := ThermParms\left(2, 3.2\times 10^6 \frac{1}{m^3\cdot K} J\right) \qquad BB := ThermParms\left(5, 2.8\times 10^6 \frac{1}{m^3\cdot K} J\right)$$

$$CC := ThermParms\left(8, 4.5\times 10^6 \frac{1}{m^3\cdot K} J\right)$$

$$All := augment(AA, BB, CC)$$

result of silty clay.xls

All

Example of the import data (Σ*q*: total heat input; *T*: temperature; θ: water content)

Time (s)	Probe 1			Probe 2			Probe 3		
	Σ*q* (J m^{-1})	*T* (^{0}C)	θ	Σ*q* (J m^{-1})	*T* (^{0}C)	θ	Σ*q* (J m^{-1})	*T* (^{0}C)	θ
0.0	0.00	15.99	0%	0.00	16.21	0%	0.00	15.72	0%
0.5	3.04	16.28	0%	2.97	16.59	0%	2.99	15.86	0%
1.0	6.08	16.53	0%	5.94	16.89	0%	6.00	16.07	0%
1.5	9.12	16.73	0%	8.91	17.10	0%	9.01	16.28	0%
2.0	12.17	16.91	0%	11.88	17.28	0%	12.01	16.46	0%
2.5	15.21	17.09	0%	14.86	17.45	0%	15.02	16.63	0%
3.0	18.25	17.25	0%	17.83	17.61	0%	18.02	16.79	0%
3.5	21.30	17.41	0%	20.80	17.76	0%	21.03	16.94	0%
4.0	24.34	17.56	0%	23.77	17.91	0%	24.03	17.08	0%
4.5	27.38	17.69	0%	26.74	18.03	0%	27.04	17.21	0%
5.0	30.43	17.81	0%	29.71	18.16	0%	30.05	17.33	0%
5.5	33.47	17.93	0%	32.68	18.27	0%	33.05	17.46	0%
6.0	36.52	18.05	0%	35.65	18.36	0%	36.06	17.57	0%
6.5	39.56	18.15	0%	38.62	18.49	0%	39.06	17.68	0%